

Pavel Semaev

Energy efficient CO₂ refrigeration units for fishing vessels

June 2021



Norwegian University of
Science and Technology

Energy efficient CO₂ refrigeration units for fishing vessels

Pavel Semaev

MSc. in Sustainable Energy

Submission date: June 2021

Supervisor: Prof. Armin Hafner

Co-supervisor: Ignat Tolstorebrov

Norwegian University of Science and Technology
Department of Energy and Process Engineering

Preface

This is the Master Thesis of Pavel Semaev, written during the final year of the Sustainable Energy master program of the Department of Energy and Process Engineering at the Norwegian University of Science and Technology (NTNU). The research work was done during the spring semester of the year 2021.

I want to thank Ignat Tolstorebrov and Professor Armin Hafner for their guidance and advice. Thanks also to Eirik Starheim Svendsen and Muhammad Zahid Saeed for their helpful advice and practical suggestions regarding the Dymola software, and Engin Söylemez for help with the conference paper. In truth, I could not have achieved the current standards without a strong support group. I would also like to thank my fellow students, providing me with a good study environment.

Finally, I must express my profound gratitude to Agnes and my parents for providing me with support and encouragement throughout the final year.

Trondheim, June 2021

A handwritten signature in black ink that reads "Pavel Semaev". The signature is written in a cursive style with a large initial 'P'.

Pavel Semaev

Abstract

Reduction in greenhouse gas emissions from the fishing sector is an effort that requires the development of innovative new technology, and that requires research. This master thesis is a part of the CoolFish project, led by SINTEF Ocean, with multiple research and industrial partners. The project aims to develop environmentally friendly systems for cooling, freezing, and heating onboard fishing vessels.

This thesis describes the architecture and performance of a prototype industrial CO₂ transcritical system for refrigerated seawater (RSW). The design presented was developed by NTNU to be implemented at MMC First Process. The CO₂ system will cover cooling demands in air conditioning (AC), RSW and low-temperature freezing. Five simulation models for the CO₂ system were developed using Engineering Equation Solver (EES) and Dymola/Modelica for optimization regarding system performance, energy efficiency, and applicability for future installations:

- **CASE 1:** Single throttling. One evaporating temperature level at -5 °C (Refrigerated sea water temperature production).
- **CASE 2:** Double throttling with auxiliary compressor configuration. Two evaporating temperature levels at -5 °C (RSW) and 5 °C (AC).
- **CASE 3:** Triple throttling with parallel compression. Three evaporating temperature levels at AC, RSW and low temperature frozen storage (LT) at -25 °C.
- **CASE 4:** Similar as in CASE 2 with the utilization of a high-pressure ejector. Two evaporating temperature levels at AC and RSW.
- **CASE 5:** Similar to CASE 2 with the utilization of a high-pressure ejector. Two evaporating temperature levels at RSW and LT.

Optimal high pressure, pressure in the intermediate pressure receiver, the effectiveness of internal heat exchangers and effectiveness of ejectors were thoroughly investigated to optimize the specified cases. The research shows that the COP of the transcritical CO₂ system varies with the pressure in the gas cooler; a maximum COP occurs at an optimal discharge pressure depending on the outlet temperature from the gas cooler. Based on the cycle evaluation, correlations of the optimal discharge pressure are obtained for each specified case. Further, dynamic models of the CO₂ unit are presented. The simulations was done with respect to realistic operating conditions, focusing on the chilling and the temperature maintenance period.

The results indicate that the length of the maintenance predominantly affects the overall system performance. During maintenance, the loads are low and primarily occurs due to the transmission losses. While the length of the maintenance period varies, it can be argued to be the most prolonged operational period for fishing vessels going far to the sea. Therefore correct system control, ensuring the best possible COP at maintenance is essential to ensure low system power consumption, hence lowering the fuel consumption onboard in the range of [7% – 12%]. Further, the results show a high-performance increase utilizing a high-pressure ejector (CASE 4), especially at higher ambient temperatures. The ejector solution provides stable refrigeration capacity at 440 kW at RSW whilst achieving a COP in the range of [3, 0 – 3, 5]. The proper control of the refrigeration system should ensure efficient cooling onboard fishing vessels in warmer climates. One example of such control evaluation is the influence of internal heat exchangers (IHX) on system performance. Based on calculations performed by EES, the benefits of IHX on system COP and cooling at RSW is observed only at higher ambient temperatures (above 30 °C). Therefore, it is advised to bypass internal heat exchangers at seawater temperatures lower than 30 °C.

Sammendrag

Reduksjon i klimagassutslipp fra fiskesektoren er en innsats som krever forskning og utvikling av nyskapende teknologi. Denne masteroppgaven er en del av CoolFish prosjektet, ledet av SINTEF Ocean i samarbeid med flere forsknings- og industripartnere. Prosjektets mål er å utvikle miljøvennlige systemer for kjøling, frysing og oppvarming om bord på fiskefartøy.

Denne oppgaven beskriver arkitekturen og ytelsen til en prototype industriell CO₂ transkritisk system for nedkjølt sjøvann (RSW). Systemet som blir presentert er utviklet av NTNU for å implementeres ved MMC First Process. CO₂ anlegget vil dekke kjølebehov for klimaanlegg (AC), RSW og frysing ombord ved lave temperaturer (LT). Fem simuleringsmodeller for CO₂ systemet ble utviklet ved hjelp av "Engineering Equation Solver" (EES) og Dymola/Modelica for optimalisering av systemytelse, energieffektivitet og anvendelighet for fremtidige installasjoner.

- **CASE 1:** Enkel struping med et fordamping temperaturnivå på -5 °C (RSW).
- **CASE 2:** Dobbel struping med parallel kompressor. To fordamping temperaturnivå på +5 °C (AC) og -5 °C (RSW).
- **CASE 3:** Trippel struping med parallel kompresjon. Tre fordamping temperaturnivå på AC,RSW og lav temperature (-25 °C) fryselager.
- **CASE 4:** Lignende som i CASE 2 med bruk av en ejektor. To fordamping temperaturnivå (AC, RSW).
- **CASE 4:** Lignende som i CASE 3 med bruk av en ejektor. To fordamping temperaturnivå (AC, LT).

Optimal høytrykk, trykk i mellomtrykkmottakeren, virkningsgrad til interne varmevekslere og virkningsgrad til ejektorene ble grundig undersøkt for å optimalisere de nevnt modellene. Resultatene viser at COP (virkningsgrad) for det transkritiske CO₂ systemet varierer med høytrykket; maksimalt COP oppstår ved et optimalt høytrykk avhengig av utløpstemperaturen til gasskjøleren. Basert på syklusevalueringen blir det utviklet korrelasjoner for hvert spesifisert simuleringsmodell. Videre, presenteres de dynamiske simuleringsmodeller av CO₂ enheten. Simulasjonene ble testet under realistiske driftsforhold, med fokus på nedkjøling og "vedlikeholdsperioden".

Resultatene indikerer at lengden på vedlikeholdsperioden påvirker den generelle systemytelsen. Under vedlikehold er belastningen lav på grunn av infiltrasjonstap. Selv om lengden av vedlikeholdsperioden varierer, kan det hevdes at den er den lengste driftsperioden for fartøy som går langt ut i sjøen. Riktig systemkontroll er viktig for å sikre best mulig COP ved denne perioden og for å sikre lavt strømforbruk i systemet. Dette resulterer i lavere drivstoffbruk om bord [7% – 12%]. Videre viser resultatene en økning i ytelse ved bruk av ejektor (CASE 4), spesielt ved høyere omgivelsetemperaturer. Ejektor løsningen gir en stabil kjølekapasitet ved RSW, samtidig som det oppnås en forsvarlig COP. Resultatene peker også på at riktig kontroll av kjølesystemet skal sikre effektiv kjøling ombord på fiskefartøy i varmere klima. Et eksempel på slik kontrollevaluering er innflytelsen av virkningsgraden av interne varmevekslere (IHX) på systemytelsen. Basert på beregningene utført ved hjelp av EES, observeres fordelene med IHX på systemets COP og kjøleeffekt på RSW bare ved høyere omgivelsetemperaturer. Derfor anbefales det å omgå interne varmevekslere ved sjøvansstemperaturer lavere enn 30 °C.

Table of Contents

List of Figures	xiii
List of Tables	xvii
1 Introduction	1
1.1 Motivation	1
1.2 Task description	1
1.3 Overview	1
1.4 Goal and Structure	2
1.5 CoolFish project	3
2 Theory and Literature Review	4
2.1 Refrigeration Principle	4
2.2 CO ₂ refrigeration systems	6
2.2.1 Subcritical	6
2.2.2 Transcritical	7
2.3 Industrial refrigeration with CO ₂	7
2.3.1 Transcritical Industrial Systems	8
2.3.2 Cascade Systems	9
2.3.3 Indirect system	10
2.4 Methods on improving the energy efficiency of CO ₂	10
2.4.1 Internal heat exchanger	12
2.4.2 Two stage expansion with auxiliary compression	13
2.4.3 Expanders in transcritical CO ₂ systems	14
2.4.4 Ejectors	14
2.5 Refrigeration at fishing vessels	16
2.5.1 RSW systems	16
2.5.2 Heat loads in RSW systems	17
2.5.3 CO ₂ RSW systems on board	17
2.5.4 Combined RSW and freezing systems with CO ₂	18
3 System Design	20
3.1 Principle Design 1 (CASE 1, CASE 2 and CASE 3)	20
3.2 Principle design 2 (CASE 4)	22
3.3 Principle design 3 (CASE 5)	23

3.4	Description of components	25
3.4.1	Compressors (C1, C2 and C3)	25
3.4.2	Sea water Gas Cooler (GC2)	25
3.4.3	Internal Heat Exchangers (IHX1 and IHX2)	26
3.4.4	RSW (EVAP1)	26
3.4.5	AC evaporator (EVAP2)	27
3.4.6	Danfoss Multi Ejector (HP and LP Ejector)	27
4	Methodology	29
4.1	Simulation Tools	29
4.2	Compressor efficiency	29
4.2.1	Volumetric flow of the compressor	29
4.2.2	Isentropic efficiency	30
4.3	Internal Heat Exchangers	30
4.4	Ejector	31
4.5	Simulation models in Dymola	32
4.5.1	Compressors	32
4.5.2	Flooded shell and tube evaporators	34
4.5.3	Gas cooler (GC1 and GC2)	35
4.5.4	Expansion devices	35
4.5.5	RSW circuit (CASE 1, CASE 2 and CASE 4)	36
4.5.6	AC circuit	37
4.6	Statistical validation	37
5	Results	38
5.1	Steady state performance	38
5.1.1	CASE 1: 3 RSW compressors	38
5.1.2	CASE 2: 2 RSW and 1 AC compressors	41
5.1.3	CASE 3: 1 RSW, 1 AC and 1 LT compressors	46
5.1.4	CASE 4: HP ejector	49
5.1.5	CASE 5: LP ejector	53
5.2	Dynamic loads performance	57
5.2.1	Validation by comparison with EES results	57
5.2.2	Models comparison (CASE 1, CASE 2 and CASE 4)	57
5.2.3	CASE 4 - ejector efficiency	60

6 Discussion	62
6.1 Suggested control strategy	62
6.2 Overview of system improvements	63
7 Conclusion	65
8 Further Work	67
Bibliography	68
Appendix	70

List of Figures

1	Logo of the CoolFish project	3
2	Carnot refrigeration process	4
3	Simple closed vapor compression cycle	5
4	P-h diagram and T-s diagram for a single refrigeration cycle, referring to schematics in Figure 3	6
5	Comparing logP-h diagrams of a transcritical cycle vs a subcritical one	7
6	Transcritical cycles with different values of ambient temperature	8
7	Cascade system of CO ₂ and NH ₃ , principle sketch	9
8	Cascade system of CO ₂ and NH ₃ , Ts diagram	10
9	Indirect cascade system with pump circulation.	10
10	Losses of an idealised subcritical refrigeration cycle	11
11	Losses of an idealised transcritical refrigeration cycle	11
12	Transcritical cycles with different values of condensation pressure	12
13	Transcritical cycles with an internal heat exchanger scheme and Ph diagram	12
14	Auxiliary compression system configuration	13
15	Auxiliary compression system p-h diagram	13
16	Schematic of refrigeration system equipped with a two-phase ejector	15
17	Ph diagram of refrigeration system equipped with a two-phase ejector	15
18	Ph diagram, processes of expansion and compression in the ejector	16
19	A simplified schematic of the RSW system	17
20	Characteristics chilling curves for an arbitrary RSW chilling system (37)	17
21	A simplified schematic of the CO ₂ and NH ₃ system circuit installed at MS Kvannøy (38)	18
22	Principle sketch of the CO ₂ unit	20
23	Gas coolers configuration (Part of Figure 22)	21
24	RSW flooded evaporator (EVAP1) with a medium pressure reciever (MPR) (Part of Figure 22)	21
25	Principle sketch of the CO ₂ unit equipped with a multi ejector rack	22
26	The ejector configuration close up (Part of Figure 25)	23
27	Principle sketch of the CO ₂ unit with ejectors	23
28	The ejector configuration close up (Part of Figure 27)	24
29	Compressor type: HGX46/ 400-4 ML CO2T (10)	25
30	Alfa Laval AXP112 Brazed plate heat exchanger	26
31	Alfa Laval AXP52 Brazed plate heat exchanger	26
32	RSW cooler	27

33	AC evaporator (EVAP2)	27
34	Danfoss Multi Ejector Design (14)	28
35	Schematic of internal heat exchanger configuration	30
36	Schematic of a two phase ejector	31
37	CASE 1 compressor controller, snipped from Dymola	33
38	CASE 2 and 4: C1 compressor controller , snipped from Dymola	34
39	Simplified flooded evaporator: AC circuit, snipped from Dymola.	34
40	DSH and condenser unit. Snipped from Dymola	35
41	RSW loop. Snipped from Dymola	36
42	CASE 1: Refrigeration capacity vs sea water temperatures [$P_{GC} = 90 [bar]$]	39
43	CASE 1: COP as a function different discharge pressures at sea water temperatures of 30, 35 and 40 °C, for the CO ₂ system with IHX efficiencies values 0,1, 0,54 and 0,9	39
44	CASE 1: COP vs discharge pressure at different seawater temperatures [$\eta_{IHX} = 90\%$]	41
45	CASE 2: Refrigeration capacity vs seawater temperature [$P_{GC} = 90[bar]$]	42
46	CASE 2: Refrigeration capacity RSW vs AC pressure [$P_{GC} = 90 [bar]$]	43
47	CASE 2: AC Refrigeration capacity vs pressure after first expansion [$P_{GC} = 90[bar]$]	43
48	CASE 2: COP vs discharge pressure at different seawater temperatures	44
49	CASE 2: refrigeration capacity at RSW vs discharge pressure at different seawater temperatures, [$\eta_{IHX} = 10\%$]	45
50	CASE 3: Refrigeration capacity vs seawater temperature	47
51	CASE 3: Refrigeration capacity at LT vs Pressure at LT	47
52	CASE 3: COP vs discharge pressure at different seawater temperatures	48
53	CASE 3: RSW refrigeration capacity vs discharge pressure at different seawater temperatures	49
54	CASE 4: RSW Refrigeration capacity vs seawater temperature [$P_{GC} = 90 [bar]$ and $\eta_{ejector} = 30\%$]	50
55	CASE 4: RSW and AC Refrigeration capacity vs seawater temperature [$P_{GC} = 90[bar]$, IHX bypass]	50
56	CASE 4: Optimum high pressure considering COP at $T_{RSW} = 30 , 35$ and $40 [^{\circ}C]$, [IHX bypass]	51
57	CASE 4 ($\eta_{ejector} = 30\%$, IHX bypass, $P_{GC} = 90 [bar]$) vs CASE 2 (IHX bypass, $P_{GC} = 90 [bar]$)	52
58	Systems COP: CASE 4 ($\eta_{ejector} = 30\%$, IHX bypass, $P_{GC} = 90 [bar]$) vs CASE 2 (IHX bypass, $P_{GC} = 90 [bar]$)	52
59	CASE 4 ($\eta_{ejector} = 30\%$, IHX bypass, $P_{GC} = 90 [bar]$) vs CASE 1 ($\eta_{IHX} = 10\%$, $P_{GC} = 90 [bar]$)	53
60	CASE 5 ($\eta_{ejector} = 30\%$, $\eta_{IHX} = 30\%$, $P_{GC} = 90 [bar]$ and C1, C2 – RSW and C3 – LT)	54

61	CASE 4: Optimum high pressure considering COP at $T_{RSW} = 30 [^{\circ}C]$, $35 [^{\circ}C]$ and $40 [^{\circ}C]$, [$\eta_{IHx} = 30\%$]	55
62	CASE 4 vs CASE 5 ($\eta_{ejector} = 30\%$, $\eta_{IHx} = 30\%$, $P_{GC} = 90 [bar]$)	55
63	CASE 1, CASE 2 and CASE 4 comparison	58
64	Energy demand during chilling and maintenance period [$T_{SW} = 17 [^{\circ}C]$, $P_{GC} = 90 [bar]$ and $\dot{Q}_{Maintenance} = 30 [kW]$]	59
65	Energy demand during chilling and maintenance period [$T_{SW} = 27 [^{\circ}C]$, $P_{GC} = 90 [bar]$ and $\dot{Q}_{Maintenance} = 60 [kW]$]	60
66	CASE 4 with utilizing $\eta_{ejector} = 10\%$, $\eta_{ejector} = 20\%$ and $\eta_{ejector} = 30\%$; $T_{GCout} = 22 [^{\circ}C]$	60
67	Energy demand during chilling and maintenance period altering ejector efficiency [$T_{GCout} = 32 [^{\circ}C]$, $P_{GC} = 90 [bar]$ and $\dot{Q}_{Maintenance} = 60 [kW]$]	61
68	Optimal gas cooler pressure lines for the reviewed system configurations at seawater temperatures $30 [^{\circ}C]$ or higher, [$\eta_{IHx} = 30\%$]	64

List of Tables

1	CASE 1: reference system [$\eta_{IHX} = 30\%$ and $P_{GC} = 90$ [bar]]	38
2	CASE 1: Optimum discharge pressure and refrigeration capacity at given sea water temperature and IHX efficiency	40
3	CASE 2: reference system, [$\eta_{IHX} = 30\%$ and $P_{GC} = 90$ [bar]]	42
4	CASE 2: RSW and AC refrigeration capacity at different seawater temperatures, at optimum P_{AC} , [$P_{GC} = 90$ bar]	44
5	CASE 2: RSW and AC refrigeration capacity at different seawater temperatures, at optimum P_{GC} , considering systems COP, $\eta_{IHX} = 90\%$	45
6	CASE 2: RSW and AC refrigeration capacity at different seawater temperatures, at optimum P_{GC} , considering \dot{Q}_{RSW}	46
7	CASE 3: reference system, [$\eta_{IHX} = 30\%$ and $P_{GC} = 90$ [bar]]	46
8	CASE 3: RSW, AC and LT refrigeration capacity at different seawater temperatures, at optimum P_{GC} , considering systems COP	48
9	CASE 3: RSW, AC and LT refrigeration capacity at different seawater temperatures, at optimum P_{GC} , considering \dot{Q}_{RSW}	49
10	CASE 4: reference system [$\eta_{ejector} = 30\%, \eta_{IHX} = 30\%$ and $P_{GC} = 90$ bar]	49
11	CASE 4: RSW, AC and LT refrigeration capacity at different seawater temperatures, at optimum P_{GC} , considering systems COP	51
12	CASE 5: reference system [$\eta_{ejector} = 30\%, \eta_{IHX} = 30\%$, $P_{GC} = 90$ [bar], $C1, C2 - RSW$ and $C3 - LT$]	53
13	CASE 5: reference system [$\eta_{ejector} = 30\%, \eta_{IHX} = 30\%$, $P_{GC} = 90$ [bar] and $C1, C2, C3 - RSW$]	54
14	Validation of simulation models [$P_{GC} = [75$ bar – 95 bar] and $T_{GCout} = 22$ [°C]] .	57
15	Validation of simulation models [$P_{GC} = 90$ [bar] and $T_{GCout} = [15^\circ C - 32, 5^\circ C]$] .	57

Nomenclature

Abbreviations

<i>AC</i>	Air Conditioning
<i>C</i>	Compressor
<i>CO₂</i>	Carbon dioxide
<i>COP</i>	Coefficient Of Performance
<i>CVCC</i>	Closed Vapor Compression Cycle
<i>DHW</i>	Domestic Hot Water
<i>DX</i>	Direct Expansion
<i>EES</i>	Engineering Equation Solver
<i>EVAP</i>	Evaporator
<i>GC</i>	Gas Cooler
<i>GHG</i>	Green House Gas Emissions
<i>GWP</i>	Global Warming Potential
<i>HFC</i>	Hydrofluorcarbons
<i>HP</i>	High Pressure
<i>HP</i>	High pressure
<i>HTC</i>	High Temperature Circuit
<i>HX</i>	Heat Exchanger
<i>IHE</i>	Internal Heat Exchanger
<i>IHX</i>	Internal Heat Exchanger
<i>LP</i>	Low pressure
<i>LT</i>	Low Temperature
<i>LTC</i>	Low Temperature Circuit
<i>MA%E</i>	Mean absolute per cent error
<i>MP</i>	Medium Pressure
<i>MPR</i>	Medium Pressure Receiver
<i>ODP</i>	Ozone Depletion Potential
<i>Ph</i>	Pressure enthalpy
<i>Pr</i>	Pressure Ratio
<i>R22</i>	Chlorodifluoromethane
<i>R717</i>	Ammonia
<i>R₁₂</i>	Dichlorodifluoromethane
<i>R_{134a}</i>	Tetrafluoroethane
<i>R₇₁₇</i>	Ammonia

RSW Refrigerated Sea Water
SH Space Heating
TBV Three Way Bypass Valve
Ts Temperature Entropy

Symbols

ΔQ Capacity difference [*kW*]
 Δs Entropy difference [$\frac{J}{K}$]
 \dot{m}_R Refrigerant mas flow [*kg/s*]
 \dot{m}_{mn} Motive nozzle mas flow [*kg/s*]
 \dot{m}_{sn} Suction mas flow [*kg/s*]
 \dot{Q}_C Evaporator heat capacity [*kW*]
 \dot{Q}_E Evaporator heat capacity [*kW*]
 \dot{Q}_{AC} AC refrigeration capacity [*kW*]
 \dot{Q}_{IHx} IHX heat capacity [*kW*]
 \dot{Q}_{LT} LT refrigeration capacity [*kW*]
 \dot{Q}_{RSW} RSW refrigeration capacity [*kW*]
 \dot{V}_{flow} Volumetric Flow Rate [m^3/h]
 \dot{W}_{ideal} Ideal Mechanical Work [*kW*]
 \dot{W}_{real} Real Mechanical Work [*kW*]
 $\eta_{ejector}$ Ejector Efficiency [-]
 η_{IHx} IHX Efficiency [-]
 η_{is} Istentropic Compressor Efficiency [-]
 Φ_m Mas entertainment ratio [-]
 Π Suction Pressure Ratio [-]
 ρ Density [m^3/kg]
 C_P Heat Capacity [*kJ/kgK*]
 h Enthalpy [*kJ/kg*]
 P Pressure [*bar*]
 P_{AC} Pressure at AC [*bar*]
 $P_{diff\ out}$ Ejector pressure downstream of the diffusor [*bar*]
 P_{GC} Discharge Pressure [*bar*]
 P_{lift} Pressure Lift [*bar*]
 P_{LT} Pressure at LT [*bar*]
 P_{OPT} Optimal High Pressure [*bar*]
 $P_{sn\ in}$ Ejector suction pressure [*bar*]

s	Entropy [$\frac{J}{K}$]
T_H	Condensing temperature [$^{\circ}C$][K]
T_L	Evaporating temperature [$^{\circ}C$][K]
T_{SW}	Sea Water Temperature [$^{\circ}C$]
T_{tank}	Temperature in RSW tank [$^{\circ}C$]
v	Specific volume [m^3/kg]
W_{Ca}	Carnot Work [kW]

1 Introduction

1.1 Motivation

Fishing vessels are a significant energy consumer and are accountable for a big share of emissions related to the seafood product value chain. The refrigerant leakage is a big part of these emissions. According to the International Maritime Organisation, the release of refrigerants from global shipping is estimated at 8,400 tons, or 15 million tons CO₂ equivalent emissions and is responsible for 1.9% of total Norway's emissions (38)(5). The Montreal Protocol Technology and Economic Assessment Panel (TEAP) reported that 70% of the global fishing fleet uses R22 as their main refrigerant in 2016 (35). The EU F-Gas Regulation 517/2014 will phase down the supply of the hydrofluorocarbons to the EU market by 79% compared to the levels in 2009-2012 (26). The regulations have made hydrofluorocarbons obsolete while natural refrigerants, like CO₂ and NH₃ more popular because of close to no impact on the environment.(20).

Chilling fish in refrigerated seawater (RSW) is an important method of conserving fish. Big fishing vessels have more than 1000 m³ of RSW tanks (20). This makes the refrigerant plant one of the largest electricity consumer on board, around 50% of the total energy consumption (30). The fishing industry is thereby adapting to improved and more environmentally friendly technologies (30). There are many possible designs for an RSW system on board of a boat. CO₂ based RSW systems are relatively new to the industry and are not as dominating as NH₃ systems (38). CO₂ is a non-toxic and non-flammable refrigerant, which are critical required properties particularly for the systems installed in fishing vessels.

1.2 Task description

This master thesis is a continuation of the Project work performed during the fall of 2020. This thesis aims to follow up on implementation of a CO₂ refrigeration system at MMC First Process. This unit will be applied to test CO₂ components developed and applied by MMC. One task was to develop simulation models in Dymola, which will be validated with EES models and performance data available from the commissioning phase in 2021. The developed systems were evaluated in terms of system performance, energy efficiency, and applicability for future installations at fishing vessels. The task to be considered:

- Review of relevant literature, e.g. maritime and industrial refrigeration, energy efficiency etc.
- Describe the CO₂ refrigeration system with ejector at the high and low temperature stage and develop a draft matrix for the commissioning period.
- Develop models of the system with EES and Dymola/Modelica.
- Validate theoretical results and models with the first performance data available during the commissioning phase (if possible).
- Analyze the results in terms of system performance, energy consumption, and applicability of the refrigeration system at higher seawater temperatures.
- A Master Thesis report including a discussion section.
- Proposal for further work.
- Draft version of a scientific paper based on the results.

1.3 Overview

As stated in Section 1.2, this Master Thesis is a continuation of the Project Work performed during the fall semester of 2020, and is a part of the Coolfish project. This section will review which tasks have been completed during which period.

Project Work

The Project Work aimed to develop simulation models of the CO₂ refrigeration unit at MMC First Process. Three simulation models were built using Engineering Equation Solver (EES) and were used to evaluate the cooling unit. To obtain the best performance of the unit, a proper evaluation of the influence of some of the components on its performance was carried out, hence enabling optimization of the system.

Continuation of the Project Thesis

This master thesis will further focus on the CO₂ refrigeration system at MMC First Process. Therefore, some of the reviewed relevant literature and theory of the project thesis are relevant for the Master Thesis. In agreement with my supervisors, Armin Hafner and Ignat Tolstorebrov, it was decided to reuse some of the relevant parts of the project thesis. This enabled more time to develop skills in Dymola and develop effective simulation models both in EES and Dymola. Two simulation models were developed in EES and three with Dymola during the semester. The systems were further evaluated in regards to system performance and energy efficiency.

1.4 Goal and Structure

The task presented in Section 1.2 will be carried out throughout the spring semester. The thesis is of eight parts, which are presented below:

Theory and Literature review

Containing relevant literature regarding cooling and freezing. Including but not limited to; refrigeration principle, CO₂ refrigeration systems, industrial refrigeration with CO₂ energy efficiency and refrigeration at fishing vessels.

System design

This chapter contains detailed description of the CO₂ refrigeration system and possible configurations. This section will also present an overview of relevant components in the refrigeration system, including but not limited to; compressors, evaporators, ejectors, internal heat exchangers and gas coolers.

Methodology

Describes the methodology and procedure that was used developing the simulation models for the refrigeration unit. The method of developing initial steady state models in EES, and the method for developing dynamic models using Dymola. Second part will present some of the equations used in the simulations, regarding the efficiencies of compressors, the internal heat exchangers and ejectors.

Results

This chapter contains a presentation and discussion of results of the developed models under different ambient conditions. The results of this project is shown in five cases. Lastly the developed simulation models are compared in terms of system performance, energy efficiency and applicability at fishing vessels.

Discussion Most of the results are thoroughly discussed in the "Results" section. This chapter will discuss some of the key findings and technicalities in a broader perspective, and will focus on steady state performance analysis.

Conclusion

Containing the most significant findings of this thesis, from the simulation models and literature review. Key finding from comparison of the five cases will be presented and focused upon with predicted systems COP and refrigeration capacity.

Further Work

Some of the tasks and experiments have been left for the future due to lack of time. This section gives a series of proposal for further work to be done in later research.

Appendices

This chapter contains other relevant information. Including EES-scripts, detailed Dymola models and Ohrid conference paper based on some of the results in the following master thesis.

1.5 CoolFish project

The aspiration of this project is to take part in the development of energy efficient and climate friendly systems for heating, cooling and freezing on board fishing vessels. These are important steps to maintain shelf life and quality of the fish, and reducing CO₂ and greenhouse gas emissions. To accomplish this, the fishing sector needs new solutions and technology, that maybe previously were not economically feasible.



Figure 1: Logo of the CoolFish project

This project is funded for four years, beginning in 2019, and has three main objectives:

- **Energy efficiency:**
Development and implementation of energy efficient refrigeration systems to be used on board fishing vessels.
- **Industry design case:**
Development of integrated refrigeration and heating systems in the industry.
- **Climate and environment:**
Promote the effect of new sustainable refrigeration systems, and increase awareness of the effects on climate and environment non sustainable units have.

The CoolFish project includes research partners SINTEF Ocean (project manager), SINTEF Energy and NTNU. Industrial partners are MMC First Process, Selvåg Senior/Sørheim Holding, Danfoss, Øyangen, Perfect temperature group (PTG), Gasnor, Bluewild and Isotherm Inc. (USA).. Other partners that are involved are Institute of Refrigeration, South Bank University and Johnson Controls DK.

2 Theory and Literature Review

Chapter two will investigate relevant literature and present the most important theory for the topics covered in this project. Including but not limited to: industrial refrigeration, CO₂ refrigeration, energy efficiency, refrigeration at fishing vessels.

2.1 Refrigeration Principle

Heat is transferred naturally in the direction of decreasing temperature: from a high-temperature reservoir to lower temperature reservoir, and is driven by the temperature difference (16). Thereby, for a refrigeration process, it is not achievable for heat to flow from a colder reservoir to a warmer reservoir without any work or energy input into the process. This can be visualized by a Temperature-entropy (Ts) diagram, seen in Figure 2. The process operates between two temperature levels, the high temperature (T_H) and the low temperature (T_L). Moving low-temperature heat (Q_L) up to T_H , it is necessary for work input (W).

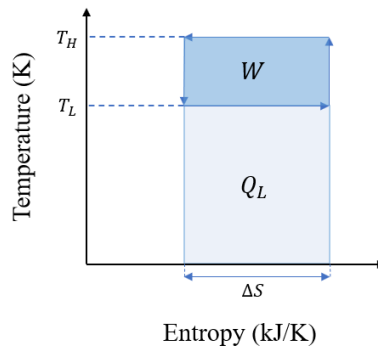


Figure 2: Carnot refrigeration process

Figure 2, illustrates a Carnot refrigeration process, where we can find isotherm condensation and evaporation, along with isentropic compression and expansion. The required work (W_{Ca}) can be thereby expressed by Equation 1.

$$W_{Ca} = (T_H - T_L) * \Delta S \quad (1)$$

To express the performance of such a refrigeration system, it is common to use a power factor, also known as the coefficient of performance (COP). It is a dimensionless factor, referring to a ratio of useful thermal energy output overwork (energy) input. For the Carnot refrigeration system it can be expressed by Equation 2.

$$COP_{Ca} = \frac{Q_L}{W_{Ca}} = \frac{T_L}{T_H - T_L} \quad (2)$$

where the low-temperature heat (Q_L) is expressed by the following equation.

$$Q_L = T_L * \Delta S \quad (3)$$

Carnot process is useful, as it gives a theoretical maximum value of system performance. As a consequence of unavoidable and irreversible losses in a real system, the actual system's COP cannot be greater or equal to the Carnot COP (COP_{Ca}).

Several different refrigeration principles exist, including natural ice open systems, evaporative open systems, closed vapour compression process, absorption systems and more. The most frequently

used and focused upon in this theses is the closed vapour-compression refrigeration cycle or CVCC. The system utilizes a large amount of absorbed heat in the evaporation and then releases in the condensation of a working fluid. CVCC utilizes a compressor to circulate the working fluid and an expansion valve to release pressure from condensation to evaporation pressure. A simple CVCC is shown schematically in Figure 3.

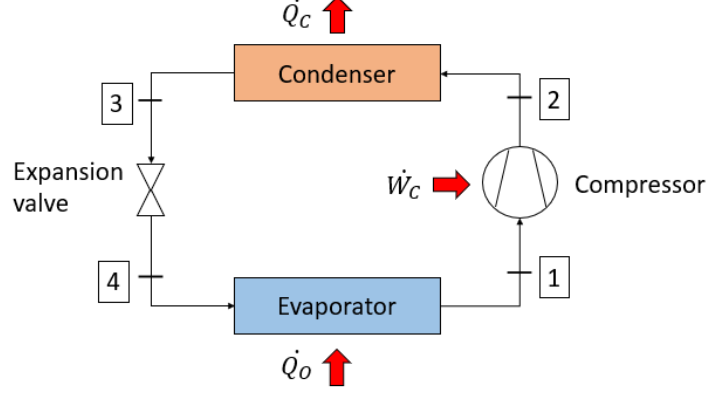


Figure 3: Simple closed vapor compression cycle

Temperature-entropy (T-s) and pressure-enthalpy (p-h) diagrams are often used to better understand CVCC. Each refrigerant has a unique p-h and T-s diagram. Using Figure 3 with its corresponding T-s and p-h diagram in Figure 4, the four stages of the closed vapor-compression refrigeration cycle is described below:

- **1-2 Compression:**

If we assume an adiabatic (isentropic) compression without any extra losses, the isentropic work will be $\dot{W}_{is} = \dot{m}_R * (h_{2s} - h_1)$. The actual compression, including the losses can be calculated as:

$$\dot{W}_C = \frac{\dot{W}_{is}}{\eta_{is}} = \frac{\dot{m}_R * (h_2 - h_1)}{\eta_{is}} \quad (4)$$

where η_{is} is the isentropic efficiency.

- **2-3 Rejection:**

Condensation takes place at constant pressure (isobaric process). Condensation removes first the super heat down to dew point curve and then brings the refrigerant into liquid form. If the heat loss to surroundings is neglected, the heat rejected from the condenser can be expressed as the sum of heat removed by evaporation and compression heat:

$$\dot{Q}_C = \dot{Q}_O + \dot{W}_C = \dot{m}_R * (h_2 - h_3) \quad (5)$$

where \dot{W}_C is the work performed by the compressor and \dot{Q}_O is the heat absorbed by evaporation.

- **3-4 Expansion:**

The expansion is assumed to be an isenthalpic process. This process decreases the temperature and the pressure of the refrigerant.

$$h_3 = h_4 \quad (6)$$

- **4-1 Evaporation:**

The working fluid absorbs the heat and evaporates, resulting in all liquid turning to gas before it leaves the evaporator. The amount of heat absorbed during the process is accumulated as latent heat in the working fluid vapour and can be calculated as:

$$\dot{Q}_O = \dot{m}_R * (h_1 - h_4) \quad (7)$$

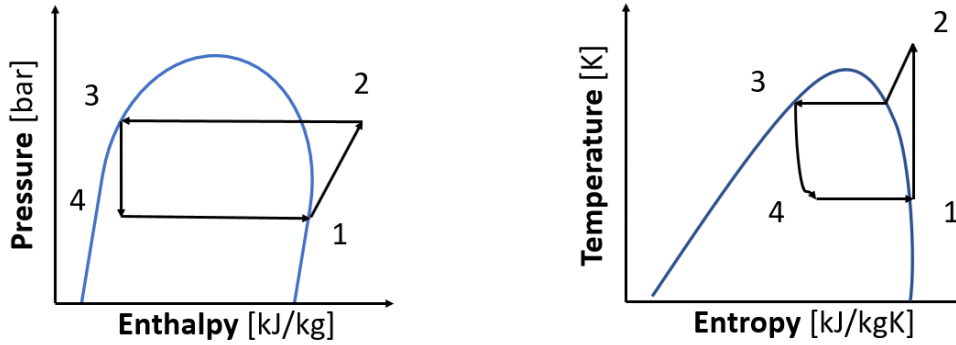


Figure 4: P-h diagram and T-s diagram for a single refrigeration cycle, referring to schematics in Figure 3

2.2 CO₂ refrigeration systems

CO₂ as a refrigerant was first introduced by Alexander Twining in 1850 (20). Refrigeration system using CO₂ was developed during the following years and peaked in the 1920s and 1930s. As a result of the introduction of synthetic refrigerants, like R-12 (CFC-12) in 1938, the CO₂ was gradually faded out and totally out of use in the 1960s (7). The low values of GWP (Global Warming Potential) and ODP (Ozone Depletion Potential) for the refrigerant were the main reasons for the renewed interests in the use of CO₂ in the 1990s. CO₂ is a natural refrigerant, alongside propane, butane, water, ammonia and water. Compared to these and other refrigerants, CO₂ is very different because of the low critical temperature (31,1 °C), the high triple point (5.18 bar) and the high pressure in general (e.g. 57 bar at ambient temperature, 20 °C). The comparison of various properties between CO₂, NH₃ and R134a are reviewed in the table below.

Refrigerant	R134a	NH ₃	CO ₂
Natural substance	NO	YES	YES
Ozone Depletion Potential (ODP)	0	0	0
Global warming potential (GWP)	1300	-	0
Critical Pressure [bar]	40,7	113	73,6
Critical Temperature [°C]	101,2	132,4	31,1
Triple point pressure [bar]	0,004	0,06	5,18
Triple point temperature [°C]	-103	-77,7	-56,6
Flammable or explosive	NO	YES	NO
Toxic	NO	YES	NO

The reviewed properties of CO₂ have made this refrigerant popular to achieve a low temperature in the food and refrigeration industry. The refrigerant requires higher design pressure but gives a high specific volumetric capacity, almost ten times higher than other refrigerants (16). This results in smaller compressor sizes and a reduction in diameter at the low side refrigerant line by 60-70 % when compared to HFC systems (11). The compactness of the system is also a significant benefit, especially on ships where space is limited. The CO₂ can be used as a refrigerant in several different system configurations, including subcritical and transcritical.

2.2.1 Subcritical

The conventional refrigeration system that we are familiar with is subcritical, meaning the entire range of pressures and temperature is below the critical point and above the triple point. Operating pressures are normally in the range of 5.7 to 35 bar (or -55 to 0 °C) As a result of the low critical

temperature, in theory, CO₂ suffers from great expansion losses compared to other refrigerants. In practice, CO₂ subcritical systems are still favourable than other refrigerants, achieving a higher COP due to: higher compressor efficiencies, more efficient evaporation, and condensation heat transfer and much less temperature loss at a given pressure loss in heat exchangers and pipe system (16). To achieve a low temperature in the industrial refrigeration system, the subcritical CO₂ system can be used as a bottoming cycle for cascade systems. These systems can be designed in various ways, e.g. pump circulating systems, CO₂ in volatile secondary "brine" systems, direct expansion systems, or combinations of those (7).

2.2.2 Transcritical

As a result of the low critical temperature of the refrigerant, operation at the transcritical area needs to be taken into consideration. A transcritical process is operating at a pressure higher than the critical one, which results in heat rejection at gliding temperature instead of heat absorption at a constant temperature in the subcritical region. The temperature glide can be utilized and can be advantageous as the heat rejection causes a significant temperature rise in the heat receiving fluid. In that case, the Carnot cycle suffers from a significant temperature loss, whilst a transcritical CO₂ enables a good temperature match. CO₂ heat pumps for tap water heating is utilizing this principle and achieves good results.

In many cases, the temperature glide of the transcritical system is a disadvantage, and the CO₂ should be operated in the subcritical region. However, this is not always an option. For example, the CO₂ system in boats cooled by seawater is operating subcritical during the winters and transcritical in the warmer seasons (in warmer climates). Although latest modifications of the CO₂ system with parallel compression and ejector technology have made it possible to achieve a high COP at even high ambient temperature (9). These solutions have been inspired by CO₂ application in the supermarket heating and cooling (8), and residential heat pumps (29). This is discussed extensively in Section 2.3.

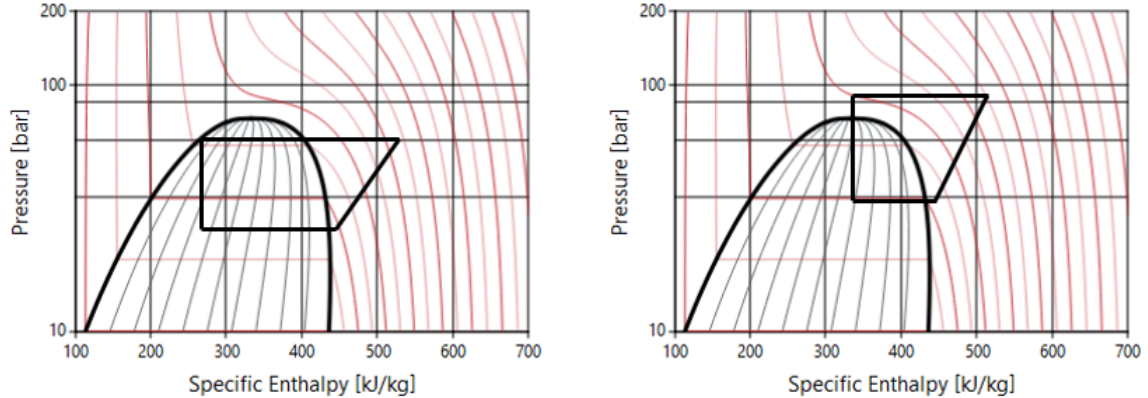


Figure 5: Comparing logP-h diagrams of a transcritical cycle vs a subcritical one

2.3 Industrial refrigeration with CO₂

Air conditioning, commercial refrigeration, and industrial refrigeration have one thing in common: the main objective is to cool some substance. A mechanical vapour compression cycle is present in all of these systems. Characteristics that separate industrial refrigeration from other systems is the evaporating temperatures extending down to -35 °C or -50 °C, and the refrigeration capacity is in the range between 300 kW and 1,5 MW (7). CO₂ as a refrigerant has a pressure of 6.8 bar(abs) at -50 °C and 5.2 bar(abs) at -56.6 °C as the lowest limit, much lower compared to R22 and R717 (7). This makes CO₂ an efficient refrigerant in industrial applications. However, the low critical pressure of CO₂ gives the refrigerant its limitations in industrial applications without special

considerations. The main consideration is that condensation using air or seawater is not possible within a subcritical refrigeration system. This has resulted in new pressure range components and special solutions concerning the level of design pressure. These solutions will be presented further in Chapter 2.

2.3.1 Transcritical Industrial Systems

The transcritical system operates in the range of 6 to 90 bar, where the transcritical fluid is cooled before it is flashed down to lower pressure. This is a good solution at comparatively small refrigeration capacities, such as air conditioning systems in a car or domestic heat pumps (21). In industrial applications, the transcritical refrigeration system may not be an ideal solution, for reasons of:

- The high pressure of the transcritical system demands special equipment and components in industrial sizes. The cost of these components and large refrigeration volumes under high system pressure, increases the investment price of the system, making it less economically feasible (21).
- The possible fluctuations in ambient temperature in the transcritical area will decrease the refrigeration capacity. Even a small temperature increase of 5 Kelvin in the transcritical area, will drastically decrease the cooling effect. An ambient temperature of 30 °C gives a 129 kJ/kg enthalpy difference. Increasing the ambient temperature to 35 °C, gives a new enthalpy difference of 84 kJ/kg, about a 35% reduction from the original one. This reduces the cooling effect of the system, as it is defined as an enthalpy difference multiplied with the mass flow. Figure 6 illustrates the reduction of the cooling effect, where ΔQ is the lost effect.

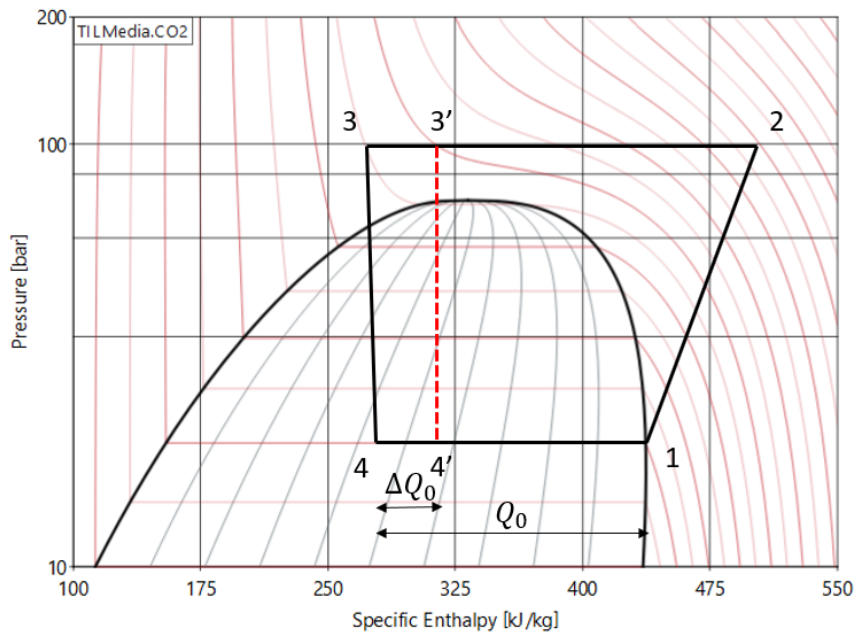


Figure 6: Transcritical cycles with different values of ambient temperature

In the subcritical cycle, the condensing pressure depends on the heat transfer characteristics of the condenser and refrigerant used. In a transcritical cycle, the condensing pressure depends primarily on the compressor capacities and the resistance of flow in a throttling valve. Allowing head pressure to float and match the condensation temperature, will improve the COP of the system, and in some cases outperform conventional systems (32). Methods on improving the COP of the transcritical

CO₂ system will be discussed extensively in section 2.4. Other advantages of a stand-alone CO₂ systems are mentioned below:

- The direct impact results from the release of CO₂ due to leakage from the refrigeration system, is negligible, as it is non-toxic, and has no Global Warming Potential (GWP) and Ozone Depletion Potential (ODP).
- CO₂ has good safety characteristics, making it an ideal fluid to be used with large quantities.
- CO₂ has in general low-pressure drop and corresponding temperature drop, which results in smaller refrigeration components that is advantageous considering the availability of space in ships.
- The refrigerant is inexpensive.

In combination with the advantages mentioned in the list above, the stand-alone CO₂ refrigeration systems becomes more relevant in industrial refrigeration.

2.3.2 Cascade Systems

A cascade system is a system with more than one cooling cycle connected with a single heat exchanger. The heat exchanger works as a condenser for the low-temperature circuit (LTC) and an evaporator for the high-temperature circuit (HTC). Thus, the cascade system allows heat transfer with a significant temperature difference whilst achieving a good COP (32). Furthermore, the CO₂ is condensed at a low temperature by another cooling cycle, achieving a CO₂ cycle in the subcritical region. Thus, cascade systems are an efficient way of maintaining low condensation temperature. Another advantage is the possibility of having two different temperature levels, low and medium, in one system. The cascade system is, however, more complex and requires more floor space than a stand-alone CO₂ system (21). Figure 8 and Figure 7 show a principle sketch and a T-s diagram of a cascade system of NH₃ and CO₂.

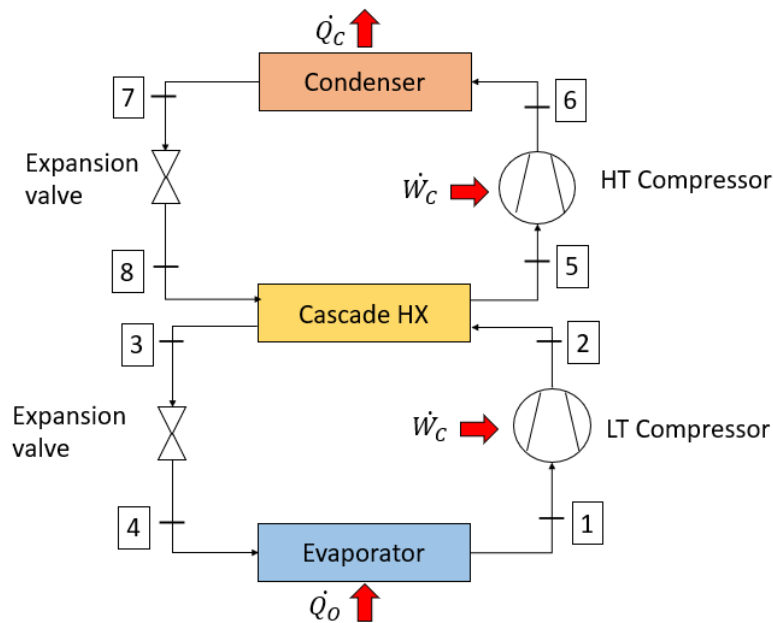


Figure 7: Cascade system of CO₂ and NH₃, principle sketch

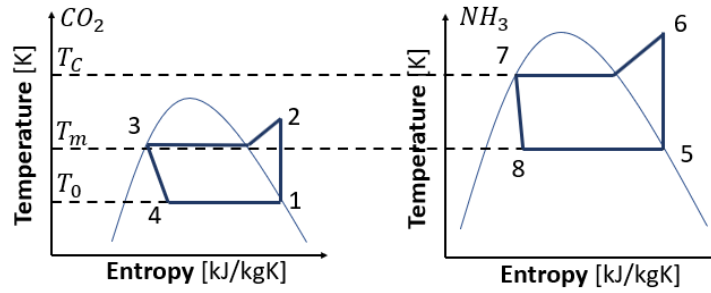


Figure 8: Cascade system of CO_2 and NH_3 , Ts diagram

2.3.3 Indirect system

Another way of avoiding the high condensation pressure of CO_2 is by using an indirect system. In this system, CO_2 is used as a volatile secondary fluid and is pumped to cold rooms where it evaporates. This allows evaporation and condensation to happen at the same pressure level, the possibility of using standard industrial components and condensing CO_2 in the subcritical region. Another advantage is reducing ammonia charges, making this system more compact than a stand-alone ammonia system (21).

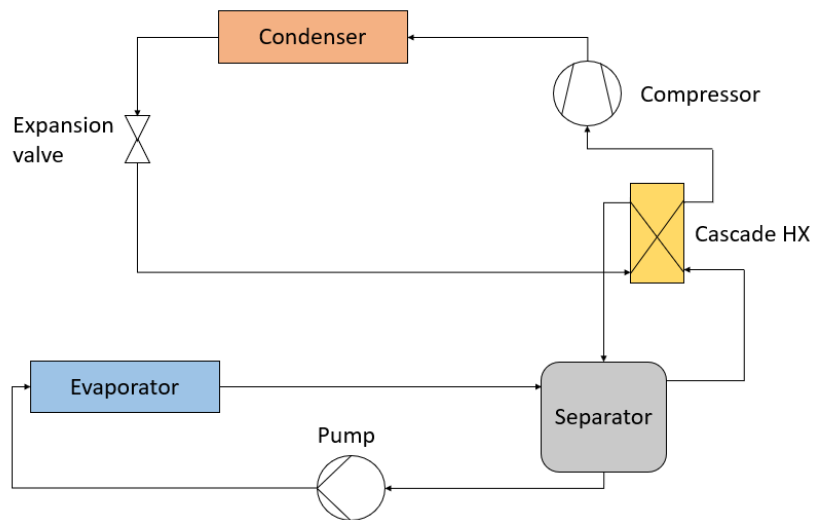


Figure 9: Indirect cascade system with pump circulation.

2.4 Methods on improving the energy efficiency of CO_2

Process losses, i. e. expansion losses and superheat losses, are responsible for the exergy losses of the idealized cycle in a traditional compression vapour refrigerant cycle. These losses result in extra energy consumption and can be easily visualized in a Ts diagram, as illustrated in Figure 10. Assuming the condensation temperature equal to the ambient one, the white rectangle, is the Carnot work necessary to obtain the refrigerant effect. In Figure 11, the same representation is made for the transcritical cycle. Comparing Figure 10 and 11, it is evident that the compression cycle is penalized when the condensation pressure exceeds the critical pressure of CO_2 .

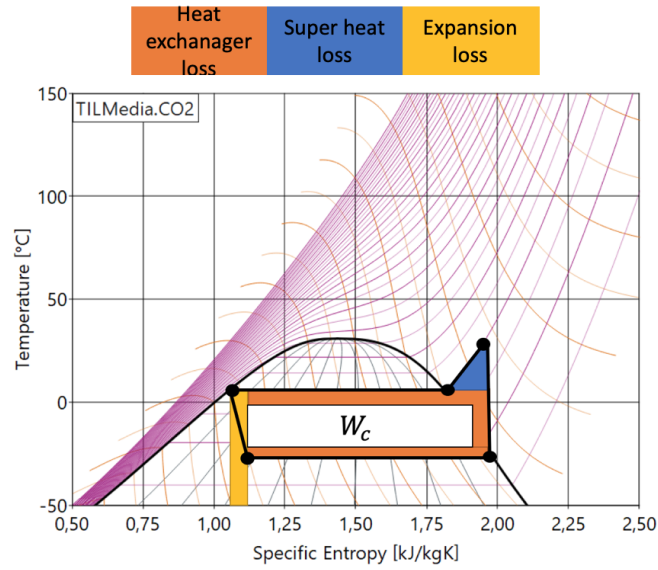


Figure 10: Losses of an idealised subcritical refrigeration cycle

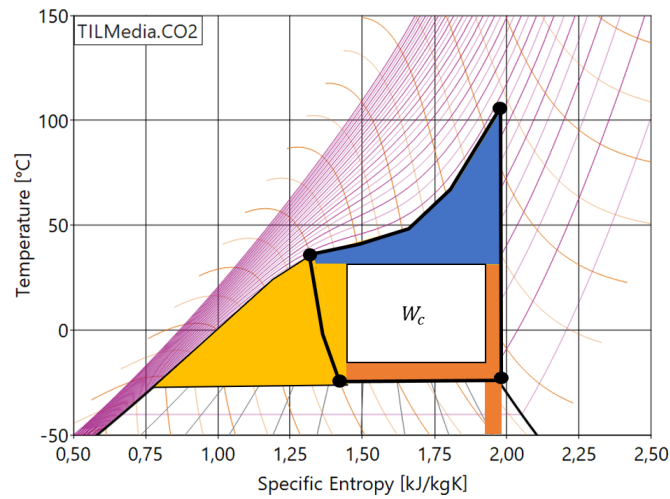


Figure 11: Losses of an idealised transcritical refrigeration cycle

As previously mentioned the condensing pressure of a transcritical cycle depends on the compressor capacities and the flow resistance of the throttling valve. The valve main task is therefore to keep the cycle upper pressure at the most optimal value to ensure a good system COP. The optimal pressure value is the one that finds the best trade of between the compressor work, W_{in} , and compressor refrigeration capacity, Q_O . Figure 12 illustrates the percentage increase of refrigeration capacity is larger than the increase in compressor work, meaning a better system COP: $\frac{\Delta Q_O}{Q_O} < \frac{\Delta W_C}{W_C}$. Consequently, the valve may not provide the right mass flow to the evaporator, and the feeding must be ensured in other ways. Methods on ensuring the right feeding of an evaporator, finding the optimal cycle upper pressure and improving the energy efficiency of CO₂ transcritical cycles are presented further.

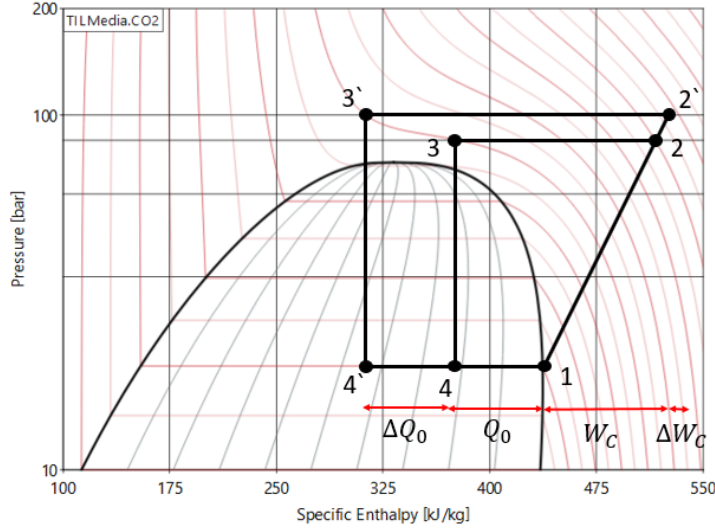


Figure 12: Transcritical cycles with different values of condensation pressure

2.4.1 Internal heat exchanger

The internal heat exchanger (IHX) has two main functions. First, the IHX superheats the gas leaving the evaporator, and second, the IHX subcools the liquid leaving the condenser simultaneously. This reduces the expansion losses and increases the refrigeration capacity of the system, but the increase in temperature at the compressor's inlet will increase the superheat loss and the compressor work. Consequentially, the IHX will be beneficial if the refrigeration capacity is increasing more the gas specific volume at the inlet of the compressor (16) or by this formula addressing Figure 13:

$$\frac{h_1 - h_6}{h_1 - h_4} * \frac{v_1}{v_2} > 1 \quad (8)$$

The value will be below 1 if pressure drop on the gas side in the IHX is taken into account. The pressure drop decreases the refrigeration capacity as it increases the specific volume of the gas (16).

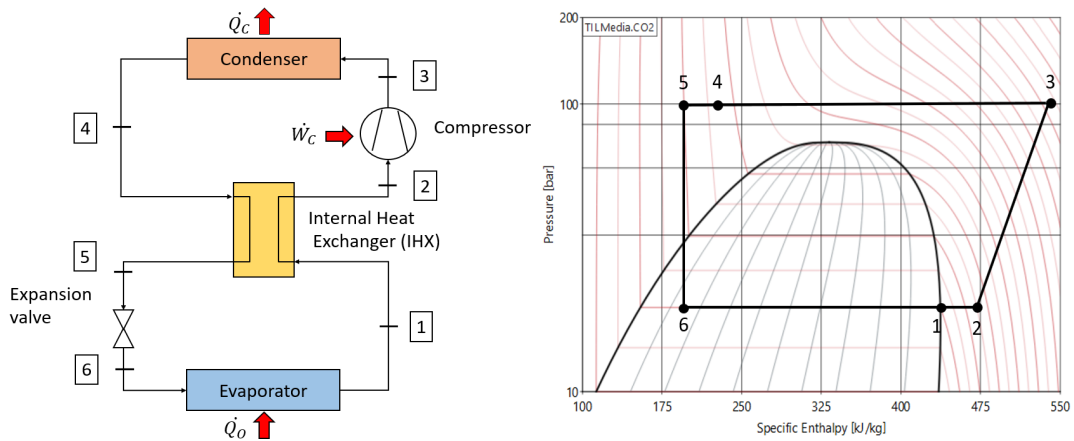


Figure 13: Transcritical cycles with an internal heat exchanger scheme and Ph diagram

The influence of IHX in a transcritical CO₂ system has been investigated in several relevant studies. Rigola et al. did a numerical and experimental study showing the possibilities using transcritical

CO₂ system and stated that “The inclusion of an internal heat exchanger (IHX) in the refrigeration cycle significantly increases the COP with a reasonable IHX size. COP increases more when ambient temperature increases” (28). In another study, Torrella et al. analysed the performance of IHX in a transcritical CO₂ system and showed an increase of efficiency of the system by 12% (13).

2.4.2 Two stage expansion with auxiliary compression

In larger industrial systems, it can be beneficial to use two-stage expansion with auxiliary compression. This system uses the auxiliary compressor to remove vapour at intermediate pressure from the first expansion, as illustrated in Fig 14 and its log p-h diagram in Fig 15. The expansion loss will reduce as the vapour fraction at point 31 can be separated and compressed separately back to the upper pressure, point 32 to point 22, by an auxiliary compressor. Consequently, the mass flow to the evaporator and the main compressor work reduces, and at the same time, the refrigeration capacity ΔQ is increased (because of the increase of the enthalpy difference over the evaporator, point 4 to point 1).

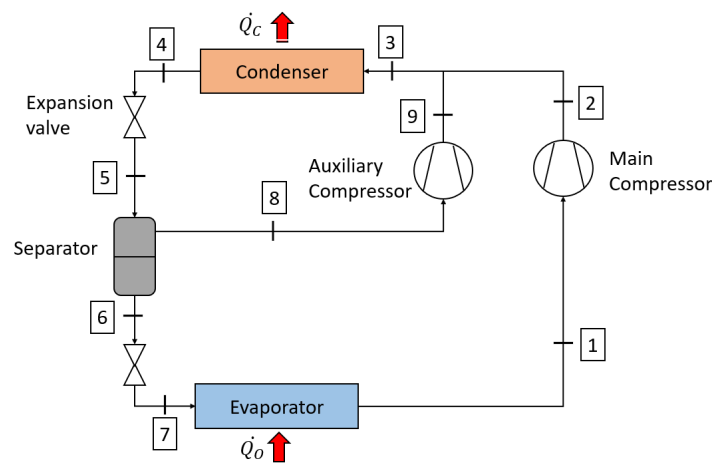


Figure 14: Auxiliary compression system configuration

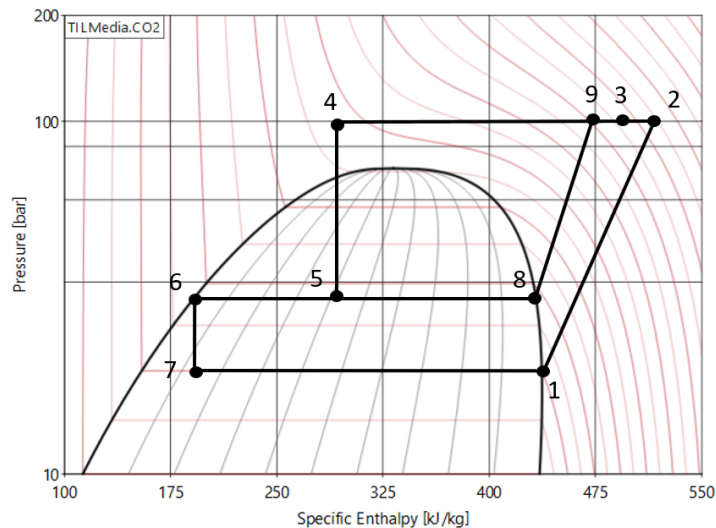


Figure 15: Auxiliary compression system p-h diagram

This is especially useful for working fluids where the high-pressure side is close to its critical pressure, as in our case with CO₂. The expansion losses are larger, and the vapour fraction at point 5 is much larger than other refrigerants. CO₂ system is also operating with high-pressure ratios, giving a better isentropic compression efficiency. Evangelos Bellos et. al. investigated CO₂ system using auxiliary compression, concluding that the maximum possible enhancement of the efficiency is 75% where there is a big temperature difference between the high-pressure side and low-pressure side, more precisely 85 Kelvin (36).

2.4.3 Expanders in transcritical CO₂ systems

Significant exergy throttling losses in a transcritical CO₂ system points to the benefits of expander usage in the system, as it increases the refrigeration effect and decreases the compressor work. Although, the energy efficiency is very dependent on the isentropic efficiency of the expansion. In a subcritical refrigeration system, the refrigerant is in two phases as it expands and is more subjected to friction loss, meaning a lower isentropic efficiency of the expansion. The transcritical CO₂ process behaves differently by the expansion process concerns single-phase refrigerant in the transcritical area. During the two-phase area, liquid and vapour densities are not much different, resulting in a higher total isentropic efficiency. The gain concerning the expansion work or cooling effect in a transcritical CO₂ system can reach 25-30% of the compressor power input (39). Much of the expander technology is still in the development face and will be not discussed further in this thesis, as they are not available on the market. This project theses will focus on applying a two-phase ejector for recovering a part of the expansion work.

2.4.4 Ejectors

The application of a two-phase ejector for recovering part of the expansion loss is well-recognized as a promising solution for highly efficient vapour-compression refrigeration systems. A conventional vapour compression system with a two-phase ejector is presented in Figure 16 and its corresponding ph diagram in Fig 17. To get a better understanding of ejectors operation, stages of the closed vapour-compression refrigeration cycle is described below, based on Fig 16 and Fig 17:

- The refrigerant leaves the gas cooler and is accelerated and expanded through the motive nozzle in point 4.
- The pressure difference between the expanded refrigerant and the refrigerant leaving the evaporator leads the low-pressure fluid (point 8) to be entrained into the suction nozzle (point 9).
- Both streams are mixed in the mixing chamber (point 5), the kinetic energy of the working fluid is transformed to a pressure increase through the diffusion nozzle (point 5 to 6).
- The working fluid enters the separator, after which vapour is compressed (point 6G to point 2) and the liquid is expanded (point 6L to 7).

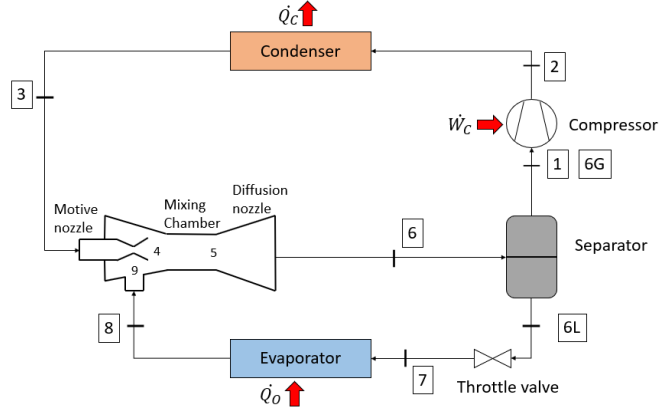


Figure 16: Schematic of refrigeration system equipped with a two-phase ejector

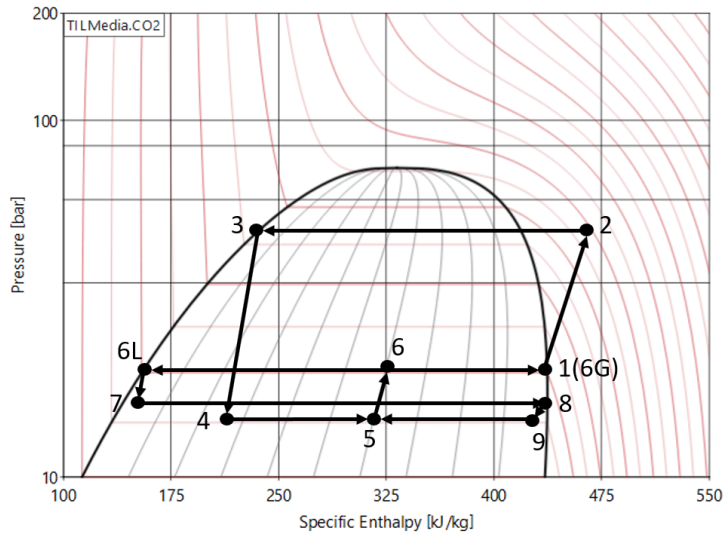


Figure 17: Ph diagram of refrigeration system equipped with a two-phase ejector

Correspondingly, when applying an ejector, the suction pressure of the compressor is increased, reducing its power input compared to a standard system. The ejector is essentially operating as a booster compressor and expander, while a throttling valve does the low-temperature expansion. The performance of an ejector is determined by four factors: mass entertainment ratio (Φ_m), pressure lift (P_{lift}), suction pressure ratio (Π) and expansion work recovery (η). They are defined as follows:

$$\Phi_m = \frac{\dot{m}_{sn}}{\dot{m}_{mn}} = \frac{\text{Suction mass flow rate}}{\text{Motive mass flow rate}} \quad (9)$$

$$\Pi = \frac{P_{diff\ out}}{P_{sn\ in}} = \frac{\text{Ejector pressure downstream of the diffuser}}{\text{Ejector suction pressure}} \quad (10)$$

$$P_{lift} = P_{diff\ out} - P_{sn\ in} \quad (11)$$

The highest possible values for mass entertainment ratio and pressure lift are desired for achieving a good COP (17) and increasing the cooling and heating capacity. Meaning a large part of the refrigerant could be pre-compressed to a higher suction pressure of the compressor. However, Paride

Gulla et al. stated that “in real applications this device is able to pre-compressed either a large amount of refrigerant with a low-pressure lift or a small amount of refrigerant with a high-pressure lift“ (17). Another essential factor to consider is the ejector efficiency ($\eta_{ejector}$) that represents the ratio between the work of isentropically compressing the refrigerant at suction nozzle pressure to the pressure in the separator, to the theoretical maximum power that could be recovered by isentropic expansion from the condensing pressure to the pressure in the separator. The following equation 12 and Figure 18, visualises the equation and makes it easier to interpret it.

$$\frac{\dot{W}_{recovered}}{\dot{W}_{recoverable\ max}} = \Phi_m * \frac{h_C - h_D}{h_A - h_B} \quad (12)$$

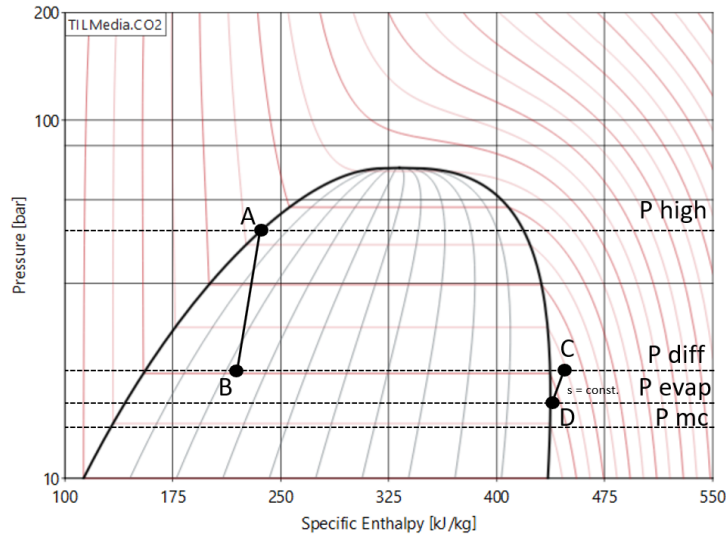


Figure 18: Ph diagram, processes of expansion and compression in the ejector

2.5 Refrigeration at fishing vessels

As a result of an increase in the development within the marine fish industry in the 1960s, the fishing vessels became more extensive, the fishing grounds were further away from shore, and the amount of catch enlarged (15). Therefore, the traditional way of preserving the fish on-board, in boxes with ice, not an efficient way of preserving the fish. Therefore, fish tanks with refrigerated seawater (RSW) were selected as the best and most efficient method in preserving the products. The RSW systems made it possible for almost all pelagic fish, frozen onshore as a whole fish and later distributed and not being processes to fish meal or oil. This industry stands for about 25% of Norway’s fish export (3). This section describes the possibilities of using CO₂ in RSW systems on fishing vessels.

2.5.1 RSW systems

Figure 19 illustrates a simplified RSW system with its main components. The refrigeration system pre-cools the seawater before the fish is loaded into the RSW tanks. The evaporating temperature usually is -5 °C, and the seawater is cooled down to about -1.5 °C before the fish is loaded (15). As the shelf life of food is strongly dependent on the temperature, further cooling of water and good circulation ensures sustainable storage of the fish before the vessel reaches shore. Big fishing vessels have several RSW tanks in different sizes to ensure the cooling of a large quantity of fish and having a flexible system.

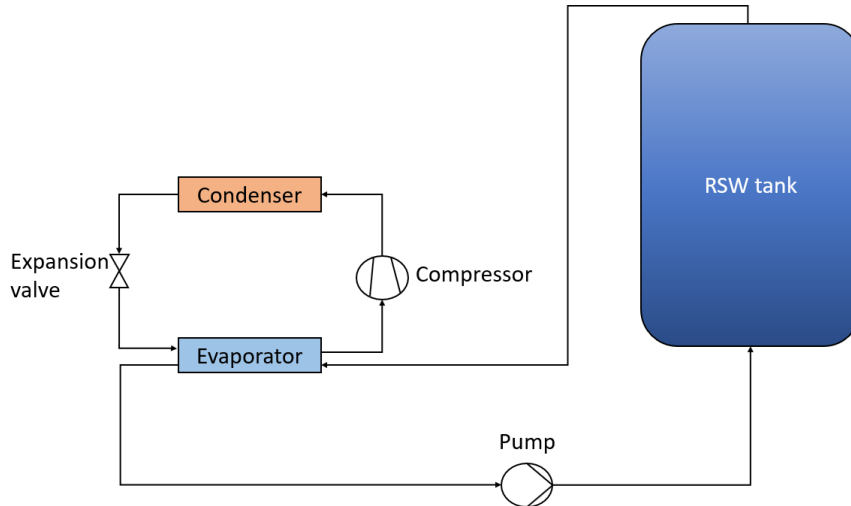


Figure 19: A simplified schematic of the RSW system

2.5.2 Heat loads in RSW systems

Figure 20 represents the characteristic chilling curve for an RSW system onboard a fishing vessel. The heat loads can be divided primarily into two parts; prechilling from original temperature (T_1) to target temperature (T_3), and chilling a mixture of seawater and fish from average temperature (T_2) to target temperature (T_3). Factors that influence the length of different periods ($\tau_{1,2,3}$) are mainly; the quantity of fish, amount of seawater and capacity of the used refrigeration system. Other heat loads in the chilling system are added due to heat transmission through the RSW tank walls and heat added by the seawater pumps (37).

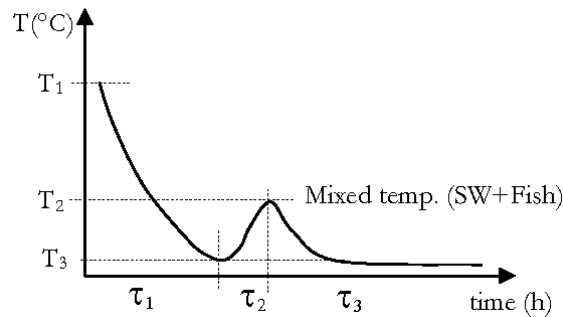


Figure 20: Characteristics chilling curves for an arbitrary RSW chilling system (37)

2.5.3 CO₂ RSW systems on board

The first CO₂ RSW-system in Norway onboard was built on MS Viking Midøy and was launched in 2012. The ship is equipped with 6 RSW tanks, where the CO₂ refrigeration system was supposed to cool only 3 of them. The capacity is 250 kW for cooling seawater to a temperature between 0 °C and -1 °, with an evaporation temperature of -5 °C. The results show that the system worked well with varying seawater temperatures, and the CO₂ system had enough capacity to cool down all 6 available tanks. Although, the second system onboard with R22 was used for increasing the capacity during cooling down of the catch (15).

The second CO₂ RSW-system in Norway was built on Trønderhav and was launched in 2014. This project was led by CADIO AS, in cooperation with NTNU and SINTEF. The refrigeration system

consists of two units with a cooling capacity of 150 kW for cooling seawater to $-1.3\text{ }^{\circ}\text{C}$. As the space in fishing vessels are limited, the evaporator and condenser heat exchangers are specially designed for these units, of a so-called "dimple type design". The system has been reported to have better efficiency and less noisy when compared to the previous R22 system. The system has worked without any problems yet (15) (38).

2.5.4 Combined RSW and freezing systems with CO₂

A combined RSW and freezing system onboard is a good way of chilling fish before freezing due to the utilization of two possible temperature levels in one system. Possible disadvantages of this kind of system are a low COP and challenges with the distribution of refrigerant. NH₃, CO₂/NH₃ and all CO₂ systems are common for newly built refrigeration systems in the Nordic region. A cascade system utilizing the different evaporation temperature of NH₃ and CO₂ is often used for both cooling and freezing at the same time.

The first cascade system, using CO₂ and NH₃ was installed at MS Kvannøy in 2002, developed by York Refrigeration in Aarhus, Denmark. Figure 21 shows the simplified system circuit of the cascade unit at the vessel. This system consists of 11 plate freezers and has a refrigeration capacity of 1350 kW at $-48\text{ }^{\circ}\text{C}$. Further, the unit consists of 9 refrigerated seawater tanks. Results from this system in operation shows a 40% reduction in product freezing time compared to R22 systems, as a consequence of utilizing the low evaporating temperature of CO₂ ($-40\text{ }^{\circ}\text{C}$ for R22 and $-48\text{ }^{\circ}\text{C}$ for CO₂) (38).

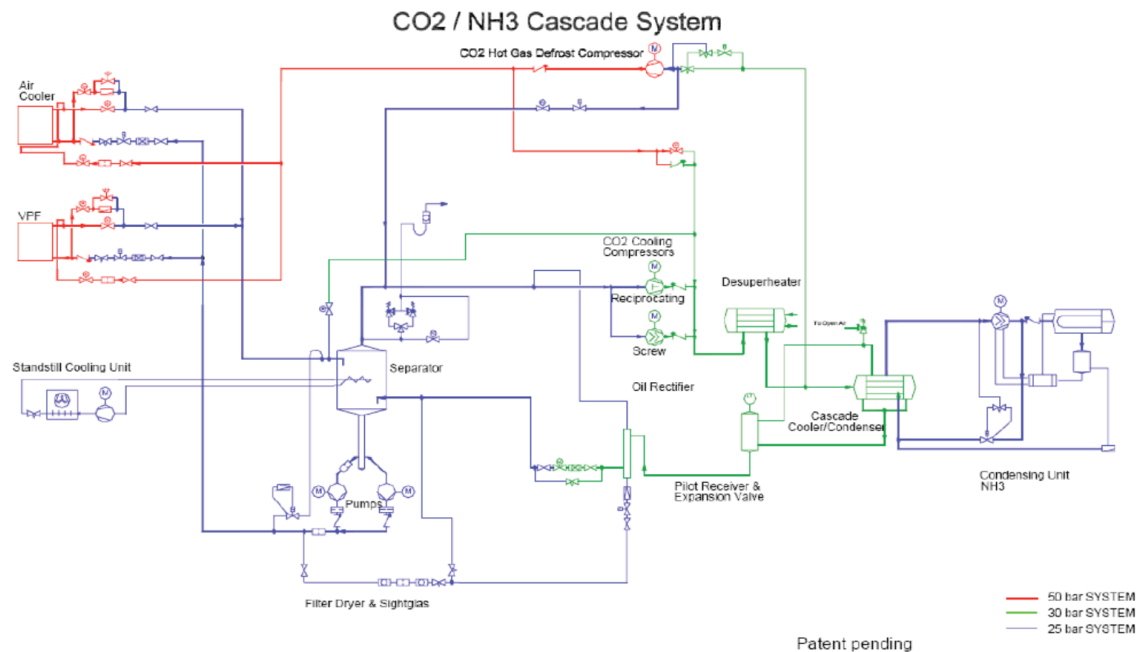


Figure 21: A simplified schematic of the CO₂ and NH₃ system circuit installed at MS Kvannøy (38)

A cascade solution was also implemented at Polar Princess in 2015. The R22 freezing system was replaced by CO₂ / NH₃ cascade freezer system with 12 plate freezers and RSW tanks. The unit consists of 3 screw compressors and 5 reciprocating piston compressors. Results for this unit are not available (38).

The previous R22 systems at MS Roaldnes has been replaced by a CO₂ only refrigeration system by Kuldeteknikk AS. The new CO₂ system increased the capacity of the fish freezing from 30 metric

ton/day to 40 metric ton/day and reduced the freezing time by 26% compared to the previous R22 system due to the lower achievable evaporating temperature. The defrost time of the CO₂ unit was also lower. The new system demanded 20% less space compared to the previous R22 system, and at the same time, easier to clean (38).

3 System Design

This chapter contains a detailed description of the CO₂ refrigeration system, that will be implemented at the MCC First Process. Including but not limiting to: general overview of system designs and description of central components.

3.1 Principle Design 1 (CASE 1, CASE 2 and CASE 3)

The company has chosen a transcritical CO₂ system for testing onshore, before implementing it on fishing vessels. The system is schematically shown in Figure 22 and contains three parallel CO₂ compressors Bock (HGX46/ 400-4 ML CO₂T). One compressor is equipped with a frequency converter, while the other two are controlled by ON/OFF. This increases flexibility regarding power consumption and operational conditions, as the compressors are activated based on the requested capacity.

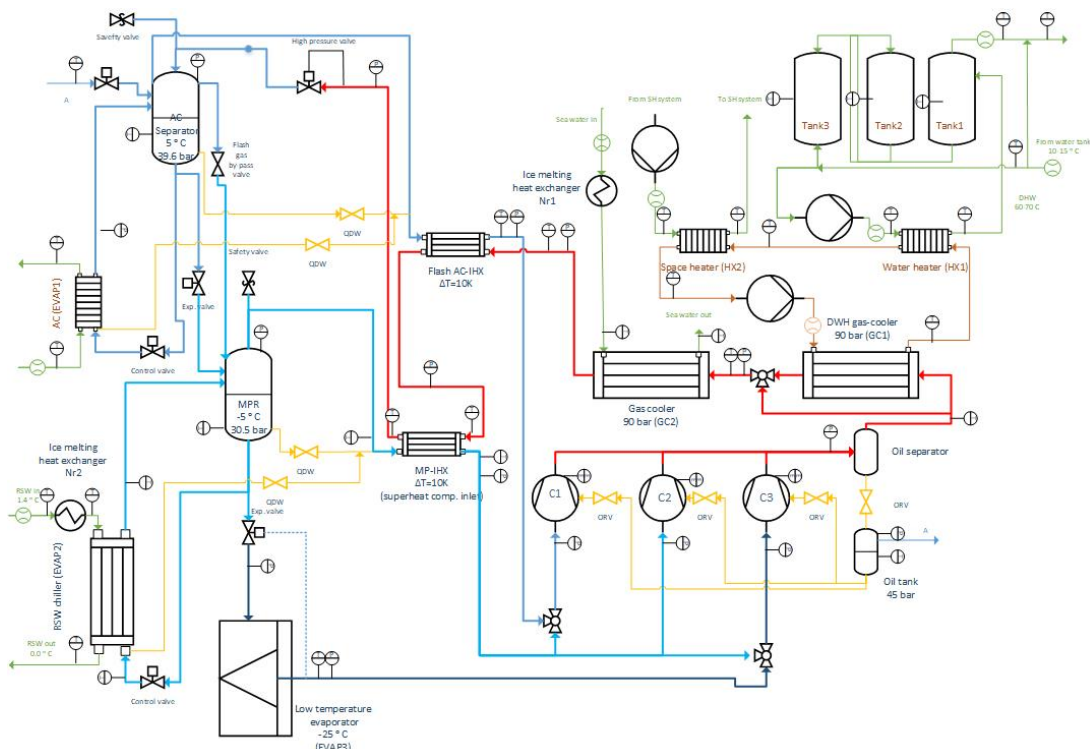


Figure 22: Principle sketch of the CO₂ unit

The system utilizes the benefits of transcritical CO₂ -loop by energy recovery from gas coolers and is designed to supply heat for Domestic Hot Water (DHW) production and Space Heating (SH). Heat is supplied to the secondary loop through the gas cooler, GC1, as shown in Figure 23. The hydronic subsystem provides heat through two heat exchangers in series, HX1 and HX2, at high and medium temperatures. The HT circuit provides DHW in a temperature range between 60-70 °C through HX1, while the remaining of the heat is utilized to SP through HX2. During operation conditions with negligible DHW and SH demands, the heat is rejected to seawater through GC2, while avoiding GC1 by a three-way bypass valve (TBV 1). The CO₂ enters the gas coolers as vapor at a set pressure of 90 bar and is cooled down by the seawater.

The main function of the CO₂ system is to provide RSW, where the cooling load is the controlling parameter. The operation of the system is focused on cooling seawater, where the setpoint temperature in the RSW tanks is approximately 0 °C. To ensure efficient cooling, CO₂ is set to enter the RSW evaporator (EVAP1) at approximately 30.5 bar and - 5 °C. EVAP1 functions as

a flooded evaporator and operates thereby in conjunction with a medium-pressure receiver, MPR, as shown in Figure 24. The receiver functions as a separator of gaseous and liquid refrigerant and ensures a feed of liquid refrigerant to the evaporator, and has a volume of 300 L. The RSW side of the system is designed to provide 450 kW cooling capacity at a seawater temperature of 15 °C and utilizing all three compressors.

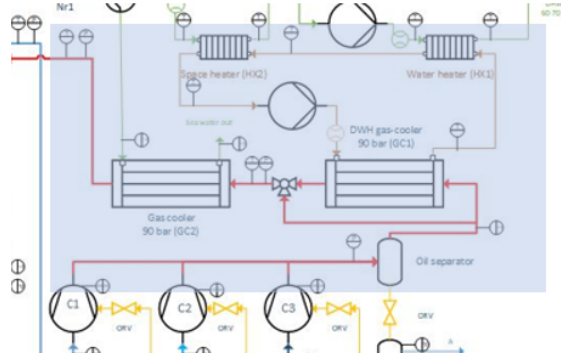


Figure 23: Gas coolers configuration (Part of Figure 22)

Integration of air conditioning (AC) into the CO₂ system is a compact and energy efficient solution. This can be done by including a flooded evaporator (EVAP2) and a separator (Ac-R) between the high-pressure regulating valve and the medium pressure receiver (MPR). AC delivery is accomplished by running parallel compressors, and in this case AC/MP compressor (C1) is responsible for delivering the cooling capacity. The AC evaporating temperature is set to be at 5 °C.

RSW system has also possibility to provide cooling load to the low temperature (LT) storage at – 25 °C. LT storage main function is storing fish that are frozen by other methods, and thus not requiring much of refrigeration capacity. The LT evaporator runs on direct expansion (DX) conditions, meaning a section of the evaporator is used for super-heating the refrigerant before entering compressor (C3).

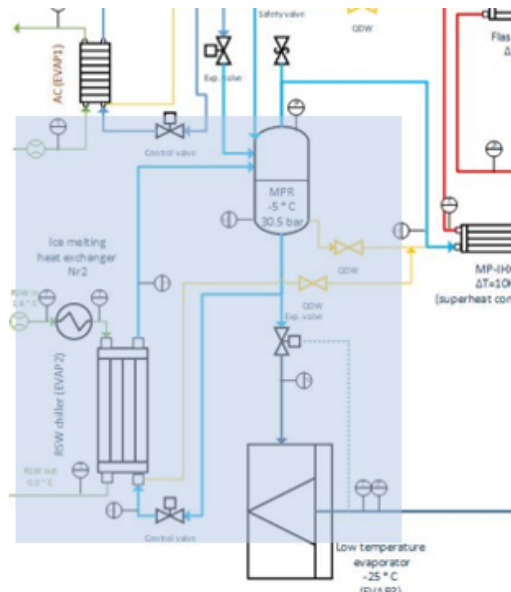


Figure 24: RSW flooded evaporator (EVAP1) with a medium pressure receiver (MPR) (Part of Figure 22)

The parallel compressors refrigeration system can operate in both the subcritical and transcritical modes depending on the seawater temperature. As the cooling load is the controlling parameter,

the vessel supplies the cooling demand, which adjusts the setpoint of the compressors' capacities. Meaning if an increase in the RSW chilling is requested, all three compressors (C1, C2, C3) are available to provide the requested capacity (CASE 1). The second mode of operation occurs during the demand of AC and RSW chilling, where (C1) is responsible for AC, while compressors, C2 and C3, for RSW chilling (CASE2). The third mode of operation occurs when the system provides AC, RSW, and LT storage, where C1 is responsible for AC, C2 is responsible for RSW and C3 is responsible for LT storage (CASE 3). Accordingly, proper capacity control is necessary to minimize energy consumption and utilizing the flexibility of this system.

3.2 Principle design 2 (CASE 4)

The transcritical CO₂ system configurations described in Section 3.1 is further modified, by installing a multi-ejector rack parallel to the high-pressure valve. The system is schematically shown in Figure 25 and contains all previously mentioned components in Section 3.1.

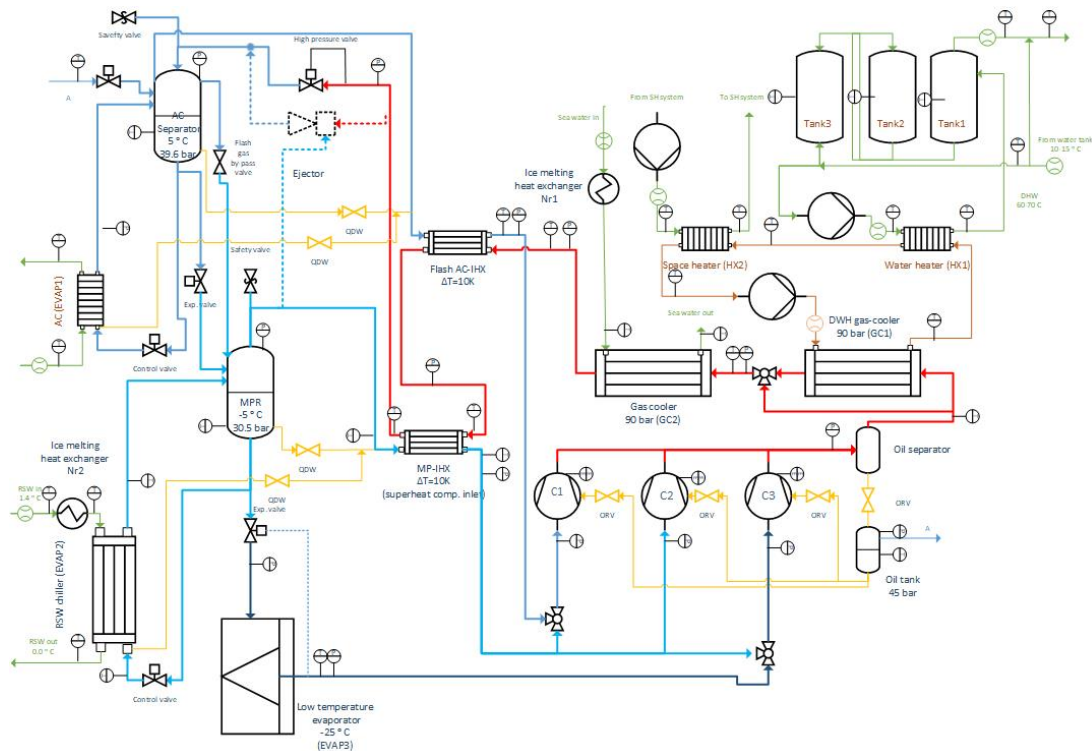


Figure 25: Principle sketch of the CO₂ unit equipped with a multi ejector rack

In this ejector-supported parallel solution, the parallel compression runs in conjunction with multi ejector rack. The basis of this modification is linked to system improvements, as the ejector provides recovery for some exergy losses during the high pressure expansion. Each ejector is regulated by the respective valves, shown in Figure 26. Therefore, the overall control is based on the idea of opened and closed fixed geometry ejectors working in parallel mode. The transcritical ejector configuration is afterward described as the fourth mode of operation (CASE 4).

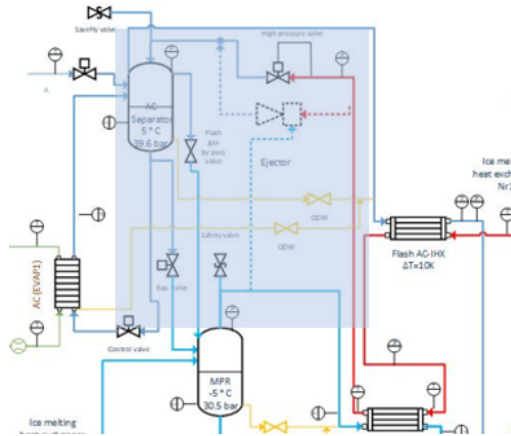


Figure 26: The ejector configuration close up (Part of Figure 25)

Based on theory from Section 2.4.4, the ejectors will maintain the optimal high pressure in any running mode, and at the same time, recover some of the work which is usually dissipated due to the throttling valve. Further, part of the refrigerant from the RSW separator, shown in Figure 26, is pre-compressed to the AC pressure, which in turn causes significant unloading of the main compressor (C2 and C3) to the detriment of the auxiliary compressor (C1). As the AC pressure is about 9 bar higher than RSW pressure, a notable energy-saving is attained, increasing systems overall COP.

3.3 Principle design 3 (CASE 5)

The CO₂ system described in in Section 3.1 is also possible to modify by installing multi ejector rack at a lower pressure, marked with dotted lines in Figure 27.

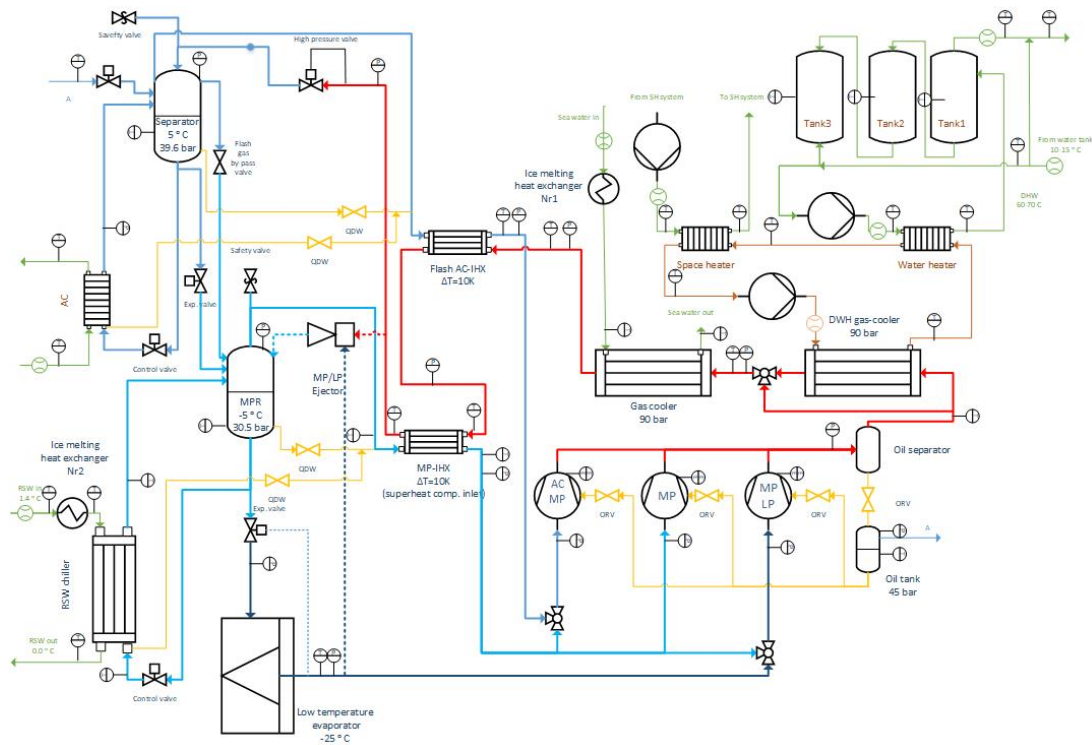


Figure 27: Principle sketch of the CO₂ unit with ejectors

The ejector lifts some of the gas from the LT evaporator (EVAP 3) to the MPR receiver. From the receiver, the gas is compressed directly by the RSW compressors (C1, C2). The ejector is therefore moving part of the LT load to the RSW compressors. Hence, reducing the load on the LT compressor. As a result, the RSW compressors operate at a higher suction pressure (30,5 bar), resulting in lower energy consumption and higher system COP. A closer look at the ejector configuration is shown schematically in Figure 28. When comparing to design solutions described earlier, Principle design 3 will not benefit from integrating air conditioning, as all refrigerant out of the gas cooler is going through the ejector motive nozzle. The described ejector configuration is afterwards described as the fifth mode of operation (CASE 5).

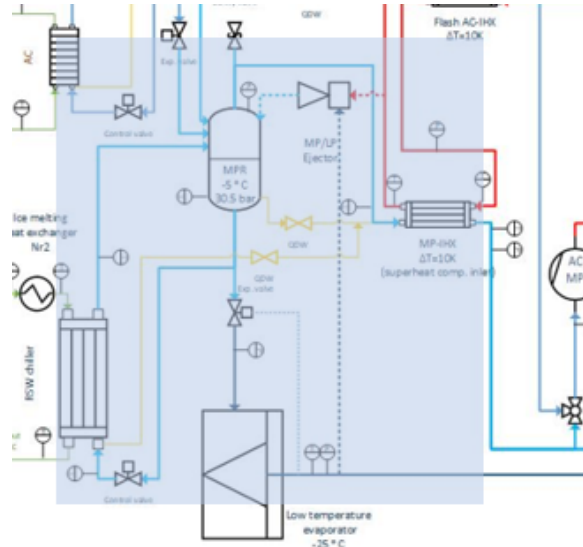


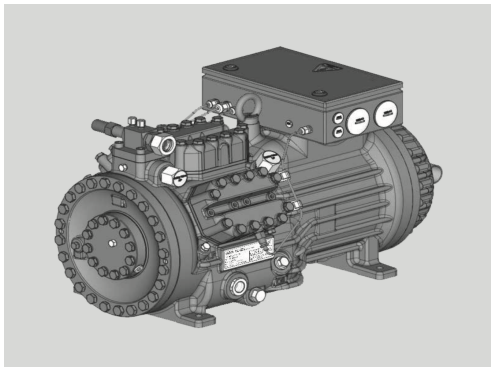
Figure 28: The ejector configuration close up (Part of Figure 27)

3.4 Description of components

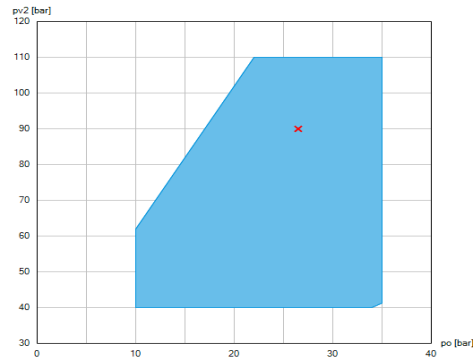
This section will present an overview of relevant components in the refrigeration system described above.

3.4.1 Compressors (C1, C2 and C3)

The CO₂ system has three semi-hermetic compressors, type: HGX46/ 400-4 ML CO₂T. These compressors are for use with CO₂ in the transcritical and/or subcritical systems, and cannot be used with other refrigerants. Each compressor has six reciprocating cylinders with suction gas cooled motor, and a swept volume of 400 m³ each. C1 is equipped with a frequency converter, with a frequency range of 20-70 Hz, enabling better system control. To ensure reliable and safe oil supply, the manufacturer has installed an oil pump independent of direction of rotation. The maximum permissible operating pressure is 100 bar for LP and 150 bar for HP(6).



(a) Figure of the compressor



(b) Areas of application

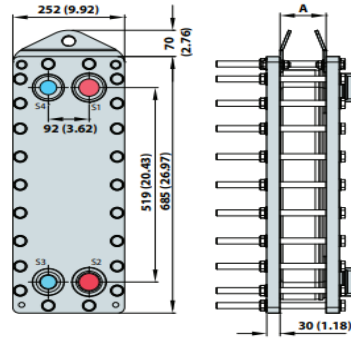
Figure 29: Compressor type: HGX46/ 400-4 ML CO₂T (10)

3.4.2 Sea water Gas Cooler (GC2)

The CO₂ system is equipped with two gas coolers in series, GC1, and GC2. The proposed heat exchanger for GC2 is Alfa Laval AXP112, manufactured by Lenntech. Alfa Laval XP is designed for applications in air conditioning and other refrigeration applications and is well suited for CO₂ applications in the transcritical area. The heat exchanger is a brazed plate heat exchanger with external frames made of carbon steel. The capacity of the heat exchanger is determined by the number of plates and can hold up to 300 plates. The heating surface consists of metal plates stacked on top of each other. Channels are formed so that the hot and cold fluid circulates in every other canal between the plates, usually in counterflow to increase the efficiency of the heat transfer (1).



(a) Figure of the plate heat exchanger



(b) Dimensional Drawing

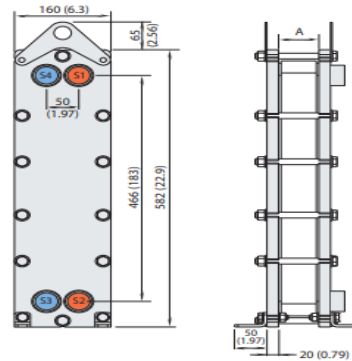
Figure 30: Alfa Laval AXP112 Brazed plate heat exchanger

3.4.3 Internal Heat Exchangers (IHX1 and IHX2)

The CO₂ unit is equipped with two internal heat exchangers, at two different pressure levels. IHX1 is at 40 bar and IHX is at 31 bar, with the main function of superheating the flash gas leaving ACR and MPR, before entering the compressors. The proposed heat exchangers are Alfa Laval AXP52. Both heat exchangers are brazed plate heat exchangers for extreme high-pressure operations and are specifically designed for applications in air conditioning and other refrigeration use. AXP is designed with external frames in carbon steel to withstand the high-pressure operations CO₂ require. According to the manufacturer the benefits of these heat exchangers are compactness, easy to install, self-cleaning, low level of service, and maintains and are gasket-free(2).



(a) Figure of the plate heat exchanger



(b) Dimensional Drawing

Figure 31: Alfa Laval AXP52 Brazed plate heat exchanger

3.4.4 RSW (EVAP1)

System RSW cooler is manufactured by Isotherm, INC in Arlington, Texas. Configuration of this heat exchanger is shell-and-tube heat exchanger, designed for usage with CO₂ and sea water. The RSW cooler has single tube and double shell passes, and is shown in Figure 32. The seawater enters the gas cooler in tube side inlet marked A, and exist in tube side outlet marked B, with a diameter of 2032 mm. The refrigerant enters the gas cooler in C1 and C2, and exist at D1 and D2. The RSW cooler is equipped with an oil drain (G1 and G2) and has an empty weight of 1361 kg. The designed cooling capacity of the RSW Cooler is 450 kW, with a CO₂ temperature -5 °C, and seawater inlet temperature 1.4 °C and outlet temperature 0 °C (10) .

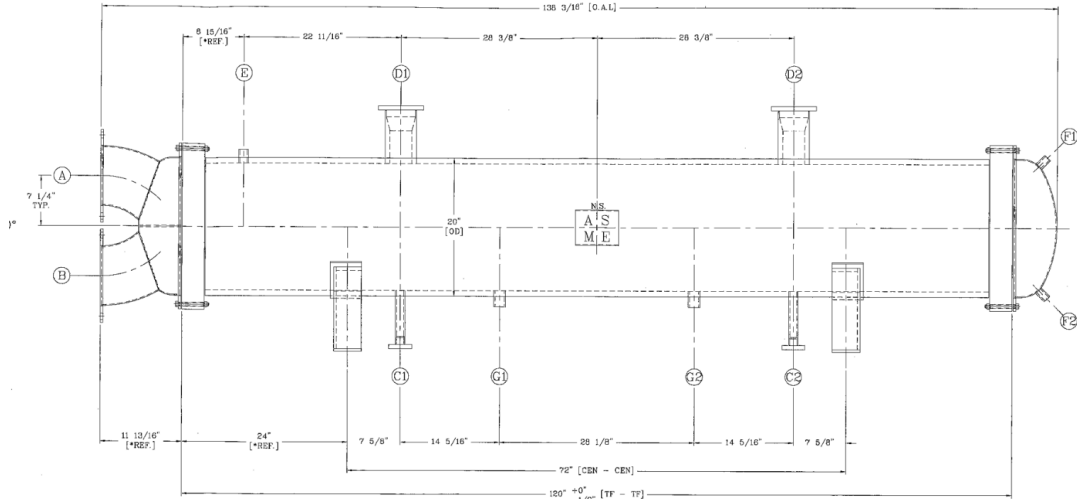


Figure 32: RSW cooler

3.4.5 AC evaporator (EVAP2)

The CO₂ system uses a shell and tube heat exchanger, as a filled evaporator for the AC configuration, as shown in Figure 33. The evaporator is manufactured by Isotherm, INC located in Arlington, Texas. The refrigerant enters the gas cooler at point C, and exists in D1 and D2. The water enters at tube side inlet. The seawater enters at tube side inlet, A, and exists at tube side outlet, B. GC2 is equipped with an oil drain located at the bottom (E3) and has a total empty weight of 680 kg.

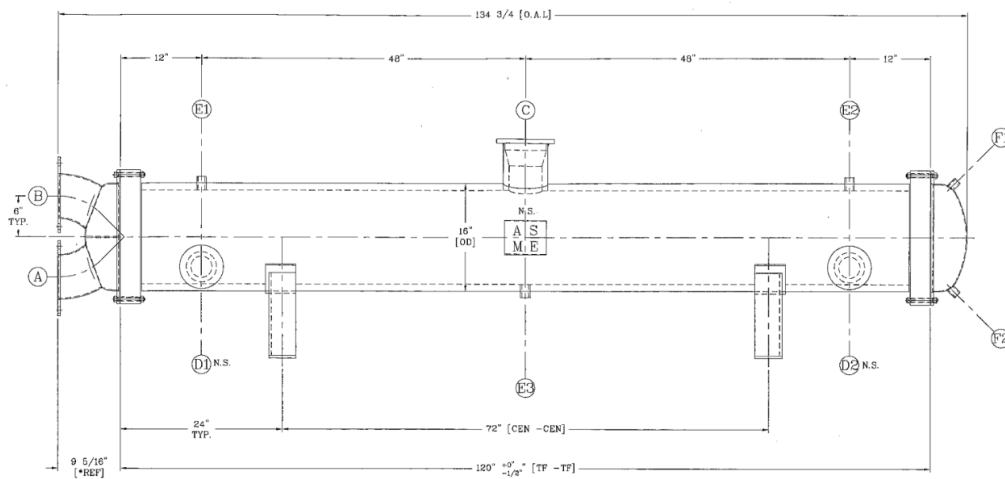


Figure 33: AC evaporator (EVAP2)

3.4.6 Danfoss Multi Ejector (HP and LP Ejector)

Danfoss provides the ejector in the CO₂ system. Danfoss Multi Ejector utilizes the high-pressure refrigerant's energy, lifting the gas from MT to the parallel compressor. As mentioned in Section

2.4.4, this will provide a reduction in needed compressor capacity, thus energy consumption. Danfoss advertises substantial energy savings by implementing the Multi ejector, especially in warmer climates (14). A typical design of the ejector used in the CO₂ refrigeration system described in Section 3.2, is presented in Figure 34. Each block has a range of ejectors mounted vertically and in different sizes. Multi Ejector are available with 4 to 6 ejectors and will match the capacity demand using different numbers and combinations of these. A built-in valve prevents backflow, hence removing the need for check valves in the suction line.

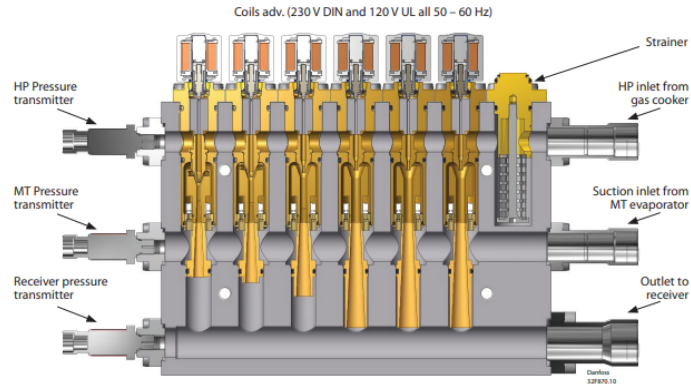


Figure 34: Danfoss Multi Ejector Design (14)

4 Methodology

This section describes the methodology and procedure that was used in developing the simulation models for the refrigeration unit. The first part presents the simulation tools that will be applied to evaluate the refrigeration system. This thesis will be based on calculations performed by EES and Dymola.

4.1 Simulation Tools

Two simulation tools can be applied to develop simulation models for the refrigeration system described in Chapter 3. The simulation tools are:

- **Engineering Equation Solver (EES)** is a software package used to solve systems of non-linear equations. It is very useful as it provides many specialized functions and equations related to thermodynamic and heat transfer problems and is widely used for mechanical engineering. It is especially very suitable to build a vapour compression refrigeration system as it does not require special coding. EES has a complete database for the properties of different refrigerant applied in refrigeration systems, such as CO₂ discussed in this project.
- **Dymola** is a modelling and simulation software based on the open Modelica modelling language. It can be used for quite complex systems and is applied for use within aerospace, automotive, robotics, process, and other applications. Compatible model libraries and a powerful modelling language are some of the key advantages related to this modelling software. The possibility to use symbolic equation processing makes the simulation of interests more efficient and robust.

4.2 Compressor efficiency

The volumetric and isentropic efficiencies are usually given by the manufacturer (16). If that is not the case, it is also possible to calculate the efficiencies from the capacity sheets for the chosen compressor. Therefore, the isentropic and volumetric efficiencies used in this project are based on data provided by BOCK. The program software developed by the manufacturer, gives the compressors power consumption \dot{W}_{real} , mass flow \dot{m}_r and discharge end temperature T_2 from provided evaporating temperature T_0 and High pressure (HP).

4.2.1 Volumetric flow of the compressor

Volumetric flow rate (\dot{V}_{flow}) is quantity of fluid that is moved per unit of time, and is given by:

$$\dot{V}_{flow} = \rho * \dot{m}_r * 3600 [m^3/h] \quad (13)$$

The mass flow of refrigerant, \dot{m}_r [kg/s], was provided by the manufacturer at the chosen evaporating temperature and HP, while the density, ρ [m³/kg], was taken from the software ‘‘RnLib’’ and ‘‘CoolPack’’. The volumetric flow decreases with increasing pressure ratio (Pr), as it decreases the mass flow. The volumetric flow of the provided compressor was therefore expressed as a function of pressure ratio:

$$\dot{V}_{flow}(Pr) = -2,2398 * Pr + 38,883 [m^3/h] \quad (14)$$

4.2.2 Isentropic efficiency

The isentropic efficiency of a compressor was given as a ratio between work done by ideal compression and the actual work done. Therefore, the efficiency η_{is} was given by:

$$\eta_{is} = \frac{\dot{W}_{ideal}}{\dot{W}_{real}} \quad (15)$$

The compressor power consumption, \dot{W}_{real} [kW], was provided by the software from the manufacturer, whilst the ideal work, \dot{W}_{ideal} [kW] was given by:

$$\dot{W}_{ideal} = \dot{m}_R * (h_{2ideal} - h_1) [kW] \quad (16)$$

where enthalpies in state 1 and state 2 were taken from the software ‘‘RnLib’’ and ‘‘CoolPack’’. The relative isentropic efficiency provides an overview of compressor behaviour over the operating map. Isentropic efficiency decreases with increasing pressure ratio, and was expressed as a function of pressure ratio:

$$\eta_{is}(Pr) = -0,0079 * Pr^2 + 0,0362 * Pr + 0,6692 \quad (17)$$

4.3 Internal Heat Exchangers

The efficiency of Internal Heat Exchangers (IHX), η_{IHX} is a fundamental measure of the IHX performance. The efficiency was calculated using the following equation:

$$\eta_{IHX} = \frac{T_2 - T_3}{T_1 - T_3} \quad (18)$$

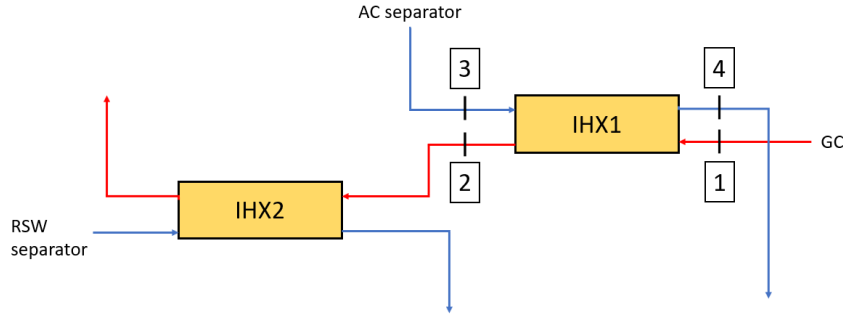
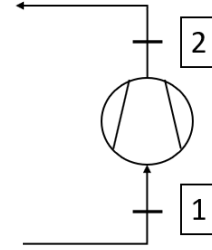


Figure 35: Schematic of internal heat exchanger configuration

Where temperature T_1 [$^{\circ}C$], is the temperature out of gas cooler and T_3 [$^{\circ}C$], is the temperature out of the AC separator. The exchangers capacity was calculated using both the low side and high side enthalpy difference, multiplied with corresponding mass flow rate:

$$\begin{aligned} Q_{IHX_{cold}} &= \dot{m}_{AC} * [h(4) - h(3)] \\ Q_{IHX_{hot}} &= \dot{m}_{GC} * [h(1) - h(2)] \end{aligned} \quad (19)$$

The efficiency of the internal heat exchanger was used as variables in further system analysis. The efficiency was used to estimate the refrigerants outlet temperature T_2 . The following efficiencies

were used in the steady state calculations: 10%, 54% and 90%. The efficiency of both heat exchangers in the CO₂ system were assumed to be equal.

4.4 Ejector

As mentioned in Section 2.4.4, the ejector is a valuable instrument that lessens the losses caused by the expansion process in a CO₂ system (8) (17). The thermodynamic modelling of ejectors has been extensively investigated in several research studies. Figure 36 shows an ejector which includes one outlet and two inlet streams, which can be separated into three sections: 1) nozzle section, 2) mixing section and 3) diffuser section. The formulas presented further are written as follows based on the state points shown in Figure 36.

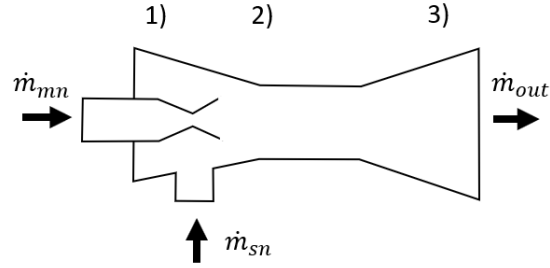


Figure 36: Schematic of a two phase ejector

The mass flow in the motive nozzle is defined as the mass flow out of the gas cooler.

$$\dot{m}_{mn} = \dot{m}_{GC} \quad (20)$$

The efficiency of ejector is defined as follows.

$$\eta_{ejector} = \frac{\dot{W}_{recovered}}{\dot{W}_{recoverablemax}} = \Phi_m * \frac{h(P_{diff out}, s_{sn in}) - h_{sn in}}{h_{mn in} - h(P_{diff out}, s_{mn in})} \quad (21)$$

where the mass entrainment ratio, Φ_m is

$$\Phi_m = \frac{\dot{m}_{sn}}{\dot{m}_{mn}} \quad (22)$$

Combining Equation 21 and Equation 22, it is possible to develop an expression for the suction mass flow, \dot{m}_{sn} .

$$\dot{m}_{sn} = \eta_{ejector} * \dot{m}_{mn} * \frac{h_{mn in} - h(P_{diff out}, s_{mn in})}{h(P_{diff out}, s_{sn in}) - h_{sn in}} \quad (23)$$

The enthalpy at the ejector outlet is calculated then by

$$h_{out} = \frac{\dot{m}_{mn} * h(P_{diff out}, s_{mn in}) + \dot{m}_{sn} * h(P_{diff out}, s_{sn in})}{\dot{m}_{mn} + \dot{m}_{sn}} \quad (24)$$

The mass flow at the outlet is

$$\dot{m}_{out} = \dot{m}_{sn} + \dot{m}_{mn} \quad (25)$$

The pressure lift the ejector can provide is calculated by the following equation.

$$P_{lift} = P_{diff\ out} - P_{sn\ in} \quad (26)$$

A different set of simulation results are obtained, varying the efficiency of the ejector. The efficiency was used to estimate the suction mass flow, which increases with the efficiency. The efficiencies used in further simulation scenarios are 10%, 20% and 30%.

4.5 Simulation models in Dymola

Creating simulation models accounting for every detail of the RSW system and its configurations is time-consuming and influences reliability and simulation time. Therefore, a number of simplifications have been made in the models, as a result of limitations in presented tool and balance between accuracy and efficiency. This sub chapter presents the simulation models with made simplifications.

A total of three models have been developed in Dymola using parameters described in Section 3:

- CASE 1: one evaporation level (RSW). The configuration utilizes all three compressors to provide the requested refrigeration capacity at RSW.
- CASE 2: double throttling and auxiliary compressor configuration. Refrigeration provided at two pressure levels, RSW and AC.
- CASE 4: similar as in CASE 2, but with utilization of a high pressure multi ejector rack. Refrigeration is provided at two pressure levels as well, RSW and AC.

The reasoning for concentration on these three cases is because of the time-limitation and consideration of which cases are able to provide most cooling based on steady state EES results in Section 5.1. This subsection describes the general approach of developing the systems in Dymola, with examples from all three system configurations. The integration tolerance of 1E-6 was chosen, based on the recommendation from (4), which is suited for thermo-fluid flow systems.

The ambition of the simulation models in Dymola was to investigate how different system configurations will perform with dynamic loads. Therefore, modeling system components are not done in this theses; including modeling the tubes between components, and accounting for pressure drop throughout the system. Further, constant heat transfer coefficient have been selected.

4.5.1 Compressors

"Efficiency compressors" from TIL library are used in the presented simulation files. The model is allowing the user to program the efficiencies, displacement volume and speed. The efficiencies used in the simulation files were calculated using equations presented in Section 4.2. Several attempts of using variable compressor efficiencies were carried out in Dymola. Modelling new custom compressors was found out to be too time-consuming, and modifying the "efficiency compressors" was unsuccessful. The limitation lies in the TIL-Component library not allowing inputs of efficiencies from components in the system configuration, which are not included in the base TIL-component library. The efficiencies are therefore assumed to be constant. This assumption is reasonable concerning stable pressure ratios at full-load operation. Although, this assumption fails to consider the decrease in efficiency at part load operations and the change in pressure ratios.

The compressors displacement volume was calculated by following formula:

$$V_{Disp} = \frac{V_{Nom}}{3600 * 60} \quad (27)$$

where the V_{Nom} was provided by the software from the manufacturer. The calculated displacement volume of one compressor described in Section 3.4.1 was $V_{Disp} = 0,00021m^3$

Further assumptions for the compressors are listed below:

- Constant volumetric efficiency at 0,8 and constant isentropic efficiency at 0,7.
- Constant speed of compressors at 60 Hz (C2 and C3 in CASE 2 and CASE 4).

CASE 1: compressors control

Figure 37 depicts the model for the CO₂ compressors and their control system for CASE 1. The compressor rack was simplified to a single unit, with a total displacement volume of $V_{Disp} = 0,00063m^3$. As seen in Figure 37, the compressor rack was regulated by a switch controller. The control strategy chosen for the compressors is as follows:

1. All three compressors are working at maximum capacity until a set temperature is reached in the RSW tank. The chosen RSW temperature for presented simulation is at $T_{tank} = -0.5^\circ C$.
2. Two compressors are turned off and one compressor is working on maintaining the set temperature in the RSW tank. The PI controller adjusts the relative displacement volume in order to maintain the temperature. The controller has an upper limit of output at 1/3.
3. If temperature in the RSW tank exceeds the set temperature again, all three compressors are turned on.

The chosen strategy reflects two compressors with ON/OFF regulations and one compressor with frequency converter.

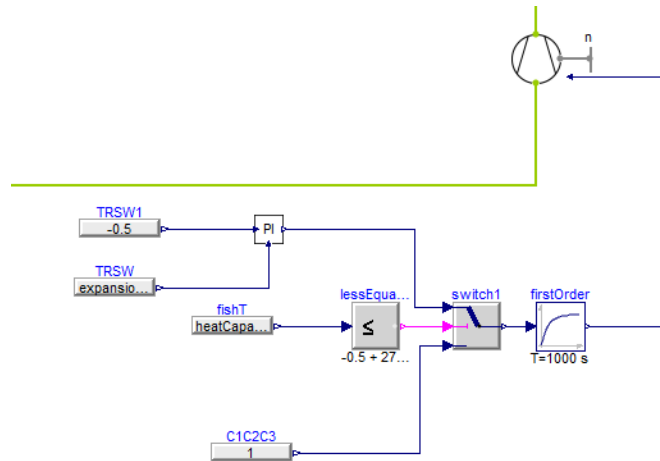


Figure 37: CASE 1 compressor controller, snipped from Dymola

CASE 2 and CASE 4

CASE 2 and CASE 4 have identical control strategies for the compressor rack. Compressor C1 is working as an auxiliary compressor, while C2 and C3 are working to provide RSW cooling. For C1, the PI controller adjusts the frequency in order to maintain suction pressure at 39,5 bar, visualized in Figure 38.

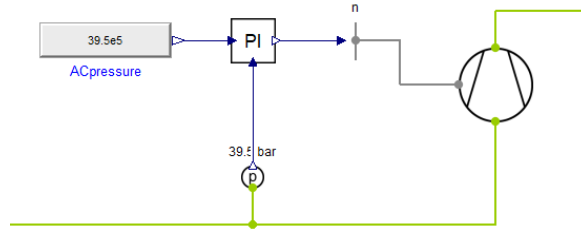


Figure 38: CASE 2 and 4: C1 compressor controller , snipped from Dymola

The compressor rack at RSW was simplified to a single unit, with a displacement volume of $V_{Disp} = 0,00042m^3$. The chosen control strategy for the compressors was similar to the one presented in CASE 1. One alteration is the upper limit for the PI-controller is set to 1/2. Deviating from the design, this models assumes two compressors are equipped with frequency controllers, which was done to improve simulation performance in Dymola.

4.5.2 Flooded shell and tube evaporators

The TIL library does not include models for flooded shell and tube heat exchangers. Therefore, a combination of components and settings were used to simulate the model.

The gravity fed heat exchangers circulation number is depended on pressure drop and heat transfer load, and in this case is assumed to be at a constant value of 1,25. In the Dymola file, shown in Figure 39 a pump is controlling the circulation ratio. This was achieved by utilizing a PI-controller that maintains the outlet quality after the evaporator at 80%. The pumps energy requirement is not taking into account later in energy calculations.

Circulation number is the rate of the liquid feed and evaporation level and can be calculated as:

$$C_n = \frac{1}{x_{out}} \tag{28}$$

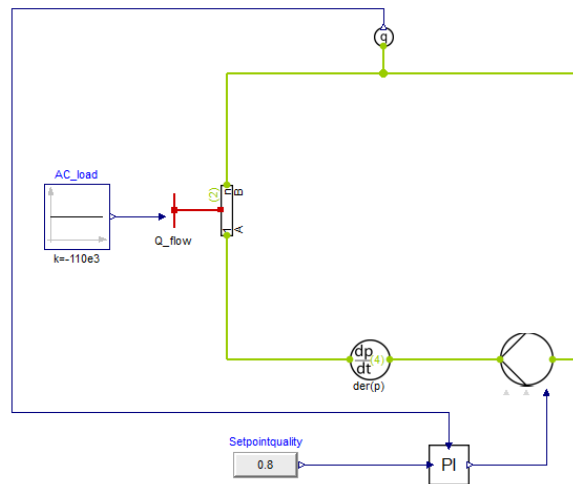


Figure 39: Simplified flooded evaporator: AC circuit, snipped from Dymola.

4.5.3 Gas cooler (GC1 and GC2)

Figure 40 depicts the model for the gas coolers. On the the high pressure side, the CO₂ was cooled down and heat is distributed to DHW and space heating, as described in Section 3.1. In Figure 40 the rejection of condensation heat was in GC2 (left gas cooler in the figure below), while some of the heat was recovered in the de-super heater unit (GC1) for DHW production (right gas cooler in the figure below).

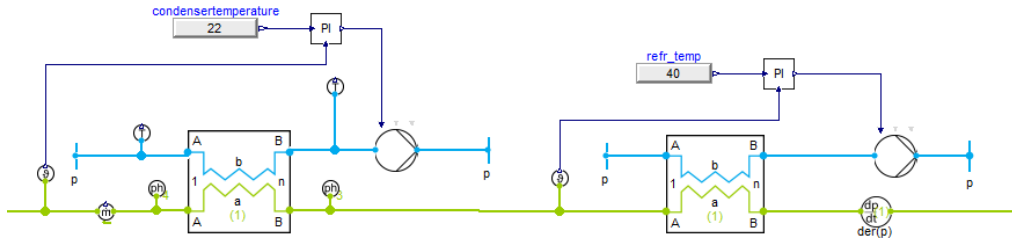


Figure 40: DSH and condenser unit. Snipped from Dymola

DHW system was not part of the focus area in simulation models and was thereby highly simplified. Accordingly, the primary purpose of GC1 is to reject heat. The water mas flow through the gas coolers is regulated by a pump, keeping the refrigerant temperature out of the gas cooler at 40 °C. To maintain the cooling capacity of the CO₂ unit, the rest of the heat is removed in the following gas cooler. The control is done similarly in GC2, keeping the temperature out of the gas cooler at 22 °C. Both gas coolers are modelled after the presented specifications in Section 3.4.2. The pressure level in the upper level is $P_{GC} = 90$ [bar] which is maintained by an expansion valve controlled by a PI-controller, regulating the effective flow area.

4.5.4 Expansion devices

High Pressure Valve (CASE 1 and CASE 2)

The high pressure was controlled by an expansion valve. The expansion valves are modeled using the "Orifice Valve" from the TIL-library. The PI-controller regulates the area of the expansion to uphold a set-point of 90 bar. The effective valve flow area at the design conditions were calculated by the equation below.

$$A_{Valve} = \frac{\dot{m}_R}{\sqrt{(P_C - P_E) * 2\rho_{inlet}}} \quad (29)$$

Medium Pressure Valve (CASE 1, CASE 2 and CASE 4)

The medium pressure valve was modelled using "Orifice Valve" from TIL-library and is regulated using a PI-controller. The PI-controller adjusts the mass flow of refrigerant, thereby the filling level of the RSW separator by changing the effective flow area of the orifice valve. The MP expansion valve controller was set to maintain a filling level of 0,5. The presented filling level will ensure suitable feeding to the RSW evaporator.

HP Ejector (CASE 4)

The ejector was modeled using the "Efficiency based ejector model" component in the TIL 3.5.0 component library. The high pressure is controlled by effective driving flow are of the ejector to uphold the set-point of 90 bar. The input parameter of the component is the effective driving flow area and the efficiency of the ejector. The effective driving flow area is controlled by a PI controller

and efficiency of ejector is defined depended on system configuration and demand for cooling at RSW and AC.

4.5.5 RSW circuit (CASE 1, CASE 2 and CASE 4)

The RSW circuit was designed to deliver seawater at a temperature of $-1,5\text{ }^{\circ}\text{C}$ to cover refrigeration for two main heat loads; namely prechilling of seawater as part of fishing preparation and chilling of seawater/fish mixture once the fish has been loaded on board the tanks. The system should also cover refrigeration for maintenance chilling, where the refrigeration system maintains a target temperature in the load. The RSW evaporator was modelled in Dymola using the pre-modelled "Shell and tube evaporator" in the TIL Component library. The entire refrigeration installation is dimensioned to have a designed evaporator capacity of 450 kW, although the actual RSW capacity depends on chosen system configuration. The manufacturer of chosen evaporator provided the needed surface area of the evaporator, and a constant heat transfer coefficient is assumed for the entire heat exchanger surface. The RSW evaporator is modelled as a gravity-fed shell and tube evaporator, as described in Section 4.5.2, and depicted in Figure 41.

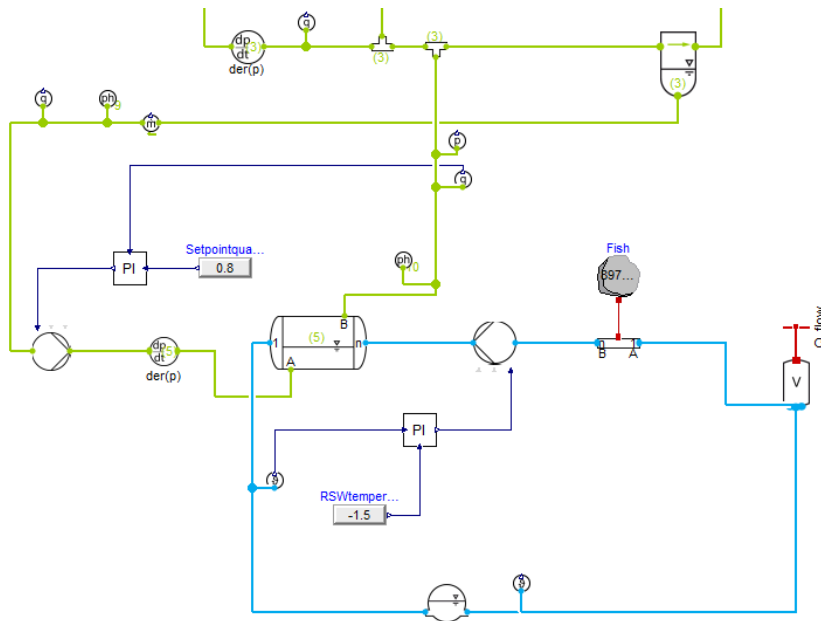


Figure 41: RSW loop. Snipped from Dymola

The seawater circuit presented in Figure 41 consists of a seawater pump, tube element connected to a lumped thermal element storing heat, a volume and an expansion tank. The RSW tank was modelled as a single volume of 118m^3 , where a continuous heat source of 30 kW is applied to the tank volume, indicating the heat accumulation through infiltration. A seawater pump regulates the seawater mass flow to keep the outlet temperature at the set-point of $-1,5\text{ }^{\circ}\text{C}$, as portrayed in Figure 41. The expansion tank sets the correct pressure value in the system and the initial temperature of the seawater in the RSW tank. A tube element is representing the load, and the load input is retrieved from the lumped thermal element. The lumped thermal element is representing the catch. The model has two input parameter; the heat capacity of the element and the initial temperature of the element. Heat capacity is modelled based on the data related to the "Energy measurement onboard pelagic purse seiner" (34), and the catch in presented simulations is assumed to be mackerel. The catch size was assumed to be 59m^3 , and the initial temperature of the element was set to $6\text{ }^{\circ}\text{C}$. The tank was assumed to be 118m^3 .

The presented RSW circuit can simulate three main heat loads:

-
- **Prechilling:** The lumped thermal element is disconnected from the tube element, and an initial seawater temperature is set in the expansion tank. The system works at full capacity up to a temperature of -0.5 °C is reached.
 - **Chilling:** The lumped thermal element is connected to the tube element, and the system is working at full capacity up to a temperature of -0.5 °C is reached in the RSW tank again.
 - **Maintenance:** System works at part load, covering refrigeration due to heat accumulation through infiltration.

4.5.6 AC circuit

The AC circuit was designed to deliver water at a temperature of 10 °C to cover all potential AC demand on board. A tube element represents the AC load, and the load input is retrieved from the spreadsheet describing the load scenario or a predefined constant load. The flow rate of CO₂ is determined to ensure a circulation ratio of 1,25. Thereby, the return stream of CO₂ has a vapour quality of 80%. Work input to the pump is neglected in the energy consumption calculation, as the main pump's function is to represent the behaviour of a gravity-fed evaporator. The model can be seen in Figure 39.

The reason for simplifying the AC circuit is the lack of data onboard fishing vessels regarding the AC demand. Further investigation and energy measurements need to be performed onboard fishing vessels to implement a proper system modelling of the AC circuit.

4.6 Statistical validation

Validation has been characterized as "comparison of the model's predictions with the real world to determine whether the model is suitable for its intended purpose" (12). Validation is an essential step for model acceptance. A broad range of methods has been proposed and used in many different fields of study. Different validation techniques can be grouped into four main sections: visual techniques, subjective assessment, deviance measures, and statistical tests. Mayer and Butler properly elucidate these categories in their paper on "Statistical validation" (12).

In this study validation technique chosen was the deviance measures. This method is based on the difference between simulated and observed values. The most frequently used measure and the measure used in this study is 'mean absolute per cent error' (MA%E). The measure is defined as:

$$MA\%E = 100[\sum(|y_i - \hat{y}_i|/|y_i|)]/n \quad (30)$$

where \hat{y}_i represents simulated values, y_i observed values, and n the number of pairs. When reviewing the errors, Kleijnen suggests 10% as an upper limit of acceptability (25).

In this study, the theoretical results and models need to be validated with the first performance data available during the commissioning phase of the RSW system. However, the commissioning phase of the project was postponed indefinitely. Therefore, validation with real-world data was not done during this master thesis. In agreement with supervisors for the project, it was decided to validate the Dymola simulation results with EES results. Unfortunately, this validation will not determine to what degree the simulations are an accurate representation of the system in real life. However, the comparison is beneficial, as both software are using various simplifications and uncertainties.

5 Results

This chapter describes the results and simulations performed with EES and Dymola. The main focus for the EES results are evaluation of optimal gas cooler pressure, influence of efficiencies of the internal heat exchangers and the ejector. Additionally, dynamic load simulations were performed with focus on energy demand during chilling and maintenance chilling. The results are presented in five cases; The first case presents the steady-state performance of the RSW system using all three compressors. Case two presents a double expansion with a parallel compressor; case three presents triple expansions, with three evaporating levels. Case four will utilize a high-pressure ejector solution, while case five will utilize the low-pressure ejector.

5.1 Steady state performance

To get an impression of the CO₂ refrigeration system described in the Chapter 4, the initial calculations were performed using the Engineering Equation Solver (EES). To obtain the best performance for the RSW system, a proper evaluation of some of the components' influence on its performance is carried out. Hence, enabling optimization of the RSW system.

5.1.1 CASE 1: 3 RSW compressors

CASE 1 represents the simplest design for the RSW system. CASE 1 utilizes all three compressors (C1, C2, and C3) to provide the requested refrigeration capacity. The system utilizes one internal heat exchanger (IHx2), where the value for the heat exchanger effectiveness used in the reference system is 30%. Table 1 represents the refrigeration capacity of the RSW system and systems COP at different seawater temperatures. The refrigeration capacity, \dot{Q}_{RSW} , and systems COP decreases with increasing seawater temperature, shown in Table 1, assuming a constant discharge pressure at 90 bar.

Table 1: CASE 1: reference system [$\eta_{IHx} = 30\%$ and $P_{GC} = 90$ [bar]]

T_{SW} [°C]	\dot{Q}_{RSW} , [kW]	COP
15	421,1	2,97
25	355,4	2,5
35	237,1	1,67

The refrigeration capacity is calculated for different ambient conditions and plotted in Figure 42. The following figure shows that the influence of IHx effectiveness, η_{IHx} , on the refrigeration capacity is small at low temperatures; at a seawater temperature of 15 °C with 90% effectiveness, the value of refrigeration capacity is 3% less when compared with 10% IHx effectiveness. Figure 42 demonstrates that the refrigeration capacity is larger at a lower efficiency of the IHx at a temperature below the critical one. With an efficient IHx, the volumetric refrigeration cooling effect [$\frac{m^3}{kW}$] of IHx will increase, and the start of the compression process will move to an area of greater superheat where the isentropic compression lines become flatter. This results in a higher enthalpy difference across the compressors, leading to more power consumption.

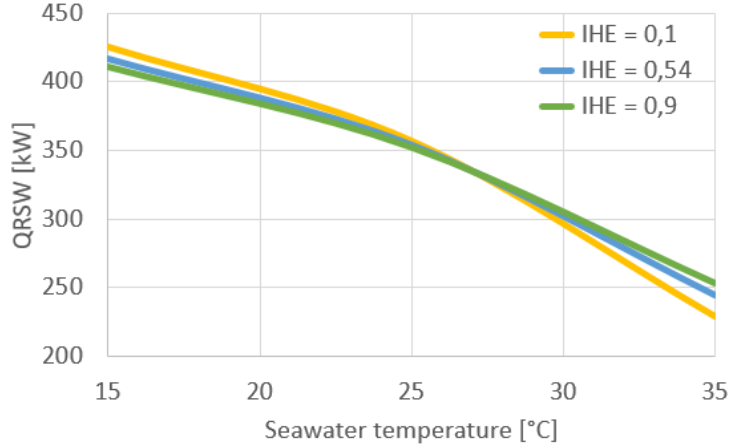


Figure 42: CASE 1: Refrigeration capacity vs sea water temperatures [$P_{GC} = 90$ [bar]]

At seawater temperatures below the critical temperature of CO_2 the increased power demand for the compressor is greater than the increased refrigeration capacity due to the liquid's subcooling leaving the condenser. Consequently, at $15\text{ }^\circ\text{C}$, the refrigeration capacity is larger with an IHX efficiency η_{IHX} of 10% compared to 90%. The improvements of \dot{Q}_{RSW} with IHX are greater at high seawater temperatures; Improvement can also see this in Figure42, where at a seawater temperature, T_{SW} of $35\text{ }^\circ\text{C}$ a 10% increase of refrigeration capacity is seen when improving the η_{IHX} from 10% to 90%.

Figure 43 presents the influence of η_{IHX} and T_{SW} , on systems COP. The temperatures chosen for the simulation are: $T_{SW} = 30\text{ }^\circ\text{C}$, $T_{SW} = 35\text{ }^\circ\text{C}$ and $T_{SW} = 40\text{ }^\circ\text{C}$ At such high seawater temperatures, it is important to keep the cycles discharge pressure at the optimal value to ensure good system COP. Along with the η_{IHX} direction, when seawater temperature (T_{SW}) and gas cooler pressure (P_{GC}) are fixed, the refrigeration system performs better with a high η_{IHX} . This is due to a larger increase in specific cooling capacity \dot{Q}_{RSW} , when compared to an increase of compressor work \dot{W}_{in} .

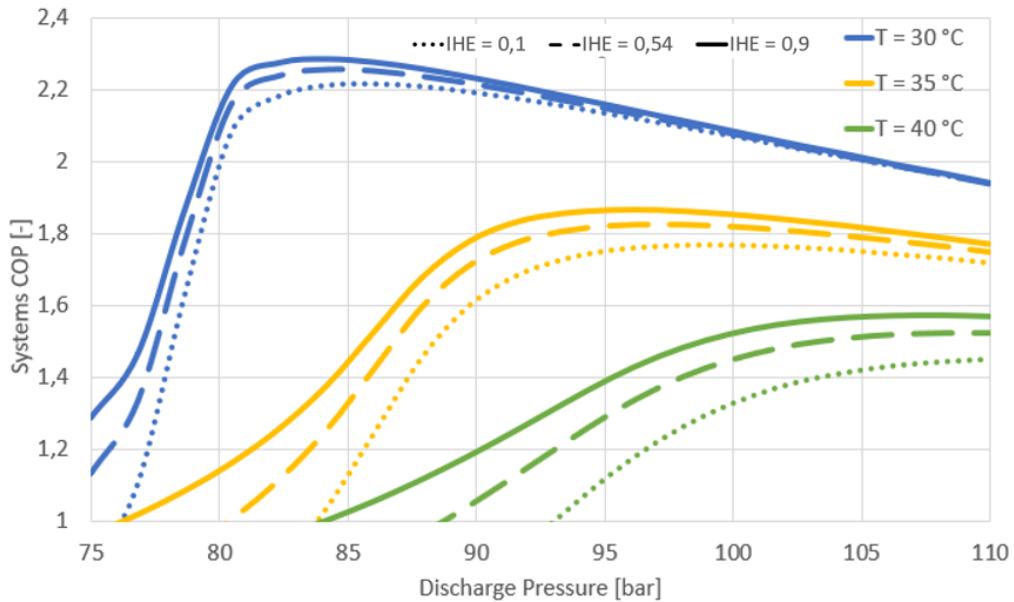


Figure 43: CASE 1: COP as a function different discharge pressures at sea water temperatures of 30, 35 and 40 °C, for the CO_2 system with IHX efficiencies values 0,1, 0,54 and 0,9

Five points can be observed in Figure 43:

- High seawater temperatures result in lower system COP. In this case, an increase in seawater temperature leads to a decrease in enthalpy h_3 and a corresponding decrease in refrigeration capacity \dot{Q}_{RSW} . At the same time, compressor work \dot{W}_{in} will increase, thus resulting in a decrease of the COP.
- Figure 43 presents that with the increase of the discharge pressure, systems COP increases gradually in all three efficiency configurations. The rising trend is close to a linear relationship. This is caused by a larger refrigeration capacity increase \dot{Q}_{RSW} , compared to the compressor work increase \dot{W}_{in} . COP is increased to the extreme value and then slowly decreased with the further increase of discharge pressure. A slight decrease in COP can be advantageous. Samer Sawahla states that at high temperatures, the lower gradient makes the system's performance less sensitive to the control of the discharge pressure (33).
- Furthermore, it is evident from Figure 43 that there exists an optimal discharge pressure that gives a maximum COP. This means that a transcritical CO₂ system should operate near its optimum pressure to achieve high efficiency. Several studies have been investigated the optimal heat rejection pressure for CO₂ transcritical cycles. In some studies, a correlation for the optimal discharge pressure was developed. S.M.Liao developed a correlation in terms of evaporating temperature and the outlet temperature of the gas cooler (22). Samer Sawahla developed a correlation in terms of the gas cooler approach temperature and ambient temperature (31). Both studies stated the importance of isentropic efficiency on the correlation developed.
- Optimum discharge pressure decreases with high IHX efficiency. Table 2 presents, among others, the optimum discharge pressure for a given seawater temperature T_{SW} and IHX efficiency η_{IHX} . To show how efficiency affects the optimum discharge pressure, pick $T_{SW} = 30$ [°C], and P_{opt} lowers down from 86,1 bar to 84,2 bar, while η_{IHX} increases from 10% to 90%. Consequently, the pressure ratio will decrease, improving the compressor performance and safety of the system. These results match the simulation performed by Ying Chen and Junjie Gu in their investigation of optimum high pressure for CO₂ transcritical refrigeration systems with internal heat exchangers (19).
- Maximum COP is obtained with a high efficient IHX. As seen earlier in this section (Figure 42), a high efficient IHX is only beneficial at seawater temperatures above $T_{SW} = 27$ [°C]. Pick $T_{SW} = 35$ [°C] and COP increases with 5% with a increase of η_{IHX} from 10% to 90%. The benefits of high efficient IHX are larger with increasing seawater temperature, which is visualised by the distance between the dotted and solid lines in Figure 43.

Table 2: CASE 1: Optimum discharge pressure and refrigeration capacity at given sea water temperature and IHX efficiency

-	T = 30 °C			T = 35 °C			T = 40 °C		
	10%	54%	90%	10%	54%	90%	10%	54%	90%
P_{opt} [bar]	86,05	84,21	84,21	98,95	97,11	97,11	110	110	108,5
\dot{Q}_{RSW} [kW]	302,1	300,9	304,4	272,2	276,1	281,4	242	253,8	257,9
COP [-]	2,21	2,25	2,28	1,77	1,83	1,86	1,45	1,52	1,57

Table 2 presents further the refrigeration capacity at the optimum discharge pressure. At seawater temperature $T_{SW} = 30$ [°C] and $\eta_{IHX} = 90\%$, the refrigeration capacity is $\dot{Q}_{RSW} = 281,4$ [kW]. This is an 16% increase when comparing it with the reference system presented in Table 1. Systems COP improves with 10% as well. At $T_{SW} = 40$ [°C], the optimum pressure is not possible. The compressors chosen for this system are not able to provide such a high pressure. Therefore at $T_{SW} = 40$ [°C], the largest refrigeration capacity is provided when P_{GC} is at 110 bar.

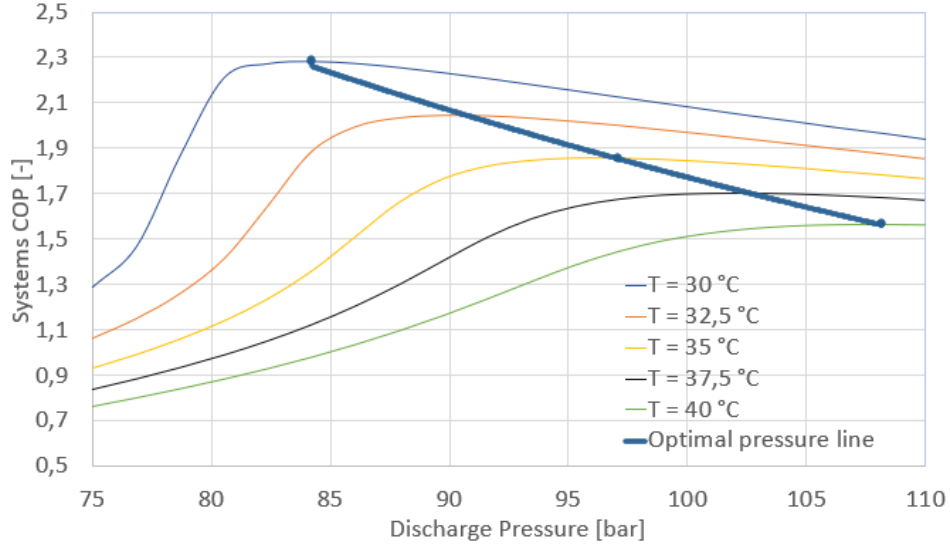


Figure 44: CASE 1: COP vs discharge pressure at different seawater temperatures [$\eta_{IHX} = 90\%$]

According to S.M. Liao, the optimal discharge pressure for a transcritical CO_2 cycle depends on three parameters: the temperature out of the gas cooler T_{GC} , the evaporating temperature $T_{RSW_{evap}}$ and the compressors isentropic efficiency η_{is} (22). In CASE 1, the evaporating temperature. The isentropic efficiency are constant, hence the optimal discharge temperature is only effected by the T_{GC} . In CASE 1, the $T_{GC} = T_{SW} + 4$ [$^{\circ}\text{C}$]. The η_{IHX} is assumed to be 90% as this will ensure the highest possible COP at the chosen temperatures. Figure 44 presents a plot where discharge pressure is varied, and the COP is plotted at different pressures for seawater temperatures. The optimum discharge pressure values were curve fitted as a function of seawater temperature.

Curve fitting the optimum discharge pressure developed in Figure 44 yields the following correlation:

$$P_{opt} = 2,4336 * (T_{SW} + 4) + 1,4614 \text{ [bar]} \quad (31)$$

The correlation can be used in the simulation to operate at the optimum discharge pressure. Although, at $T_{SW} > 40$ [$^{\circ}\text{C}$], the P_{GC} should be at 110 [bar] at all time, by the reasons off mentioned earlier in this section. This correlation is similar to the one obtained by Samer Sawalha (31). The correlation obtained by S.M.Liao et al. is different, as it considers the evaporating temperature as well (22).

5.1.2 CASE 2: 2 RSW and 1 AC compressors

CASE 2 presents the second design for the RSW system. CASE 2 demonstrates a double throttling and auxiliary compressor cycle, where C1 is the auxiliary compressor, and C2 and C3 are RSW compressors. The system uses two internal heat exchangers (IHX1 and IHX2), where the value for the heat exchanger effectiveness used in the reference system is set to 30%. CASE 2 is providing refrigeration at two temperature levels, RSW and AC. Accordingly, CASE 2 removes the vapour arising from flashing during the first expansion. An increase in seawater temperature results in more flash gas, potentially a better system COP when compared to CASE 1. C1 compressor will be further presented as the AC compressor, as one of the possibilities of utilizing the refrigeration capacity at that pressure level is to provide Air Conditioning.

Table 3 represents the refrigeration capacity at AC and RSW pressure and systems total COP. The discharge pressure is set to 90 bar while the pressure in AC receiver is set to $P_{AC} = 39,6$ [bar]

Table 3: CASE 2: reference system, [$\eta_{IHX} = 30\%$ and $P_{GC} = 90 [bar]$]

$T_{SW} [^{\circ}C]$	$\dot{Q}_{RSW} [kW]$	$\dot{Q}_{AC} [kW]$	$COP_{TOT} [-]$
15	307,9	170,3	3,4
25	299,9	103	2,8
35	268	0	1,9

($T_{AC} = 5 [^{\circ}C]$). The increased amount of flash gas due to an increase in T_{SW} decreases the AC evaporator's feeding, decreasing its refrigeration capacity. At $T_{SW} = 35 [^{\circ}C]$, the amount of expanded gas is so high that AC's refrigeration capacity is zero. However, one should note that the potential AC demand is largest when seawater (ambient air temperature) is high. Although, comparing CASE 1 and CASE 2 reference systems, at $T_{SW} = 35 [^{\circ}C]$, the RSW refrigeration capacity \dot{Q}_{RSW} increases with 13 % in CASE 2. Although, from practical point of view, refrigeration system in CASE 2 is not as simple as in CASE 1.

Systems' main function, as in CASE 1, is to provide refrigeration at RSW. The RSW refrigeration capacity is therefore calculated at different seawater temperatures and plotted in Figure 45. The following figure shows the influence of IHX effectiveness η_{IHX} on the RSW refrigeration capacity, assuming the same effectiveness for both heat exchangers, $\eta_{IHX} = \eta_{IHX1} = \eta_{IHX2}$. The influence η_{IHX} at $T_{SW} = 15 [^{\circ}C]$ on refrigeration capacity is significant; the value of refrigeration capacity increases by 36% when η_{IHX} decreases from 90% to 10%.

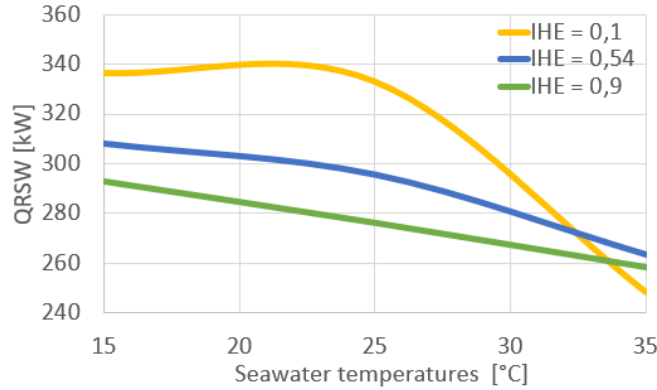


Figure 45: CASE 2: Refrigeration capacity vs seawater temperature [$P_{GC} = 90[bar]$]

As mentioned in Section 5.1.1 , the volumetric cooling effect [$\frac{m^3}{kW}$] of IHX increases with an increase of η_{IHX} , and is not beneficial at temperatures below the critical of CO_2 . The benefits of efficient heat exchangers are only seen when seawater temperature exceeds $32,5 [^{\circ}C]$ (Figure 45). The improvement of \dot{Q}_{RSW} using an efficient heat exchangers at $T_{SW} = 35 [^{\circ}C]$ is: 6% increase in \dot{Q}_{RSW} , with an increase of η_{IHX} from 10% to 54%. When comparing the efficiencies, a heat exchanger with an efficiency of 90% is not beneficial at the presented seawater temperatures.

Figure 46 presents the influence of pressure in the receiver (P_{AC}) on the RSW refrigeration capacity, \dot{Q}_{RSW} . The pressure interval chosen for the calculation is [$31bar - 57bar$] with its corresponding temperature range [$-4^{\circ}C - 20^{\circ}C$]. The following figure demonstrates the influence of η_{IHX} on the refrigeration capacity as well. At seawater temperatures $T_{SW} = 30 [^{\circ}C]$ and $T_{SW} = 35 [^{\circ}C]$, the refrigeration system produces more RSW cooling utilizing low IHX efficiencies.

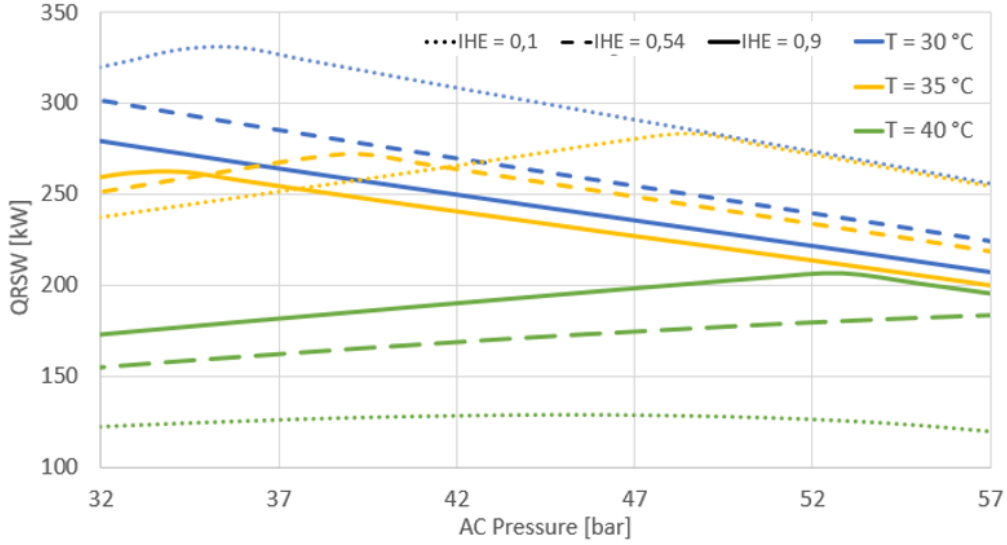


Figure 46: CASE 2: Refrigeration capacity RSW vs AC pressure [$P_{GC} = 90$ [bar]]

At $T_{SW} = 30$ [°C] the optimum pressure in the receiver is $P_{AC} = 35$ [bar] while at $T_{SW} = 35$ [°C] the optimum pressure in the receiver is $P_{AC} = 47$ [bar], both using $\eta_{IHX} = 0,1$. At $T_{SW} = 40$ [°C] the optimum pressure in the receiver is $P_{AC} = 53$ [bar], utilizing now a IHX efficiency, $\eta_{IHX} = 0,9$. At $T_{SW} = 35$ [°C], utilizing the optimum pressure and efficiency, the increase in RSW refrigeration capacity is 23% when compared to the reference system presented in Table 3. As seen in Figure 47, with higher IHX efficiency, the values of P_{AC} is reduced. In the chosen pressure interval, this is best visualised for $T_{SW} = 35$ [°C]. That is not always beneficial as it is convenient to keep the receiver pressure high thus reducing the power consumption of the system. This occurs due to the parallel compressor operating with a lower pressure ratio which increases the performance of the compressor (40). At $T_{SW} = 35$ [°C] the optimum pressure in the receiver is $P_{AC} = 47$ [bar] and the corresponding evaporating temperature is $T_{AC} = 12$ [°C], which is high comparing to existing systems. Although, S. Girotto encourages to use air conditioning systems designed for the highest temperatures possible. He presents a solution for food retailers, which eliminates the use of secondary fluid by installing AC evaporator directly into to the air handling unit (18).

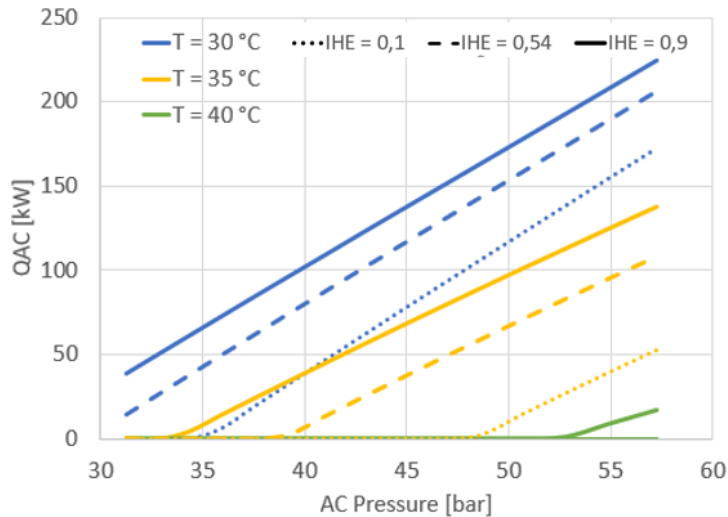


Figure 47: CASE 2: AC Refrigeration capacity vs pressure after first expansion [$P_{GC} = 90$ [bar]]

The AC refrigeration capacity \dot{Q}_{AC} is calculated at different pressure levels P_{AC} and plotted in Figure 47. As discussed previously, the refrigeration capacity decreases with increasing seawater temperature. At $T_{SW} = 40$ [°C], the amount of flash gas is so high that AC net capacity is not attainable. At $T_{SW} = 30$ [°C] and $T_{SW} = 35$ [°C] the maximum refrigeration capacity is respectively $\dot{Q}_{AC} = 224,4$ [kW] and $\dot{Q}_{AC} = 137,5$ [kW], both utilizing $\eta_{IHX} = 0,9$. The high efficiency of IHX1 and IHX2 will subcool better the refrigerant leaving the gas cooler, thus decreasing its enthalpy and increasing the potential refrigeration at the AC pressure. This is not always beneficial as it reduces the RSW refrigeration capacity \dot{Q}_{RSW} . AC load for fishing vessels is not reviewed in previous scientific publications. If the AC load for fishing vessels at different ambient temperatures is known, Figure 46 and 47 can further optimise the refrigeration system.

Table 4 summarizes the highest refrigeration capacities for RSW, using the optimum pressure at P_{AC} at the specific seawater temperatures. The chosen high pressure of the system is 90 bar in all three presented solutions. As seen in the table, the AC refrigeration capacity is negligible at chosen P_{AC} .

Table 4: CASE 2: RSW and AC refrigeration capacity at different seawater temperatures, at optimum P_{AC} , [$P_{GC} = 90$ bar]

T_{SW} [°C]	η_{IHX} [%]	P_{AC} [bar]	\dot{Q}_{RSW} [kW]	\dot{Q}_{AC} [kW]	COP_{TOT} [-]
30	10	35,9	330,8	6,1	2,4
35	10	48,6	283,8	2	2,1
40	90	52,8	206,7	0,9	1,5

Comparing with results from Table 2 (CASE 1), the benefits of an auxiliary compressor solution is only noticeable at $T_{SW} = 30$ [°C], with an increase of refrigeration capacity by 9%. At $T_{SW} = 35$ [°C] the refrigeration capacities are similar. At $T_{SW} = 40$ [°C], CASE 1 outperforms CASE 2, with a 26,22% higher RSW refrigeration capacity. This can be explained by the utilization of optimum discharge pressure in CASE 1, and using the reference pressure of 90 bar in CASE 2.

CO₂ refrigeration units have been emerging significantly on the market in the last decade. (24), especially in commercial refrigeration. Research investigating the optimal high pressure are found in several studies. Baek et al. performed a experimental study on a CO₂ refrigeration system, where they demonstrated the existence of the optimal discharge pressure under given operation conditions (23). Wang et al. investigated high pressure of a transcritical CO₂ system with double expansions and IHX. (27) Therefore, further optimization on CASE 2 regarding the discharge pressure is needed to obtain the maximum refrigeration capacity.

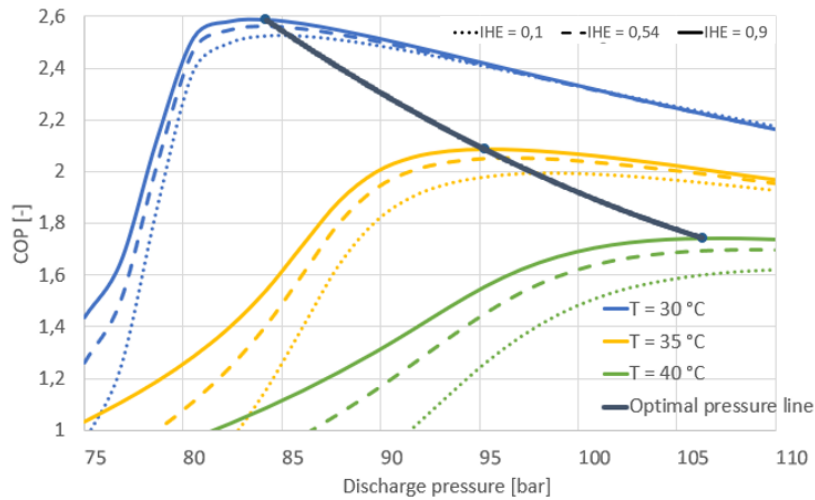


Figure 48: CASE 2: COP vs discharge pressure at different seawater temperatures

Figure 48 presents the influence of η_{IHX} and T_{SW} on systems COP. Seawater temperatures chosen in Figure 39 are, $T_{SW} = 30$ [°C], $T_{SW} = 35$ [°C] and $T_{SW} = 40$ [°C]. The pressure in the AC receiver is kept at, $P_{AC} = 40$ [bar]. As in CASE 1, the system performs better with a high efficient IHX. This is visualised in Figure 48, by the solid lines over the dotted in the three presented cases.

Assuming $\eta_{IHX} = 0,9$, and considering systems COP, the optimum discharge pressure developed in Figure 48 gives the following correlation:

$$P_{opt} = 2,209 * (T_{SW} + 4) + 9,1057 \text{ [bar]} \quad (32)$$

Table 5: CASE 2: RSW and AC refrigeration capacity at different seawater temperatures, at optimum P_{GC} , considering systems COP, $\eta_{IHX} = 90\%$

T_{SW} [°C]	\dot{Q}_{RSW} [kW]	\dot{Q}_{AC} [kW]	COP_{TOT} [-]
30	258,2	84,2	2,6
35	246,1	65,8	2,1
40	234,8	51,9	1,7

At $T_{SW} = 35$ [°C], utilizing the correlation for optimum discharge pressure (Equation 32), the increase in refrigeration capacity is 15% compared to the reference system presented in Table 3. Systems COP increases by 5%. Comparing with results presented in Table 4, the optimum discharge pressure correlation gives a considerable increase in COP; at $T_{SW} = 30$ [°C] by 8% and at $T_{SW} = 40$ [°C] by 13%. At the same time, drastic increase in AC refrigeration capacity is also noticeable. Although, the refrigeration capacity decreases at $T_{SW} = 30$ [°C] and $T_{SW} = 35$ [°C]. As mentioned before, the main task for the refrigeration unit is providing RSW cooling. Thus, further optimization of discharge pressure, considering \dot{Q}_{RSW} is investigated.

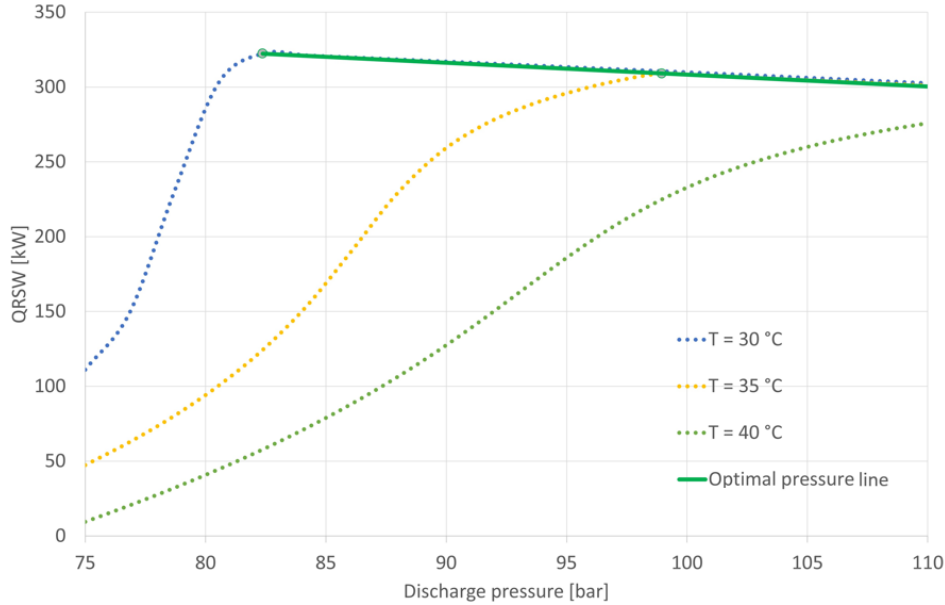


Figure 49: CASE 2: refrigeration capacity at RSW vs discharge pressure at different seawater temperatures, [$\eta_{IHX} = 10\%$]

\dot{Q}_{RSW} is calculated for different P_{GC} and plotted in Figure 49. The figure shows \dot{Q}_{RSW} at $T_{SW} = 30$ [°C], $T_{SW} = 35$ [°C] and $T_{SW} = 40$ [°C]. The system performs better with a low

efficient heat exchanger, hence Figure 49 only presents \dot{Q}_{RSW} with a $\eta_{IHX} = 0,1$. The pressure in the AC receiver is kept at $P_{AC} = 40$ [bar].

Assuming $\eta_{IHX} = 0,1$, and considering \dot{Q}_{RSW} , the optimum discharge pressure developed in Figure 49 gives the following correlation:

$$P_{opt} = 3,893 * (T_{SW} + 4) - 50,954 \text{ [bar]} \quad (33)$$

Table 6: CASE 2: RSW and AC refrigeration capacity at different seawater temperatures, at optimum P_{GC} , considering \dot{Q}_{RSW}

T_{SW} [$^{\circ}C$]	η_{IHX} [-]	\dot{Q}_{RSW} [kW]	\dot{Q}_{AC} [kW]	COP_{TOT} [-]
30	0,1	314,7	0	2,5
35	0,1	307,5	6,95	1,99
40	0,1	275,8	0	1,62

Table 6 presents shows an increase in RSW refrigeration capacity at $T_{SW} = 35$ [$^{\circ}C$] and $T_{SW} = 40$ [$^{\circ}C$] when compared to the results presented in Table 4, and the reference system (Table 3). Three points can be observed when comparing with results obtained in CASE 1 (Table 2):

- CASE 2 solution outperforms CASE 1 at presented seawater temperatures considering \dot{Q}_{RSW} ; at $T_{SW} = 30$ [$^{\circ}C$] by 3,4%, at $T_{SW} = 35$ [$^{\circ}C$] by 10% and at $T_{SW} = 40$ [$^{\circ}C$] by 7%.
- Simultaneously, CASE 2 solution outperforms CASE 1 at presented seawater considering COP; at $T_{SW} = 30$ [$^{\circ}C$] by 10%, at $T_{SW} = 35$ [$^{\circ}C$] by 8% and at $T_{SW} = 40$ [$^{\circ}C$] by 3%.
- $\eta_{IHX} = 0,1$ used obtaining results in Table 6, while in CASE 1 the largest \dot{Q}_{RSW} is achieved by utilizing $\eta_{IHX} = 0,9$

5.1.3 CASE 3: 1 RSW, 1 AC and 1 LT compressors

CASE 3 reviews the third design for the RSW system. CASE 3 presents a solution with three expansions with parallel compressors. This design allows the system to provide refrigeration at three temperature levels. Meaning, the system can provide AC, RSW, and LT refrigeration simultaneously. CASE 3 unit is similar to CASE 2, with an additional expansion valve after the MPR separator and a low-temperature dry evaporator (EVAP3). Table 7 presents the results for the CASE 3 reference system. Internal heat exchanger effectiveness and discharge pressure used in the reference system are the same as in CASE 2, $\eta_{IHX} = 30\%$ and $P_{GC} = 90$ [bar]. Evaporating temperature at low temperature is set to $T_{LT} = -25$ [$^{\circ}C$].

Table 7: CASE 3: reference system, [$\eta_{IHX} = 30\%$ and $P_{GC} = 90$ [bar]]

T_{SW} [$^{\circ}C$]	\dot{Q}_{RSW} [kW]	\dot{Q}_{AC} [kW]	\dot{Q}_{LT} [kW]	COP_{TOT} [-]
15	154	173,8	81,6	3,0
25	150,1	114,1	81,6	2,6
35	145,9	3,7	81,6	1,7

Table 7 shows a drastic decrease in RSW refrigeration capacity at all temperature levels when compared to the reference systems in CASE 1 and CASE 2. At $T_{SW} = 15$ [$^{\circ}C$] the decline is 50% when compared to CASE 2 and 63% when compared to CASE 1. This can be explained by the system utilizing only one compressor (C2) providing the RSW chilling. The refrigeration capacities at AC pressure is similar to the ones in CASE 2 as a consequence of the same discharge pressure used in both cases. The small difference can be attributed to the difference in mass flow in CASE 2

and 3, resulting in different cooling capacities of internal heat exchangers. An increase in seawater temperature drastically reduces the AC refrigeration capacity. The decrease is similar to the one in CASE 2. The RSW refrigeration capacity is not so affected by the seawater temperature, with only 0,6% decrease in \dot{Q}_{RSW} when increasing $T_{SW} = 15 [^{\circ}C]$ to $T_{SW} = 35 [^{\circ}C]$. This is graphically illustrated further in Figure 51. The LT refrigeration capacity \dot{Q}_{LT} is unaffected by the different seawater temperatures, as long as the discharge pressure is constant. The refrigeration capacity in this simulation at P_{LT} depends only on the pressure chosen for the freezing operation. Different possible capacities at LT will be further looked upon in this section.

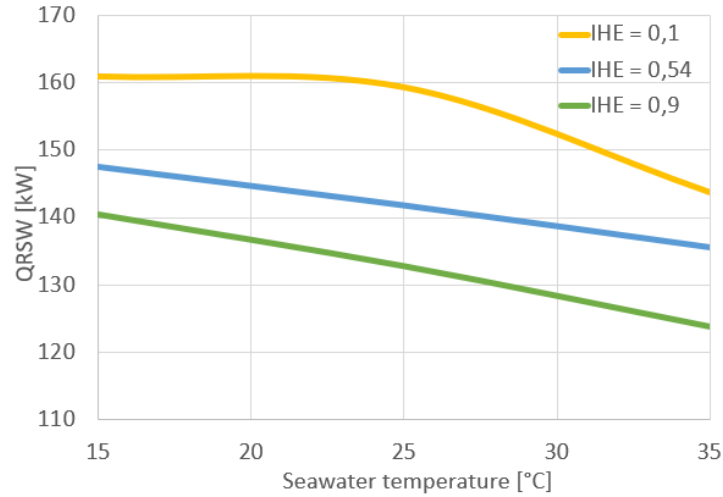


Figure 50: CASE 3: Refrigeration capacity vs seawater temperature

The RSW refrigeration capacity is calculated for different seawater temperatures and plotted in Figure 50. The plot illustrates IHX effectiveness, η_{IHx} on \dot{Q}_{RSW} , assuming the same effectiveness for both heat exchangers. The benefits of efficient IHX are not seen in the presented temperature range: RSW refrigeration capacity is larger with an efficiency of IHX at $\eta_{IHx} = 0, 1$.

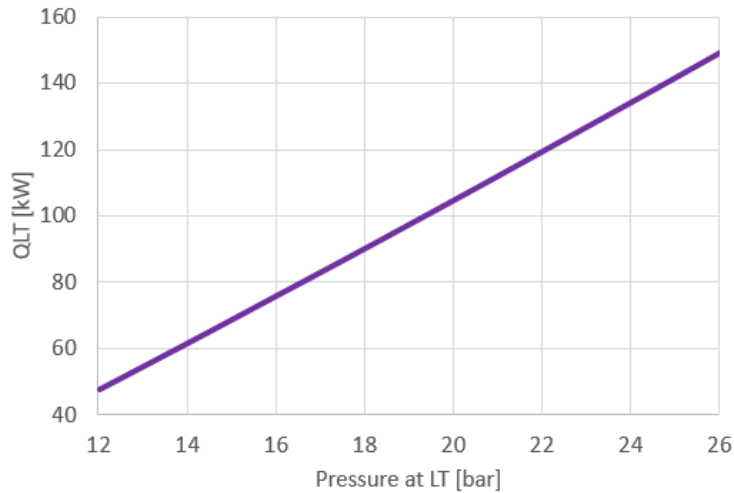


Figure 51: CASE 3: Refrigeration capacity at LT vs Pressure at LT

The LT refrigeration capacity \dot{Q}_{LT} is calculated at different pressure levels P_{LT} and plotted in Figure 51. As mentioned earlier, the \dot{Q}_{LT} is not affected by the seawater temperatures, meaning the presented line is fitting for all ambient conditions mentioned in this chapter.

Figure 52 presents the influence of η_{IHX} and T_{SW} on systems COP at different discharge pressures. T_{SW} , η_{IHX} and P_{GC} chosen for CASE 3 are the same as in CASE 1 and CASE 2 (Figure 44 and 49). The pressure in the AC receiver is kept at $P_{AC} = 40$ [bar] and LT pressure at $P_{LT} = 17$ [bar]. Similar to results obtained in CASE 1 and CASE 2, the system performs better with high efficient IHXs, when considering systems COP.

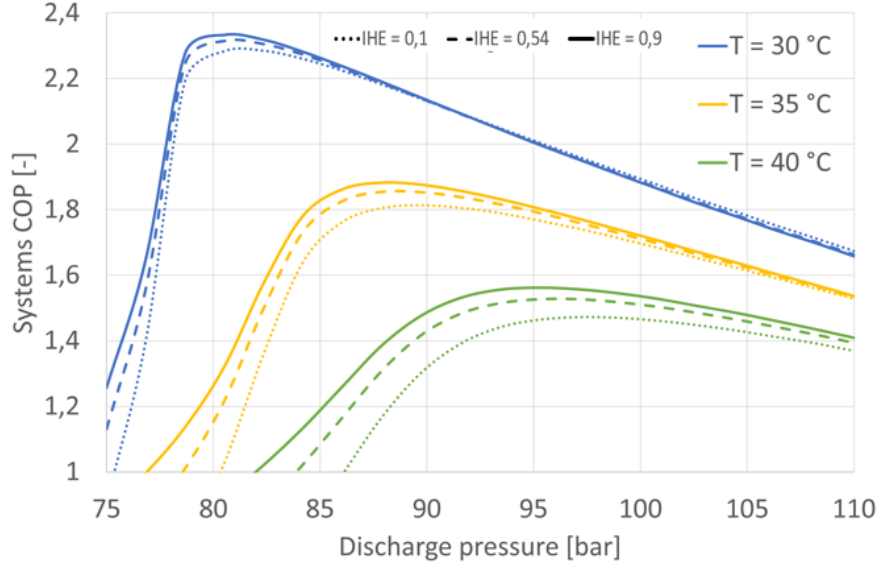


Figure 52: CASE 3: COP vs discharge pressure at different seawater temperatures

The optimum discharge pressure correlation developed for CASE 3, considering systems COP is:

$$P_{OPT} = 1,473 * (T_{SW} + 4) + 30,446 \text{ [bar]} \quad (34)$$

Table 8: CASE 3: RSW, AC and LT refrigeration capacity at different seawater temperatures, at optimum P_{GC} , considering systems COP

T_{SW} [°C]	η_{IHX} [-]	\dot{Q}_{RSW} [kW]	\dot{Q}_{AC} [kW]	\dot{Q}_{LT} [kW]	COP_{TOT} [-]
30	0,9	129,4	57,8	85,5	2,3
35	0,9	123,9	15,3	82,5	1,7
40	0,9	116,3	0	79,5	1,4

Considering RSW refrigeration capacity is still the main task of the refrigeration system, optimization of P_{GC} further is done to obtain the largest \dot{Q}_{RSW} . Based on results shown in Figure 52, the system will use $\eta_{IHX} = 0,1$. \dot{Q}_{RSW} is calculated and plotted in Figure 53 as a function of the discharge pressure.

Assuming $\eta_{IHX} = 0,1$, the optimum discharge pressure developed in Figure 53 gives the following correlation, considering \dot{Q}_{RSW} :

$$P_{OPT} = 2,601 * (T_{SW} + 4) - 8,119 \text{ [bar]} \quad (35)$$

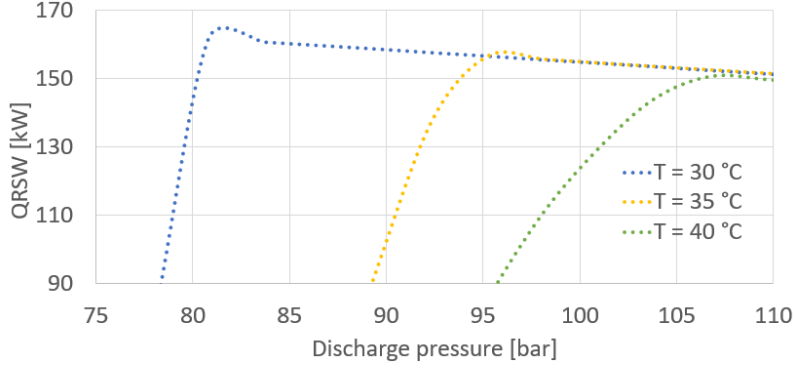


Figure 53: CASE 3: RSW refrigeration capacity vs discharge pressure at different seawater temperatures

Table 9: CASE 3: RSW, AC and LT refrigeration capacity at different seawater temperatures, at optimum P_{GC} , considering \dot{Q}_{RSW}

T_{SW} [$^{\circ}C$]	η_{IHX} [-]	\dot{Q}_{RSW} [kW]	\dot{Q}_{AC} [kW]	\dot{Q}_{LT} [kW]	COP_{TOT} [-]
30	0,1	161,9	12	85,55	2,2
35	0,1	156,5	11,4	80,3	1,7
40	0,1	151,1	2	75,1	1,4

Results in Table 9 shows an increase in RSW refrigeration capacity compared to results in Table 8; at $T_{SW} = 30$ [$^{\circ}C$] by 25%, at $T_{SW} = 35$ [$^{\circ}C$] by 26% and at $T_{SW} = 40$ [$^{\circ}C$] by 30%. CASE 3 yield smaller refrigeration capacity at RSW regardless of seawater temperature, when compared to CASE 1 and CASE 2. Although, CASE 3 yields three evaporating temperatures. Comparing systems COP in Table 8 and Table 9, at temperatures above critical one, the system performs likewise with a $\eta_{IHX} = 0,1$ and $\eta_{IHX} = 0,9$. Comparing the \dot{Q}_{AC} in Table 8 and Table 9, the AC refrigeration capacities are similar at $T_{SW} = 35$ [$^{\circ}C$] and $T_{SW} = 40$ [$^{\circ}C$]. At $T_{SW} = 30$ [$^{\circ}C$], the \dot{Q}_{AC} is almost five times larger in Table 8 than in Table 9.

5.1.4 CASE 4: HP ejector

CASE 4 represents utilization of a high-pressure multi ejector to optimize the RSW system further. As in previous sections, this solution utilizes two internal heat exchangers (IHX1 and IHX2), three pressure levels (HP, AC and RSW pressure), with three compressors (C1, C2 and C3). The ejector removes a part of the gas out of the RSW separator, hence unloading compressors C2 and C3.

Table 10: CASE 4: reference system [$\eta_{ejector} = 30\%$, $\eta_{IHX} = 30\%$ and $P_{GC} = 90bar$]

T_{SW} [$^{\circ}C$]	\dot{Q}_{RSW} [kW]	\dot{Q}_{AC} [kW]	COP_{TOT} [-]
15	404,3	83,62	3,4
25	414,5	0	2,8
35	282,2	0	2,0

Table 10 shows the refrigeration capacity at AC and RSW pressure and systems total COP. The internal heat exchangers and the ejector effectiveness ($\eta_{IHX} = \eta_{ejector}$) is set to 30% in the reference system. Table 10 shows a strong increase in RSW refrigeration capacity, when compared to the reference system in CASE 2 (Table 3). At $T_{SW} = 15$, 25 and 35 [$^{\circ}C$], the increase is accordingly 31%, 38% and 5,3% considering RSW cooling. However, the refrigeration capacity at AC is smaller in CASE 4 compared to CASE 2, while systems COPs are alike at seawater temperatures presented in Table 10.

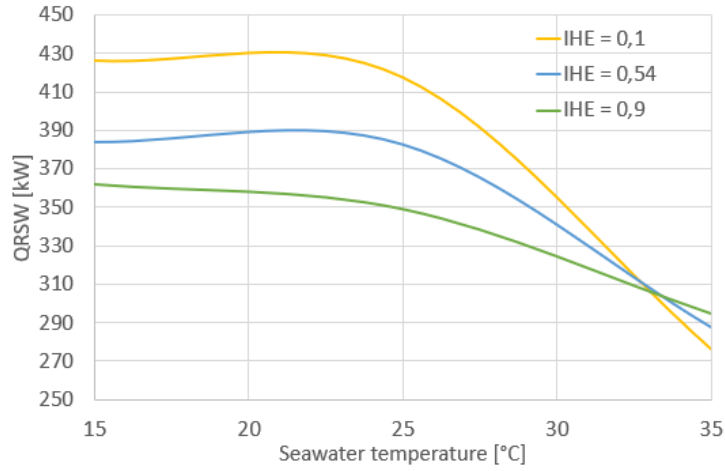


Figure 54: CASE 4: RSW Refrigeration capacity vs seawater temperature [$P_{GC} = 90$ [bar] and $\eta_{ejector} = 30\%$]

The RSW refrigeration capacity is calculated at different seawater temperatures and plotted in Figure 54. The efficiency of the ejector, is set to 30%. The influence of efficiency of the internal heat exchangers ($\eta_{IH X}$) on the refrigeration capacity is significant; at $T_{SW} = 15$ [°C] the value of RSW refrigeration capacity increases by 19% when decreasing the $\eta_{IH X}$ from 90% to 10%. The reason for the increase is the volumetric cooling effect of the internal heat exchangers increases with an increase of their efficiency. This is not beneficial at temperatures below critical temperature of CO_2 . Therefore, further analysis of the system is done by cutting of the internal heat exchangers using two bypass valves.

Figure 55 presents the influence of the efficiency of ejector on the RSW and AC refrigeration capacity. The temperature range chosen for the calculations is [15°C – 30 °C]. The efficiency of the ejector used are 0%, 20% and 30%.

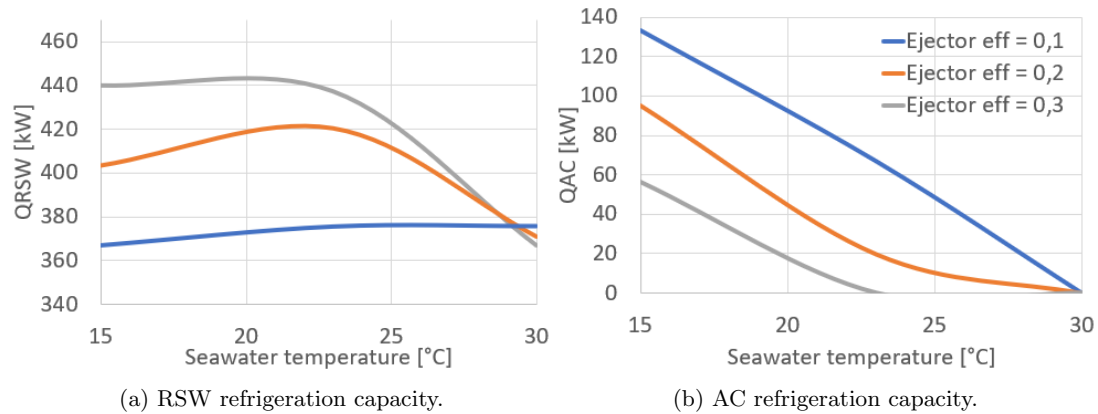


Figure 55: CASE 4: RSW and AC Refrigeration capacity vs seawater temperature [$P_{GC} = 90$ [bar], IHX bypass]

Figure 55a indicates a significant increase of the RSW refrigeration capacity utilizing an efficient ejector. At $T_{SW} = 15$ [°C] the \dot{Q}_{RSW} increases by 16% by increasing the efficiency of ejector from 10% to 30%. Although, at the same time, the \dot{Q}_{AC} decreases by 56%, shown in Figure 55b. An efficient ejector will increase the flow at the suction line, hence compressing a larger part of the RSW separator's refrigerant. Accordingly, as mentioned in Section 3.2, unloading the RSW compressors to the AC compressor's detriment, hence a smaller refrigeration capacity at AC. Another benefit utilization of an effective ejector, shown in Figure 55a, is stable RSW capacity up to around 23 °C at RSW.

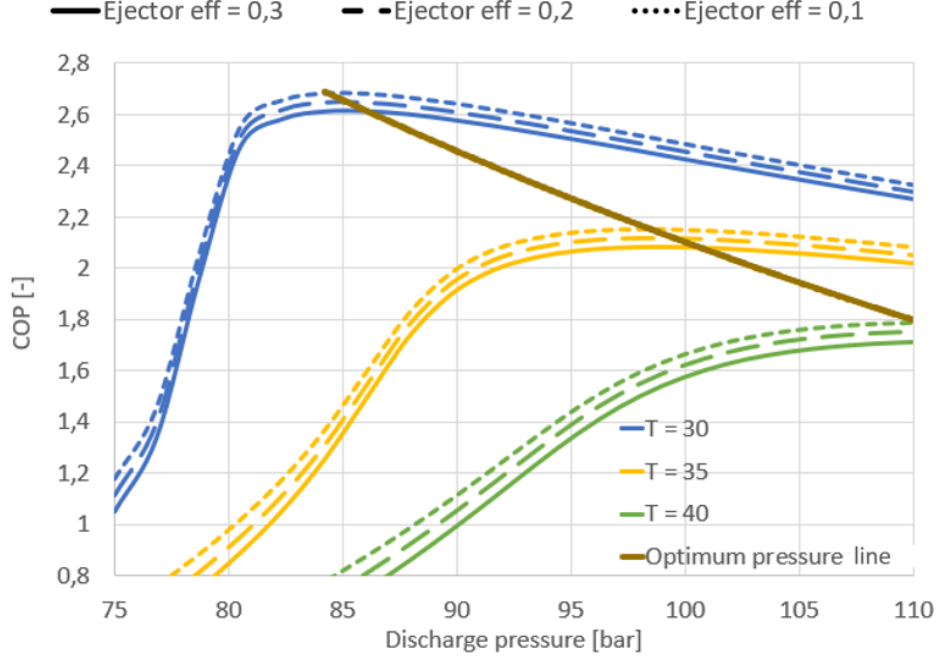


Figure 56: CASE 4: Optimum high pressure considering COP at $T_{RSW} = 30, 35$ and 40 [$^{\circ}C$], [IHX bypass]

Figure 56 presents further the influence of P_{GC} , $\eta_{ejector}$ and T_{SW} on systems COP. As in previous cases, the figure considers high seawater temperatures, $T_{SW} = 30$ [$^{\circ}C$], $T_{SW} = 35$ [$^{\circ}C$] and $T_{SW} = 40$ [$^{\circ}C$]. When seawater temperature (T_{SW}) and discharge pressure (P_{GC}) are fixed, the system gives a higher COP with a less efficient ejector. This is due to larger decrease of AC refrigeration capacity \dot{Q}_{AC} , compared to the increase of RSW refrigeration capacity \dot{Q}_{RSW} when utilizing an efficient ejector. Although, at $T_{SW} = 30$ [$^{\circ}C$] and $P_{GC} = 84,2$ [bar] the decrease in COP utilizing an efficient ejector is 2,5%.

Assuming $\eta_{ejector} = 30\%$, bypassing the internal heat exchangers, and considering systems COP, the optimum discharge pressure developed using Figure 56 gives the following correlation:

$$P_{opt} = -0,0738 * T_{SW}^2 + 7,745 * T_{SW} - 81,72 \text{ [bar]} \quad (36)$$

Table 11: CASE 4: RSW, AC and LT refrigeration capacity at different seawater temperatures, at optimum P_{GC} , considering systems COP

T_{SW} [$^{\circ}C$]	$\eta_{ejector}$ [-]	\dot{Q}_{RSW} [kW]	\dot{Q}_{AC} [kW]	COP_{TOT} [-]
30	0,1	356,3	0	2,7
35	0,1	335	0	2,2
40	0,1	304,6	0	1,9

At $T_{SW} = 35$ [$^{\circ}C$], applying the optimum discharge pressure correlation (Equation 36), the refrigeration capacity increases by 19% compared to the reference system presented in Table 10. As a result of the increase in refrigeration capacity at RSW, the COP increased by 10%. Comparing with the optimized results in CASE 2, (Table 5):

- Systems COP in CASE 4 and CASE 2 at $T_{SW} = 30$ [$^{\circ}C$] and $T_{SW} = 35$ [$^{\circ}C$] is close. Although, the refrigeration capacity at RSW is 38% larger when utilizing an ejector.

- Increase in \dot{Q}_{RSW} and COP_{TOT} is also shown at $T_{SW} = 40$ [°C]. The RSW refrigeration capacity is 30% larger in CASE 4 than in CASE 2.
- CASE 4 presents no refrigeration capacity at AC at high seawater temperatures.

Equation 36 can also be applied considering the refrigeration capacity at RSW. Figure 55 visualizes the optimum ejector efficiency at seawater temperatures higher 29 °C is $\eta_{ejector} = 10\%$. Accordingly, values in Table 10 are also optimized considering \dot{Q}_{RSW} . The results are compared to the optimized results in CASE 2, considering \dot{Q}_{RSW} (Table 6); CASE 4 outperforming CASE 2, achieving a higher \dot{Q}_{RSW} and COP_{TOT} at all considered temperature levels.

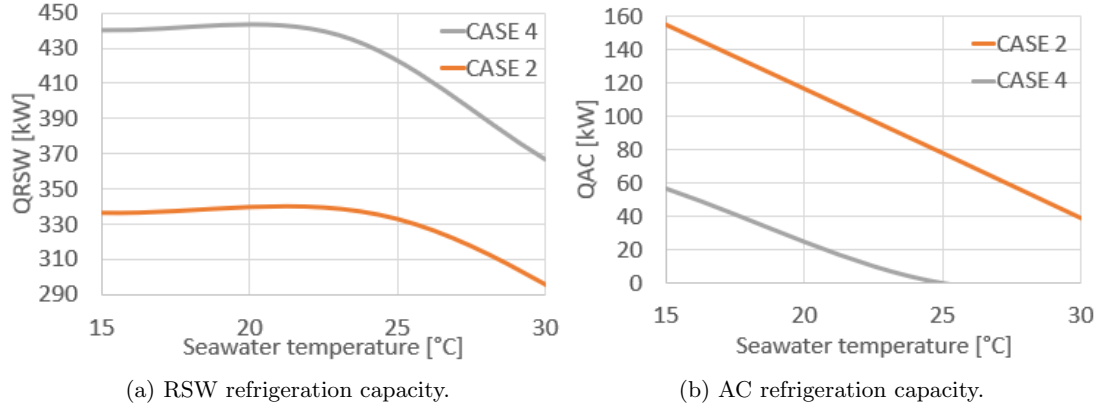


Figure 57: CASE 4 ($\eta_{ejector} = 30\%$, IHX bypass, $P_{GC} = 90$ [bar]) vs CASE 2 (IHX bypass, $P_{GC} = 90$ [bar])

Figure 57 and 58 presents the comparison of CASE 2 and CASE 4. The chosen temperature range for the calculations is [15 °C – 30 °C]. Considering refrigeration capacity at RSW, CASE 4 yields higher values when compared to CASE 2 throughout the chosen temperature interval. At $T_{SW} = 15$ [°C] the refrigeration capacity at RSW is 30% larger when applying the ejector solution. At AC pressure, CASE 2 achieves a higher refrigeration capacity than CASE 4. At $T_{SW} = 15$ [°C] the AC refrigeration capacity is 61% smaller for CASE 4 when compared to CASE 2.

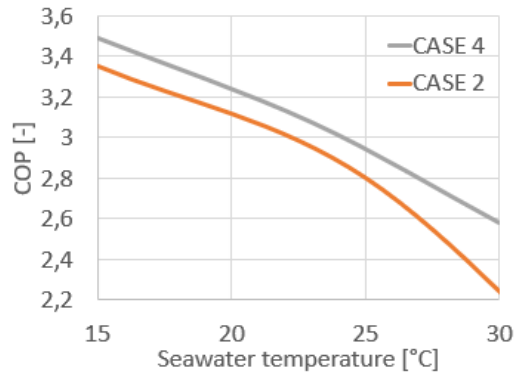


Figure 58: Systems COP: CASE 4 ($\eta_{ejector} = 30\%$, IHX bypass, $P_{GC} = 90$ [bar]) vs CASE 2 (IHX bypass, $P_{GC} = 90$ [bar])

When considering systems COP, CASE 4 achieves a higher COP at given temperatures, shown in Figure 58. At seawater temperature above 25 [°C], CASE 4 line has a lower gradient than CASE 2 line. The lower gradient is advantageous as it makes the system's performance less sensitive to the change in seawater temperature, when compared to CASE 2.

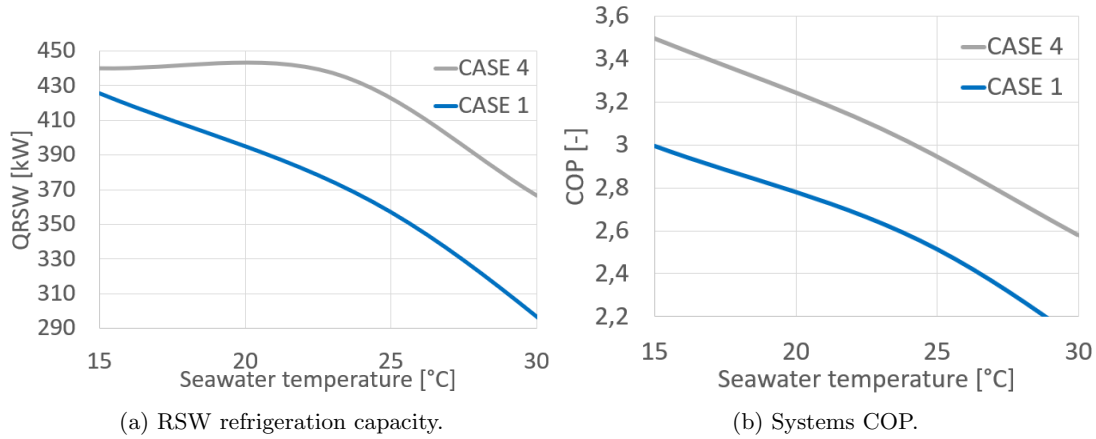


Figure 59: CASE 4 ($\eta_{ejector} = 30\%$, IHX bypass, $P_{GC} = 90$ [bar]) vs CASE 1 ($\eta_{IHX} = 10\%$, $P_{GC} = 90$ [bar])

The performance of CASE 1 and CASE 4 is evaluated and compared by calculating the \dot{Q}_{RSW} and COP at given seawater temperatures. The results are plotted in Figure 59. As can be observed in the figure above, CASE 4 achieves a higher \dot{Q}_{RSW} and COP_{TOT} throughout the temperature range. At $T_{SW} = 15$ [°C], the RSW refrigeration capacities are very close. However, at higher seawater temperatures, CASE 1 results in substantially lower COP and \dot{Q}_{RSW} when compared to CASE 4. The decrease in performance is as expected, as CASE 1 is more susceptible to high seawater temperatures than a more complex design in CASE 4. The trend in CASE 1 and CASE 4 COP and RSW capacity curves suggest CASE 4 as a better solution when applying the system at seawater temperatures above $T_{SW} = 15$ [°C]. Another advantage of CASE 4 is the possibility to provide the refrigeration at two temperature levels, although CASE 4 is not as simple as CASE 1 from a practical point of view.

5.1.5 CASE 5: LP ejector

CASE 5 reviews the fifth design for the system. CASE 5 provides a solution utilizing two evaporation pressure levels, at RSW and LT pressure. The ejector is a critical component in this system. Hot refrigerant leaving the gas cooler is then introduced to the LP ejector, sucks part of low-pressure refrigerant leaving the LT evaporator (Figure 28). Compressors C1 and C2 are providing the RSW refrigeration, while C3 is able to run as a auxiliary compressor providing cooling at LT. If an increase in RSW chilling is requested, all three compressors are available to provide the requested capacity. Accordingly, the ejector is solitary proving the LT cooling.

Table 12: CASE 5: reference system [$\eta_{ejector} = 30\%$, $\eta_{IHX} = 30\%$, $P_{GC} = 90$ [bar], C1, C2 – RSW and C3 – LT]

T_{SW} [°C]	\dot{Q}_{RSW} [kW]	\dot{Q}_{LT} [kW]	COP_{TOT} [-]
15	337,2	118,1	3,4
25	276,9	128,1	3,0
35	154,5	157,2	2,3

Table 12 presents the refrigeration capacity at RSW, LT and systems total COP. The discharge pressure is $P_{GC} = 90$ [bar], compressors C3 is running as LT compressors and $\eta_{IHX} = \eta_{ejector} = 30\%$. The increased amount of flash gas due to increase in T_{SW} , decreases the feeding of RSW evaporator, hence decreasing its refrigeration capacity. The influence of T_{SW} is significant, at $T_{SW} = 35$ [°C] the refrigeration capacity is 54% lower at RSW, when compared to at $T_{SW} = 15$ [°C]. The trend is visualized in Figure 60a. In contrast to the trend in RSW refrigeration capacity, Table 12 and Figure 60b show an increase in LT refrigeration when increasing T_{SW} . The value of LT refrigeration capacity increases by 33% when T_{SW} increases from 15 [°C] to 35 [°C].

The increase in LT refrigeration capacity can be attributed to increase in suction mass flow rate (\dot{m}_{sn}). This is a result of an increase in enthalpy difference at motive nozzle ($h_A - h_B$ in Figure 18) at higher seawater temperatures. Accordingly the systems COP at higher seawater temperature is greater, when compared to CASE 1 (Table 1), CASE 2 (Table 3), CASE 3 (Table 7) and CASE 4 (Table 10), especially at $T_{SW} = 35[^\circ C]$.

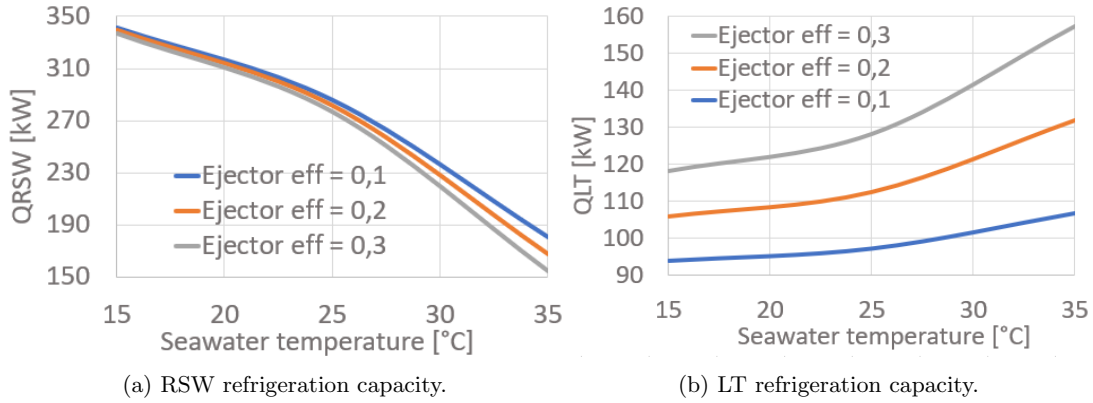


Figure 60: CASE 5 ($\eta_{ejector} = 30\%$, $\eta_{IHX} = 30\%$, $P_{GC} = 90$ [bar] and C1, C2 – RSW and C3 – LT)

Figure 60 presents the influence of $\eta_{ejector}$ on \dot{Q}_{RSW} and \dot{Q}_{AC} . The chosen seawater temperature range is $[15^\circ C - 30^\circ C]$. When considering the RSW refrigeration, the efficiency of ejector $\eta_{ejector}$ is not significant at temperatures below $25^\circ C$, shown in Figure 60a. At a seawater temperature of $15^\circ C$, the change in refrigeration capacity is 1,3% when changing effectiveness of the ejector from $\eta_{ejector} = 10\%$ to $\eta_{ejector} = 30\%$. At $T_{SW} = 35^\circ C$ the difference in \dot{Q}_{RSW} will increase to 7%. The effect of the efficiency of ejector is substantial when considering the refrigeration capacity at LT, visualized in Figure 60b. A higher efficient ejector will increase the suction mas flow \dot{m}_{sn} , thus increasing the LT evaporation capacity. The difference of refrigeration capacity is up to 24% when considering seawater temperatures presented in Figure 60. Figure 60 further displays an increment in LT refrigeration capacity when increasing T_{SW} discussed previously in this chapter.

When an increase in the RSW chilling is requested, all three compressors (C1, C2, C3) are available to provide the requested capacity. Accordingly, a decline in refrigeration capacity at LT is noted. The mas flow at the LT evaporator (EVAP 3) is now equal to the suction mas flow of the ejector \dot{m}_{sn} . \dot{Q}_{RSW} , \dot{Q}_{AC} and COP_{TOT} are then calculated and presented in Table 13.

Table 13: CASE 5: reference system [$\eta_{ejector} = 30\%$, $\eta_{IHX} = 30\%$, $P_{GC} = 90$ [bar] and C1, C2, C3 – RSW]

T_{SW} [$^\circ C$]	\dot{Q}_{RSW} [kW]	\dot{Q}_{LT} [kW]	COP_{TOT} [-]
15	414	43,5	3,2
25	341,4	54,5	2,8
35	196	88	2

Table 13 presents an expected decline in \dot{Q}_{LT} when compared to the values in Table 12. The increase of \dot{Q}_{RSW} is smaller than the decrease of \dot{Q}_{AC} , thus resulting in a reduction of systems COP as well. The \dot{Q}_{RSW} and its development at higher seawater temperatures is identical to the one found in CASE 1. The decrease results from both solutions utilizing all three compressors to deliver RSW cooling and one expansion from HP to RSW pressure. The trend considering \dot{Q}_{RSW} and \dot{Q}_{LT} is similar as in Table 12 and Figure 60.

Figure 61 presents the influence of discharge (P_{GC}) on systems COP. The pressure interval chosen for the calculations is $[75bar - 110bar]$, while the seawater temperatures chosen for the calculations are $T_{SW} = 30 [^\circ C]$, $T_{SW} = 35 [^\circ C]$ and $T_{SW} = 40 [^\circ C]$. At such high seawater temperatures, the control of discharge pressure is important to achieve high system COP, as shown in previous cases.

Figure 61 also demonstrates the benefits of an efficient ejector when the ambient temperatures exceed the critical temperature of CO₂. When T_{SW} and P_{GC} are fixed, the system yields higher COP utilizing $\eta_{IHX} = 30\%$. This is due to a larger increase in \dot{Q}_{LT} , when applying a more efficient ejector.

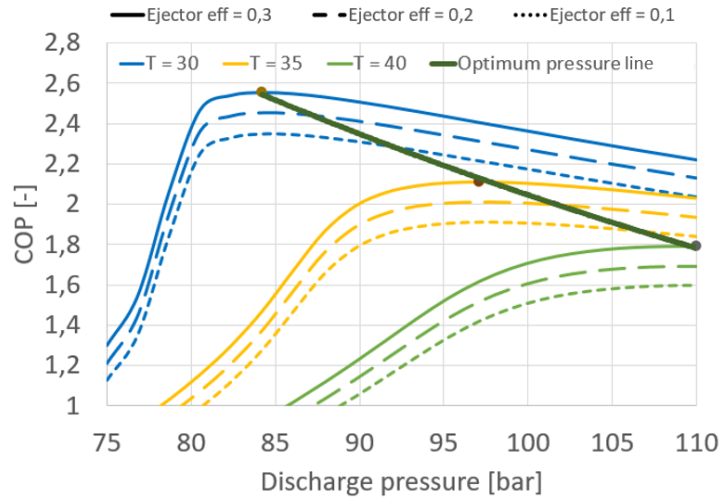


Figure 61: CASE 4: Optimum high pressure considering COP at $T_{RSW} = 30$ [°C], 35 [°C] and 40 [°C], [$\eta_{IHX} = 30\%$]

Assuming $\eta_{ejector}$, and considering systems COP, the optimum discharge pressure developed in Figure 61 gives a following correlation:

$$P_{OPT} = -0,0002 * T_{SW} + 2,593 * T_{SW} + 6,6 \text{ [bar]} \quad (37)$$

Figure 62 presents the comparison of system performance of CASE 4 and CASE 5 with respect to RSW refrigeration capacity and systems overall COP.

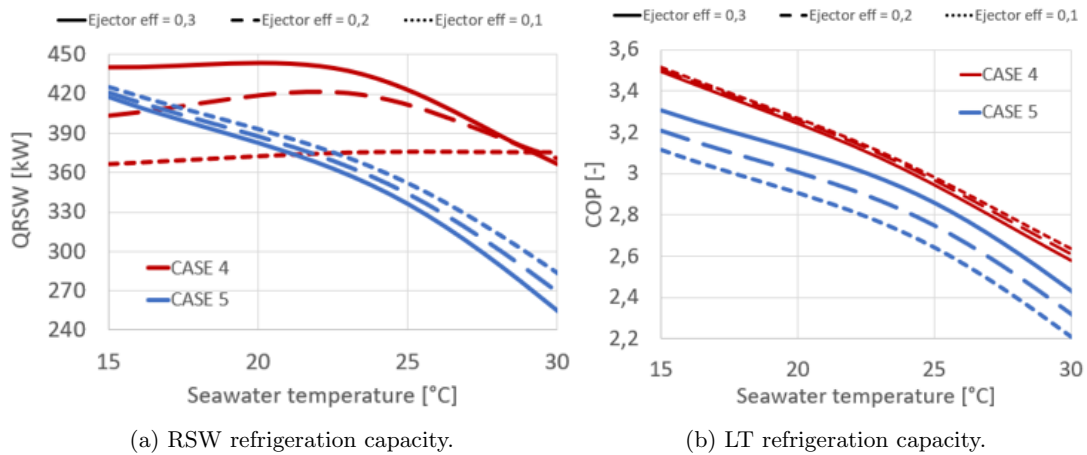


Figure 62: CASE 4 vs CASE 5 ($\eta_{ejector} = 30\%$, $\eta_{IHX} = 30\%$, $P_{GC} = 90$ [bar])

Three points can be observed from Figure 62:

- As shown in Figure 62b, CASE 4 results in higher system COP throughout the presented temperature range, achieving the maximum COP at 15 °C. Comparing to maximum COP

for CASE 5, the difference is 7% in COP. The difference is a result of CASE 4 using an auxiliary compressor to remove vapour from flashing after first expansion.

- Figure 62a shows CASE 4 results a more stable RSW capacity when compared to CASE 5. The difference is partly due to CASE 4 utilizing double throttling and auxiliary compressor, which are beneficial at high seawater temperatures. Furthermore, CASE 4 results in higher capacity at RSW, when utilizing $\eta_{ejector} = 30\%$. The difference is in a range of $[20kW - 80kW]$, depending on seawater temperature and chosen ejector efficiencies.
- Good COP in CASE 4 (HP ejector) is obtained with a low efficient ejector, while CASE 5 (LP ejector) performs better with a high efficient ejector. When considering \dot{Q}_{RSW} , the results show an apposite trend.

5.2 Dynamic loads performance

This section presents results from simulations performed with Dymola. The results are presented in three cases; 1) CASE 1: RSW system utilizing three compressors to provide the RSW cooling demand, 2) CASE 2: Double expansion with an auxiliary compressor, 3) CASE 4: similar to CASE 2 with utilization of a high pressure ejector.

5.2.1 Validation by comparison with EES results

The simulation models are validated by comparison of the results in EES and Dymola. It should be noted that validation is a non-trivial task as both numerical simulation programs have uncertainties in their calculations. The main aim of the validation is to ensure that the simplified regulation system which are utilized in all cases in Dymola, are sufficient to provide realistic system performance at dynamic cooling loads. Mean absolute percent error (MA%E) is used for validation, as described in Section 4.6.

Table 14 shows the COP and \dot{Q}_{RSW} MA%E error obtained with Dymola and EES models at different gas cooler pressures. The pressure interval chosen for the calculations is [75bar – 95bar], where a total of 10 pressure levels are analyzed. The temperature of refrigerant out of the gas cooler was set at a stable 22°C and full load operations was set up for all systems.

Table 14: Validation of simulation models [$P_{GC} = [75 \text{ bar} - 95 \text{ bar}]$ and $T_{GCout} = 22 [^{\circ}C]$]

Simulation model	COP error [MA%E]	\dot{Q}_{RSW} error [MA%E]
CASE 1	5,95	4,81
CASE 2	4,42	1,56
CASE 4	4	1,20

In Table 15, the variation of the COP and \dot{Q}_{RSW} are compared between the Dymola and EES models at different T_{GCout} , to evaluate the reliability of simulation calculations. This time, a total of 10 temperature points are analyzed in the following temperature interval, [15°C – 32,5°C]. The discharge pressure is at a constant 90 bar.

Table 15: Validation of simulation models [$P_{GC} = 90 [\text{bar}]$ and $T_{GCout} = [15^{\circ}C - 32,5^{\circ}C]$]

Simulation model	COP error [MA%E]	\dot{Q}_{RSW} error [MA%E]
CASE 1	6,19	4,87
CASE 2	3,80	1,95
CASE 4	3,35	4,67

The comparison shows that the Dymola model calculates the COP and \dot{Q}_{RSW} , within an MA%E error of 10% when compared to EES results. Based on the recommendation from Kleijnen (25), the presented errors are acceptable.

5.2.2 Models comparison (CASE 1, CASE 2 and CASE 4)

RSW chilling onboard fishing vessels can be divided to three time periods: 1) Prechilling, 2) Chilling and 3) Maintenance (34). The RSW chilling period begins when the last fish has been loaded in the RSW tank. Accordingly, the initial seawater temperature in the tank will be in the range of the initial fish temperature and the prechilled seawater temperature. Based on field measurements, the initial temperature of the prechilled seawater of 3°C is used in the following simulation scenarios (34). The average temperature in the catch when the chilling period begins is assumed to be 6 °C.

Figure 63 show the temperature development within the heat capacitor, representing the catch. At time 0, as the refrigeration system is engaged, there is a rapid decrease in temperature considering all three presented cases. As the temperature is decreasing, a smaller temperature gradient is noticeable. Figure 63a show the COP for the chilling period, considering CASE 1, CASE 2 and CASE 4. Notice a significant change in COP after the inflection point. The increase in system COP is a result of suction pressure increase during the maintenance period. The increase in suction pressure is a result of the control strategy chosen to resemble the gravity-fed evaporators (Section 4.5.2) and the seawater pump controller for RSW (Section 4.5.5). To ensure an 80% outlet quality of the refrigerant and seawater outlet temperature of $-1,5\text{ }^{\circ}\text{C}$, the system pressure increases, hence the increase in system COP. Figure 63a illustrates a larger increase increase for CASE 4 in COP as a result of the ejector providing the requested maintenance cooling without utilization of RSW compressors. Accordingly, RSW and AC cooling is provided by the auxiliary compressor, therefore a substantial increase in systems COP is noticed.

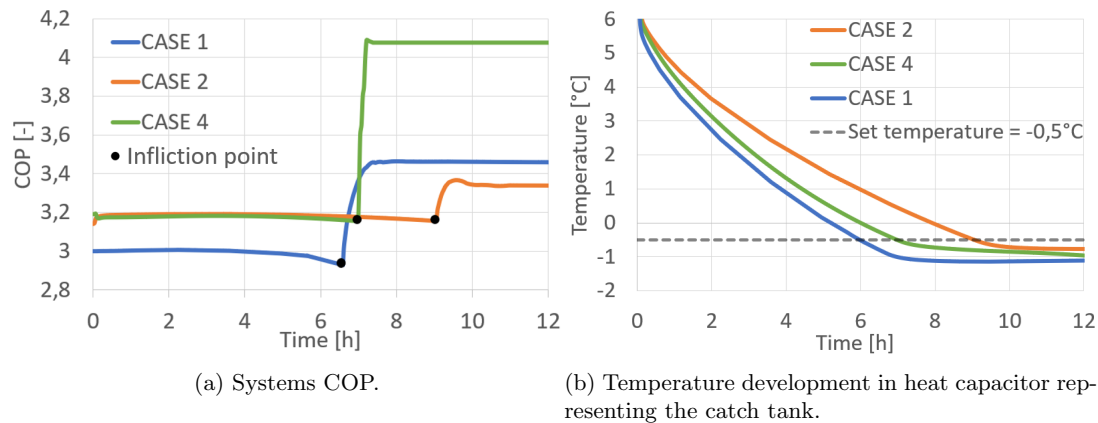


Figure 63: CASE 1, CASE 2 and CASE 4 comparison

Figure 63b show a considerable difference in chilling time. The chilling time is the time taken to lower the temperature of seawater in the RSW tank from its initial temperature to a given temperature. The set temperature is $-0,5\text{ }^{\circ}\text{C}$, and is marked as a dotted horizontal line in Figure 63b. From the figure above, it may be concluded that the rate of cooling is faster for CASE 1 compared to CASE 2 and CASE 4. The difference in cooling time is 19% and 53%, respectively. The increase in chilling time can be explained by the decrease in refrigeration capacity utilizing CASE 2 and CASE 4, due to their system architecture described in Section 5.1.2 and 5.1.4.

When considering systems COP, CASE 1 yields a lower value at full load operation when compared to CASE 2 and CASE 4, visualized in Figure 63a. CASE 2 and CASE 4 yield a higher systems COP during the chilling period. The difference is a result of CASE 4 and CASE 2 applying an auxiliary compressor after the first expansion. As explained before, CASE 4 results in higher systems COP at part load operation. CASE 2 yield a smaller increase after the inflection point, when compared to CASE 1, as a result of utilizing two compressors (C1 and C2) to provide the requested cooling. If no AC cooling is requested during maintenance, CASE 2 is able to function as CASE 1 by turning of the auxiliary compressor, thus achieving higher system COP shown in Figure 63a.

Maintenance chilling onboard fishing vessels last until the vessel is stationed at the harbour and ready for unloading. During maintenance, the loads are primarily due to the transmission losses. The length of this period can reach up to 39 hours for vessels going far to the sea, which can potentially translate to 48-67% of overall system performance time (34). Accordingly, high system COP is crucial to ensure a sound overall efficiency of the refrigeration system. As can be seen in Figure 63a there is a large difference in systems COP between the initial and maintenance chilling periods. Taking into account a long maintenance period and results in Figure 63, CASE 4 can be argued to be a superior solution considering the overall system efficiency; CASE 4 provides a fast chilling time, resulting potentially in better preservation of the catch, and in high system COP

during maintenance chilling.

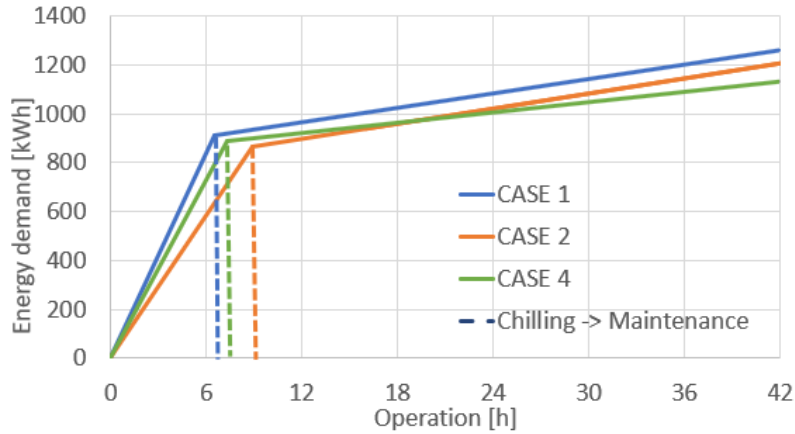


Figure 64: Energy demand during chilling and maintenance period [$T_{SW} = 17$ [°C], $P_{GC} = 90$ [bar] and $\dot{Q}_{Maintenance} = 30$ [kW]]

Figure 64 shows the share of energy demand during chilling and maintenance. Less energy demand throughout the trip will result in better system performance and less fuel consumption considering electric power onboard fishing vessels is provided by a petrol engine. As shown in the figure above, the period length of maintenance chilling predominantly affects overall energy demand. CASE 1 results in a less chilling time when compared to CASE 2 and CASE 4, visualised in Figure 64. CASE 4 results in less hourly energy demand during maintenance compared to CASE 1 and CASE 2. The difference is visualised by a smaller gradient for the CASE 4 line in comparison with the CASE 2 line, shown in Figure 64,. After 42 hours of operation, CASE 4 yields an overall lower energy demand compared to CASE 1 and CASE 2. The difference is 9% and 13%, respectively, as a result of a better balance between COP and chilling time for CASE 4.

Figure 65 presents the overall energy demand, now at a higher ambient temperature, $T_{SW} = 27$ [°C]. The high seawater temperature increases the refrigerant’s temperature out of the gas cooler and the transmission losses at RSW tanks. The initial temperature of the prechilled seawater in RSW tanks is assumed to be identical as in the previous case. Considering the result in Figure 65, CASE 4 is arguably the favourable solution. Compared to CASE 1 and CASE 2, the difference in chilling time is 14% and 50%, respectively. Additionally, CASE 4 results in less hourly energy demand compared to CASE 1 and CASE 2 visualized in Figure 65 throughout the maintenance period. CASE 2 is arguably to be the least attractive solution due to long chilling time and higher energy demand throughout the chosen time interval. The low performance of CASE 2 when compared to CASE 1 is explained by “built in” AC capacity.

The results are as expected due to a reduction in energy consumption utilizing an ejector for warmer climates (8), (17). As already indicated in Section 5.1.4 and 5.1.5, CASE 4 is less sensitive to high ambient temperatures when compared to CASE 1 and produce more refrigeration capacity than CASE 2 at full load operation. Additionally, CASE 4 delivers the requested cooling RSW, applying only the auxiliary compressor (C1) throughout the maintenance period. After 42 hours of operation, the difference in energy demand is 380 kWh when comparing CASE 4 to CASE 1 (24% difference) and 525 kWh when comparing CASE 4 and CASE 2 (33%) The substantial difference is a result of a lower chilling time and hourly energy demand throughout the maintenance period.

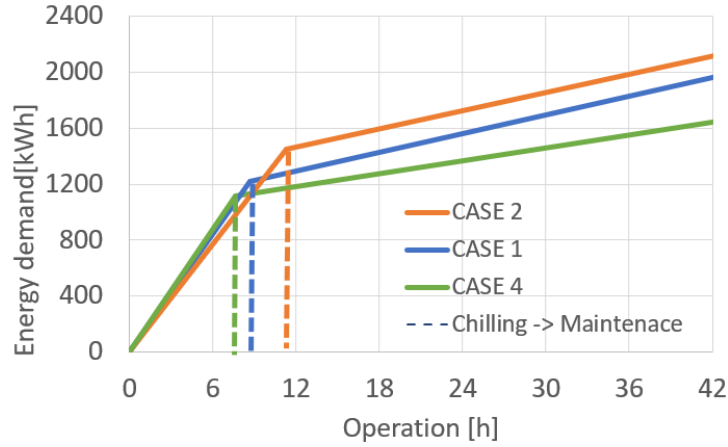


Figure 65: Energy demand during chilling and maintenance period [$T_{SW} = 27$ [°C], $P_{GC} = 90$ [bar] and $\dot{Q}_{Maintenance} = 60$ [kW]]

5.2.3 CASE 4 - ejector efficiency

The following section describes the effect of ejector efficiency, $\eta_{ejector}$, on system performance at part load and full load operation. As described in Section 2.4.4, the system is equipped with a Danfoss Multi Ejector. The following ejector has a range of ejectors installed in one unit, matching the capacity demand using different numbers and combinations of these (14). Accordingly, to replicate the control system, the input parameter for the ejector Dymola component is its efficiency, explained in Section 4.5.4. The chosen efficiencies of investigation, similar as in the initial EES calculations, are 10%, 20% and 30%.

The influence of the $\eta_{ejector}$ on temperature development of the catch and systems COP is analyzed in Figure 66. The refrigerants temperature out of the gas cooler is at 22 °C, and the discharge pressure is at 90 bar. Similar as in previous section, the set temperature is at -0,5 °C.

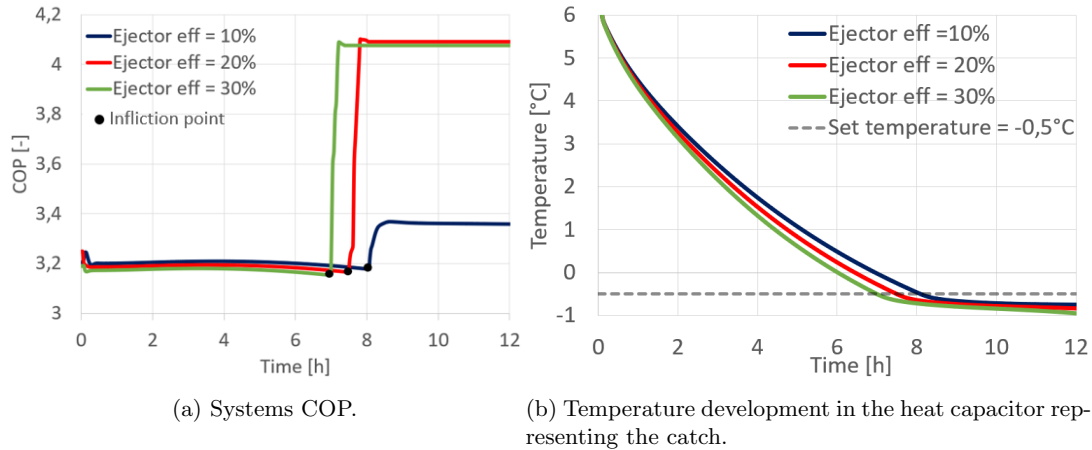


Figure 66: CASE 4 with utilizing $\eta_{ejector} = 10\%$, $\eta_{ejector} = 20\%$ and $\eta_{ejector} = 30\%$; $T_{GCout} = 22$ [°C]

Figure 66b and Figure 66a show a decrease in chilling time when utilizing an efficient ejector. As shown, a 15,6% increase in refrigeration time is noticed, when decreasing the efficiency from $\eta_{ejector} = 30\%$ to $\eta_{ejector} = 10\%$. An efficient ejector increases the flow at the suction line, consequently compressing a larger part of the gas in the RSW separator when compared to a less efficient ejector. Hence, an increase in RSW refrigeration capacity and a decrease in chilling time.

The increase in refrigeration capacity is also described and displayed in Section 5.1.4, Figure 55. During the chilling period, all three described cases yields similar system COP, shows in Figure 66a prior to the inflection point. The somewhat larger COP utilizing $\eta_{ejector} = 10\%$ is as well noticed during the initial calculations in EES in Section 5.1.4.

The maintenance period starts when the set temperature is reached in the RSW tank, visualized as the inflection point in Figure 66a. A significant increase in systems COP is noticed for all three system configuration. The systems utilizing $\eta_{ejector} = 20\%$ and $\eta_{ejector} = 30\%$ achieve a much higher COP increase than the system utilizing $\eta_{ejector} = 10\%$. The difference is due to the high-pressure ejector providing the requested cooling without using the RSW compressors, as a result of small heat loads during maintenance. An ejector with a 10% efficiency cannot provide the requested cooling; ergo, one RSW compressor (C2) is activated. The difference between the best and the worst COP is 0,72.

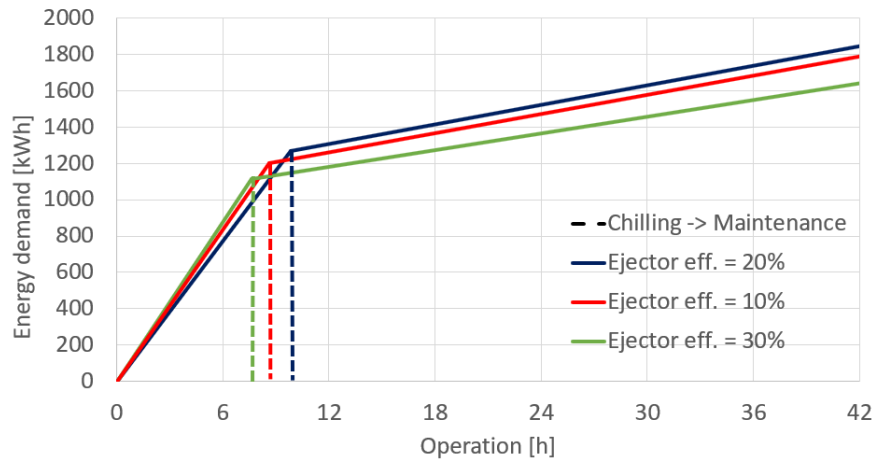


Figure 67: Energy demand during chilling and maintenance period altering ejector efficiency [$T_{GCout} = 32 [^{\circ}C]$, $P_{GC} = 90 [bar]$ and $\dot{Q}_{Maintenance} = 60 [kW]$]

It is well known that cooling systems with a series of multi-ejector configurations are reliable choices for higher ambient temperature. Figure 67 demonstrates the overall energy demand for CASE 4 utilizing multiple ejector efficiencies (10%, 20% and 30%), assuming $T_{GCout} = 32 [^{\circ}C]$. As expected, the efficiency plays a significant role in the chilling time, visualized by the dotted lines in Figure 67. The system utilizing $\eta_{ejector} = 30\%$ results in less chilling time when compared to $\eta_{ejector} = 20\%$ and $\eta_{ejector} = 10\%$. The difference in chilling time is 14% and 29%, respectively.

When considering maintenance chilling, system utilizing $\eta_{ejector} = 30\%$ results in less energy demand, as a result of higher system COP during chilling and maintenance. Systems operating with $\eta_{ejector} = 10\%$ and $\eta_{ejector} = 20\%$ is required to activate one RSW compressor, as the ejector alone is not able to deliver sufficient cooling. After 42 hours of operation, the most efficient system is utilizing $\eta_{ejector} = 30\%$, as a result best balance of chilling time and COP at part load operations. The difference is 165 kWh comparing $\eta_{ejector} = 30\%$ and $\eta_{ejector} = 20\%$, and 227 kWh comparing $\eta_{ejector} = 30\%$ and $\eta_{ejector} = 10\%$.

6 Discussion

Majority of the results are fully discussed in Chapter 5. This chapter will discuss some of the key findings and technicalities in a broader perspective regarding the steady-state performance.

6.1 Suggested control strategy

The main findings presented in Section 5.1 indicates that Principle Design 2 reviewed in Section 3.2 to be the most efficient and versatile throughout the analyzed conditions. The design allows the system to run as CASE 1, CASE 2, CASE 3 and CASE 4 based on the ambient conditions and demanded cooling onboard the fishing vessel. System architecture 2 produces up to 450 kW cooling at RSW, 160 kW at AC and 82 kW at LT, depending on the running configurations of the system.

The calculation for the reviewed system configurations shows that the ejector has a substantial impact on overall system performance. Perhaps the most significant result was obtained by the utilization of the ejector is the increase in RSW refrigeration capacity and its stability up to a seawater temperature of 25 °C. The increase was as expected, considering ejector is known to be an excellent solution for warmer climates. System architecture 2 results in an increase in RSW cooling in the range of [5% – 48%] compared to System architecture 1. Large RSW cooling capacity is beneficial considering the quality of the product depends on the chilling time. A larger system cooling capacity at RSW will result in less chilling time, thus better preservation of the catch. A fast chilling time can be dominant factor for the high seawater temperatures.

As mentioned earlier, System Architecture 2 can run in four different system configurations. Thereby proper control is necessary to minimize energy consumption and utilize the system's flexibility regarding different load parameters during a fishing voyage. Heating loads at RSW during a voyage can be divided into three parts: 1) Prechilling, characterized with high heating loads 2) Chilling, characterized with high heating loads and necessity of decreasing of the chilling time and 3) Maintenance chilling, characterized by lower heating loads but a long period of operation.

1) Prechilling:

In order to choose the right system configuration for prechilling mode, evaluation of important parameters such as load ratio and seawater temperature must be performed. The amount of heat load for prechilling depends on which tanks are charged, the target catch size and the initial seawater temperature. Prechilling is complete when seawater reaches a set temperature and is turned off again (34). Operation time during prechilling is not as crucial a parameter as power input to the system; therefore, high COP during prechilling is often more significant than RSW cooling capacity. As indicated in Section 5.1.4 (Figure 57 and Figure 59b), CASE 4 results in higher system COP and refrigeration capacity than CASE 1 and CASE 2, throughout the depicted temperature range. Therefore, based on the results, it is advised to utilize the ejector for the prechilling mode, regardless of seawater temperature.

The AC demand is also an essential factor to take into consideration for the analysis. It can be assumed that AC demand is reliant on the ambient temperature; increase in seawater temperature will result in increase in AC demand as well. If an increase in AC chilling is requested, system Architecture 2 will function as CASE 2, bypassing the ejector through an expansion valve. CASE 2 configuration will result up to 100 kW increase in cooling capacity at AC, when compared to CASE 4 (Figure 57). By doing that, the decrease in overall COP is in the range of [0,12 – 0,4], as a result in diminishing of RSW cooling capacity and not application of a two-phase ejector for recovering part of the expansion work.

2) Chilling:

The chilling period starts when the last fish has been loaded on board the vessel, and lasts until unloading. The amount of heat load for chilling depends on the actual catch size. There is never a guarantee for how much fish will be caught; hence heat load will vary from one trip to another. The

actual catch size impacts how to optimize the refrigeration process in terms of system configuration and operation. However, one thing all chilling periods have in common is the goal of limiting the chilling period. A faster chilling period limits the quality deterioration and is, therefore, an essential factor to consider.

Consequently, RSW refrigeration capacity is a priority when choosing a suitable system configuration. Based on results depicted in Section 5.1.4, CASE 4 is the recommended configuration. The ejector solution results in the most significant cooling capacity at RSW and better system COP, regardless of ambient conditions (Figure 57 and 59). CASE 4 can provide cooling at AC (0 – 55kW, depending on T_{SW}) to a seawater temperature 25 °C, which is beneficial for the overall comfort during the fishing voyage. When considering other system configurations; CASE 2 is not favourable as a result of AC demand not being an essential factor; CASE 1 is susceptible to increase in seawater temperature (up to 60 kW difference in RSW refrigeration capacity, shown in Figure 59); CASE 3 results in low RSW cooling capacity due to only one compressor working for RSW.

3) Maintenance:

Maintenance starts when the set temperature is reached in the RSW tanks during the chilling period. During maintenance chilling, the refrigeration system maintains a set temperature in the load until the fishing vessel reaches the harbour. As indicated in Section 2.5 and 4.5, the length of the maintenance will vary, but often is considered to be the most prolonged refrigeration period onboard a fishing vessel. The heat loads during the maintenance period are low and primarily due to infiltration loss.

The suitable system configuration for maintenance chilling is depended on AC and LT cooling demand. Requested cooling at RSW is assumed to be low and is therefore not relevant when choosing the suitable configuration. If AC demand is high during the trip, CASE 2 can be considered a good solution. At a seawater temperature of 15 °C, the system can provide up to 160 kW of AC cooling. The auxiliary compressor in CASE 2 (C1 in Section 3.1) is equipped with a frequency converter, thus adjusting to the demanded cooling at AC. RSW compressors are controlled by ON/OFF regulation and are activated based on the requested RSW refrigeration capacity. As a result of low RSW heating loads during maintenance, one compressor is often sufficient (C2). If LT cooling is requested, the remaining compressor (C3) can function as LT parallel compressor; thus, the CASE 3 configuration is activated. CASE 3 can cover 82 kW of cooling load at LT (Section 5.1.3), and at the same time provide cooling at AC and RSW.

CASE 4 is a favorable solution during part load operations as well. As a result of small requested cooling, the high pressure ejector could be able to provide the requested cooling demand without utilization of the RSW compressors (C2, C3). In the same way as in CASE 5 (Section 5.1.5) the mass flow at the RSW evaporator will be equal to the suction mass flow of the ejector. Additional benefit of the control strategy is utilization of only one compressor (C1) to deliver AC and RSW cooling, thus increasing systems COP and limiting the energy usage by the refrigeration system. Further simulation using Dymola and study on heat loads during maintenance are necessary to provide a insight in system performance for described cases at part load operations.

6.2 Overview of system improvements

The performance of the CO₂ refrigeration system can be optimized by adequately controlling some of the investigated parameters. High seawater temperatures lead to a decrease in enthalpy difference at the evaporator and consequently its cooling capacity. Several options for improvements have been examined for all reviewed cases, such as gas-cooler pressure control depending on the seawater temperature, efficiency of the heat exchangers, efficiency of the ejector, and the AC receiver's pressure.

Optimal gas cooler pressure

Based on performed simulations, it is evident that there is an optimal discharge pressure, giving a maximum COP. The systems COP increases quickly with increasing gas cooler pressure to the

extreme value and slowly decreases with further gas cooler pressure. The slight decrease can be advantageous, as the lower gradient makes the system's performance less sensitive to high-pressure control. COP improvements up to 15% at high seawater temperatures [30 °C - 45 °C] was achieved by utilizing an optimum gas cooler pressure. The same trend is noticed considering refrigeration capacity at RSW as well. The optimum COP values were curve fitted at multiple seawater temperatures in the range of 30°C to 45°C, and plotted in Figure 68a.

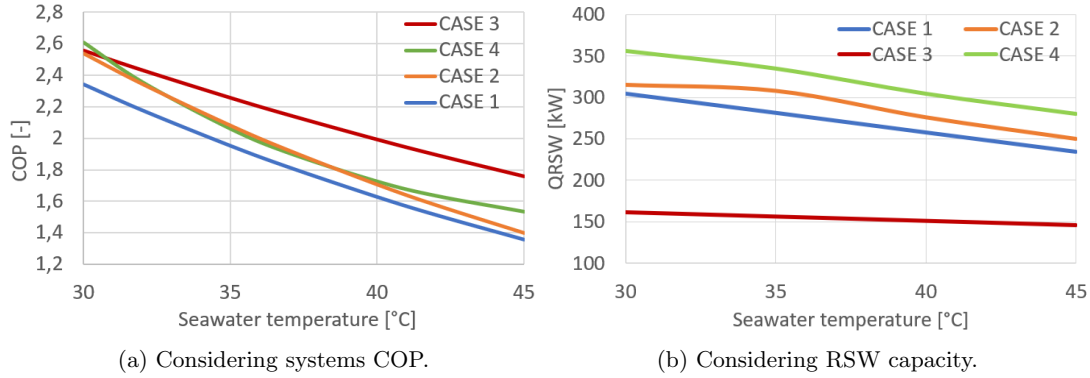


Figure 68: Optimal gas cooler pressure lines for the reviewed system configurations at seawater temperatures 30 °C or higher, [$\eta_{IHx} = 30\%$]

Figure 68a indicates what system configuration is the optimal choice when systems COP is the dominant factor. Maintenance chilling is an example of such a period. The high performance for CASE 3 considering COP is explained by the utilization of three-stage expansion with parallel compression. The optimum RSW values were curve fitted at multiple high seawater temperatures as well and plotted in Figure 68b. The results show a larger refrigeration capacity when utilizing an ejector (CASE 4). Figure 68b indicates what system configuration is the optimal choice when RSW cooling capacity is the dominant factor, such as in the chilling period.

Influence of internal heat exchangers

The influence of the efficiency of the internal heat exchanger on refrigeration capacity at RSW is considerable. Based on the results for all system configurations, the benefits of internal heat exchangers are noticed only during high seawater temperatures (above 30 °C). The reasoning is that the volumetric cooling effect of the internal heat exchangers will increase with its efficiency, and the start of the compression process will move to an area of greater superheat where the isentropic compression lines become flatter. Consequently, more power consumption by the compressors and decrease in systems COP. Based on presented calculations, it is advised to cut off the internal heat exchangers using two bypass valves at seawater temperatures lower than 30 °C, regardless of chosen system configuration.

Influence of ejectors efficiency

Results presented in Section 5.1.4 show an increase in RSW refrigeration capacity utilizing an efficient ejector. An efficient ejector result in a higher refrigeration capacity at RSW throughout the depicted temperature range. Taking into account the balance of AC and RSW cooling loads during a voyage, the correct control of Danfoss Multi Ejector described in Section 3.4.6, is essential to cover the requested cooling capacity at AC and RSW. The ejector will match the capacity demand using different number and combinations of ejectors.

7 Conclusion

An energy analysis of a prototype CO₂ trans-critical system for production of refrigerated sea water has been conducted, focusing on system performance, energy efficiency, and applicability for future installations at fishing vessels. The performance of the CO₂ system was analysed for five cases based on different system configurations using simulation software's EES and Dymola. The configurations include following options:

- **CASE 1:** All the three compressors (C1, C2, C3) are available to provide the requested RSW capacity.
- **CASE 2:** AC and RSW chilling, where compressor C1 is responsible for AC, while rest for RSW chilling.
- **CASE 3:** The system provides AC, RSW and LT cooling, where C1 is responsible for AC, C2 is responsible for RSW and C3 is responsible for LT storage. CASE 3 is a local solution of CASE 2.
- **CASE 4:** The parallel compression runs in conjunction with the ejector rack, providing AC and RSW cooling (CASE 2 + ejector).
- **CASE 5:** The parallel compression runs in conjunction with the ejector rack, providing RSW and LT cooling.

The simulation results revealed a high-performance increase utilizing a high-pressure ejector, especially at higher ambient temperatures. However, regarding the Dymola simulation models, there are still improvement opportunities regarding system simulation design. Additionally, a system will be built to conduct experiments considering predictions. The following list offers an insight into the most noteworthy discoveries made in this report:

Based on calculations made with Engineering Equation Solver:

- The influence of the efficiency of IHX on refrigeration capacity depends on the chosen system configuration. For CASE 1, the change is minor: at a seawater temperature of 15 °C with 90% effectiveness, the value of refrigeration capacity is 3% less when compared with the value at 10% effectiveness. For CASE 4, the change is 15%. However, one trend is noticed throughout all depicted operation modes. The RSW refrigeration capacity is larger, utilizing a lower efficient IHX at temperatures below the critical temperature of CO₂. Based on the presented calculations, it is advised to cut off the internal heat exchangers using two bypass valves at seawater temperatures lower than 30 °C, regardless of the chosen system configuration.
- System configurations utilizing an auxiliary compressor result in a stable RSW cooling capacity and an overall high system COP at seawater temperatures up to 25 °C.
- According to the simulation predictions, there is an optimal pressure for a maximum COP. The systems COP increases steeply with increasing gas cooler pressure to the extreme value and then slide decrease is observed with the further increasing of pressure. The slow decrease can be beneficial, as the lower gradient makes the system's performance less sensitive to the control of high pressure.
- The highest observed RSW refrigeration capacity was in CASE 4 when applying an efficient ejector. At a seawater temperature of 15 °C, the RSW refrigeration capacity was 440 kW.
- CASE 4 is arguably the superior solution compared to the others due to stable high refrigeration capacity at RSW, better COP, and cooling provided at two temperatures levels for AC and RSW.
- For CASE 5, an increase in LT refrigeration capacity is observed when increasing the seawater temperature. The increase can be attributed to an increment in suction mass flow rate at hotter ambient conditions. Accordingly, systems COP is more stable when compared to other system configurations.

Based on calculations performed with Dymola/Modelica:

- Considerable difference in chilling time is observed when utilizing ejector at high seawater temperature $T_{SW} = 28^{\circ}C$ (up to 53% difference). A faster chilling time limits food quality deterioration and is an essential factor when comparing system configurations.
- CASE 1, CASE 2 and CASE 4 were compared regarding power input during chilling and maintenance period. Length of maintenance chilling largely affects on the overall system performance. Accordingly, high system COP during the time period is essential to ensure as low power input as possible, resulting in overall lower fuel consumption.
- CASE 4 yields the best results considering maintenance chilling, with $COP = 4,1$ assuming seawater temperature at $18^{\circ}C$. The high COP is a result of the ejector providing the requested maintenance cooling without utilizing the RSW compressors. As a result of higher system performance during maintenance for CASE 4, the difference in power consumption is in the range of [9% – 33%], depending on the seawater temperature and hours of operation.
- CASE 2 is arguably the least attractive solution due to the long chilling time and higher power consumption throughout the chosen time period. The low performance of CASE 2 when compared to CASE 1 is explained by "built in" AC capacity.
- Considering CASE 4, the ejectors efficiency plays a significant role regarding the chilling time and power consumption throughout the maintenance period. A significant decrease in COP is noticed during maintenance applying an efficiency of 10%, assuming $T_{SW} = 28 [^{\circ}C]$. The low performance is explained by ejector not being able to cover the RSW cooling demand without using RSW compressor.

8 Further Work

This chapter reviews suggestion for further work. Some of the points are improvements for the models that already are developed, others regarding the extension of the work.

Measurements

The discoveries of this thesis are limited as a result of made assumptions and simplifications. Especially the results regarding the control strategy for Dymola simulations may alter from the control strategy implemented in reality. It is, therefore, essential to validate the simulation models with data from the future commissioning phase. Further, acquiring information on AC demands would also be helpful to generate simulation models and results that better reflect the energy flow of the RSW system.

Economical analysis

Energy- and economic analysis may be performed to conclude which system configuration is most economically rational to invest in. The analysis should be carried out as a comparative analysis between system configurations, evaluating the difference in power (fuel) consumption when accounting for conditions mentioned in this thesis.

Detailed simulations in Dymola

Improvement on the Dymola models presented in this report should focus on eliminating assumptions regarding constant heat transfer coefficients, pressure and heat loss. The compressors should be modelled as separated units with efficiency models and develop a more sophisticated control method for full and part load operations. Developing a model for a gravity-fed shell and tube heat exchanger should be focused on as well.

A single simulation model should be built with Dymola representing CASE 1, CASE 2, CASE 3, CASE 4 and CASE 5 in one model. Based on the results presented in this thesis, a control system should take advantage of the exemplary system configuration depending on ambient conditions and requested cooling. Thus, an optimized algorithm accounting for all variables should be developed and further implemented at full and part load operations. The model should also implement the gas cooler pressure equations developed in EES and a control valve bypassing the internal heat exchangers at certain operational conditions.

Thermal storage

Thermal storage integration with chilling systems could optimize the CO₂ system by implementing it for LT freezing. When the requested RSW cooling is at its maximum, potentially thermal storage could cover the LT freezing demand. The proposed thermal storage implementation is possible to examine in Dymola.

Bibliography

- [1] Alfa laval axp112 brazed plate heat exchanger. (accessed: 10.01.2021). URL: <https://www.lenntech.com/products/Alfa-Laval/AXP112/AXP112-Brazed-plate-heat-exchanger/index.html>.
- [2] Alfa laval axp52 brazed plate heat exchanger. (accessed: 10.01.2021). URL: <https://www.lenntech.com/products/Alfa-Laval/AXP52/AXP52-Brazed-plate-heat-exchanger/index.html>.
- [3] External trade in goods. export of fish, by species. (accessed: 05.02.2021). URL: <https://www.ssb.no/en/utenriksokonomi/statistikker/muh/aar>.
- [4] Modelica buildings library - user guide. (accessed: 04.05.2021). URL: <https://simulationresearch.lbl.gov/modelica/userGuide/bestPractice.html>.
- [5] Third imo ghg study 2014: Executive summary and final report. *International Maritime Organization*, 2015. doi:<https://unstats.un.org/sdgs/report/2020/The-Sustainable-Development-Goals-Report-2020.pdf>.
- [6] *GEA Bock HG Compressors for CO₂ Applications*. 2018.
- [7] Danfoss A/S. *Industrial Refrigeration, Ammonia CO₂ Applications*. 2014.
- [8] Armin Hafner, Sven Forsterling and Krzysztof Banasiak. Multi-ejector concepts for r-744 supermarket refrigeration. *International Journal of Refrigeration*, 2014.
- [9] Pradeep Bansal. A review - status of CO₂ as a low temperature refrigerant: Fundamentals and rd opportunities. *Applied Thermal Engineering*, 2012.
- [10] Bock. Hgx46/440-4 ml co2 t, areas of application. (accessed: 04.02.2021). URL: <https://vap.gea.com/stationaryapplication/Pages/Product.aspx?ItemObjectID=HGHAx2&Size=HGx46&ProductID=3768>.
- [11] M. H. Kim , J. Pettersen and Bullard. Fundamental process and system design issues in CO₂ vapor compression systems. *Process in Energy an Combustion Sceince*, 2004.
- [12] D.G. Mayer and D.G. Butler. Statistical validation. *Ecological Modelling*, 1993.
- [13] E. Torella, D. Sanches, R. Llopis and R. Cabello. Energetic evaluation of an internal heat exchanger in a CO₂ transcritical refrigeration plant using experimental data. *International Journal of Refrigeration*, 2011.
- [14] Danfoss. Low pressure lift ejector system: Multi ejector solution incl. multi ejector low pressure (lp 935/1435/1935) and ak-pc 782a. 2020.
- [15] Kristina N. Widell, Tom Ståle Nordtvedt and Trygve Magne Eikevik. Natural refrigerants in refrigerated seawater systems on fishing vessels. *12th IIR Gustav Lorentzen Natural Working Fluids Conference*, 2016.
- [16] Tryge M. Eikevik. *Compendium for Heat Pumping Processes and Systems*. 2015.
- [17] Paride Gullo, Martin Ryhl Kærn, Michal Haida, Jacek Smolka and Stefan Elbel. A review of current status of capacity control techniques for two-phase ejectos. *International Journal of Refrigeration*, 2020.
- [18] Sergio Giroto. Direct space heating and cooling with refrigerant CO₂. *Atmosphere Europe*, 2018.
- [19] Ying Chen and Junji Gu. The optimum pressure for CO₂transcritical refrigeration systems with internal heat exchangers. *International Journal of Refrigeration*, 2005.
- [20] T.M. Hansen. *Alternatives to HCFC as Refrigerant in Shipping Vessels*. 2000.
- [21] Christian Heerup. Master module 2 - industrial systems. *Natural Refrigerant CO₂*, 2009.

-
- [22] S.M. Liao, T.S. Zhao and A. Jakobsen. A correlation of optimal heat rejection pressures in transcritical carbon dioxide cycle. *Applied Thermal Engineering*, 2000.
- [23] Changhyun Baek, Jaehyeok Heo, Jongho Jung, Honghyun Cho and Yongchan Kim. Optimal control of the gas-cooler pressure of a CO₂ heat pump using eev opening and outdoor fan speed in the cooling mode. *International Journal of Refrigeration*, 2013.
- [24] Mo Se Kim, Dae Hoon Kong, Min Soo Kim and Minsung Kim. Investigation on the optimal control of gas cooler pressure for a CO₂refrigeration system with an internal heat exchanger. *International Journal of Refrigeration*, 2017.
- [25] Jack P. C. Kleijnen. *Statistical Tools for Simulation Practitioners*. Marcel Dekker, 1987.
- [26] Ralf Schneider, Ann-Christin Kring. F gases regulation (eu) 517/2014. *Friedhelm LOH Group*, 2019.
- [27] Zhe Wang, XueHong Wu, W Zhang and Y. Lu. Thermodynamic analysis and experimental research of transcritical CO₂cycle with internal heat exchanger and dual expansion. *International Journal of Air-Conditioning and Refrigeration*, 2013.
- [28] Joaquim Rigola, Nicolas Ablanque, Carlos D. Perez-Segarra and Assensi Oliva. Numerical simulations and experimental validation of internal heat exchanger influence on CO₂ trans-critical cycle performance. *International Journal of Refrigeration*, 2010.
- [29] Silvia Minetto, Luca Cecchinato, Riccardo Brignoli, Sergio Marinetti and Antonio Rosetti. Water-side reversible CO₂ heat pump for residential application. *International Journal of Refrigeration*, 2016.
- [30] Valentina Ruiz. Analysis of existing refrigeration plants onboard fishing vessels and improvement possibilities. *Second International Symposium on Fishing Vessel Energy Efficiency*, 2012.
- [31] Samer Sawalha. Theoretical evaluation of trans-critical CO₂systems in supermarket refrigeration. part 1: Modeling, simulation and optimization of two system solution. *International Journal of Refrigeration*, 2008.
- [32] Samer Sawalha. Master module 3: Commercial refrigeration. *Natural Refrigerant CO₂*, 2009.
- [33] Samer Sawalha. Master module 3: Commercial refrigeration. *Leonardo project NARECO₂*, 2010.
- [34] Eirik Starheim Svendsen and Marte Schei. Energy measurement onboard pelagic purse seiner. 2020.
- [35] Technology and Economic Assessment Panel. Montreal protocol on substances that deplete the ozone layer. 2016. URL: https://ozone.unep.org/sites/default/files/2019-05/TEAP_TFXXVII-4_Report_September2016.pdf.
- [36] Evangelos Bellos and Christos Tzivanidis. A comparative study of CO₂ refrigeration systems. *Energy Conversion and Management: X*, 2019.
- [37] J. A. Thorsteinssona, P. Jenssna, T. Condrab and P. Valdimarssona. Transient simulation of refrigerated and chilled seawater system. *SIMS*, 2003.
- [38] A. Hafner, C.H. Gabriellii and K. Widell. *Refrigeration units in marine vessels*. 2018.
- [39] Zhenying Zhang, Yitai Ma, Minxia Li and Li Zhoa. Recent advances of energy recovery expanders in the transcritical CO₂ refrigeration cycle. *HVACR Research*, 2013.
- [40] Ángel Á. Pardiñasa , Armin Hafner and Krzysztof Banasiak. Novel integrated CO₂ vapour compression racks for supermarkets. thermodynamic analysis of possible system configurations and influence of operational conditions. *Applied Thermal Engineering*, 2017.
-

Appendix

Appendix A: EES script

```

Function flow_rsw(m_AC;m_ACgas)
If (m_AC<m_ACgas) Then m_RSWadd=(m_AC-m_ACgas) Else m_RSWadd=0
flow_rsw:=m_RSWadd
End

```

```

Function flow_ac(m_AC;m_ACgas)
If (m_AC<m_ACgas) Then x_ACadd=0 Else x_ACadd=1
flow_ac:=x_ACadd
End

```

"Initial data"

```

T_RSWinn=1,4
T_RSWout=0,0
T_RSWev=-5
T_ACev=1
T_LTev=-15
T_RSW=30 "RSW temperature to gas-cooler"
T_4GC=T_RSW+4
P_GC=90
T_overheating=10
n_AC=1 "number of AC compressors"
n_RSW=2 "number of RSW compressors"
n_LT=0 "number of LT compressors"
e_effIHE1=0,5 "efficiency of the IHE1, set to 0.556 for 10k overheating"
e_effIHE2=0,5
e_ejector=0,3 "ejector efficiency"

```

"Volumetric flow of compressor RSW"

```
V_compRSW=-2,2398*Pr_RSW+38,883
```

"Volumetric flow of compressor AC"

```
V_compAC=-2,2398*Pr_AC+38,883
```

"Volumetric flow of compressor LT"

```
V_compLT=-2,2398*Pr_LT+38,883
```

"Pressure ratio RSW"

```
Pr_RSW=P_GC/P_RSWev
```

"Pressure ratio AC"

```
Pr_AC=P_GC/P_ACev
```

"Pressure ratio LT"

```
Pr_LT=P_GC/P_LTev
```

"Evaporation pressure AC"

```
P_ACev=p_sat(R744;T=T_ACev)
```

"Evaporation pressure LT"

```
P_LTev=p_sat(R744;T=T_LTev)
```

"Evaporation pressure RSW"

```
P_RSWev=p_sat(R744;T=T_RSWev)
```

"Isentropic efficiency of RSW compressor"

```
n_isRSW=-0,0079*Pr_RSW^2+0,0362*Pr_RSW+0,6692
```

"Isentropic efficiency of AC compressor"

```
n_isAC=-0,0079*Pr_AC^2+0,0362*Pr_AC+0,6692
```

"Isentropic efficiency of LT compressor"

```
n_isLT=-0,0079*Pr_LT^2+0,0362*Pr_LT+0,6692
```

"massflow of RSW compressor"

```
m_RSW=(V_compRSW*rho_1RSW/3600)*n_RSW
```

"Density at suction point RSW compressor"

```
rho_1RSW=density(R744;T=T_coldIHE2out;P=P_RSWev)
```

"massflow of AC compressor"

```
m_AC=(V_compAC*rho_1AC/3600)*n_AC
```

"Density at suction point AC compressor"

```
rho_1AC=density(R744;T=T_coldIHE1out;P=P_ACev)
```

"massflow of LT compressor"

```
m_LT=(V_compLT*rho_1LT/3600)*n_LT
```

"Density at suction point LT compressor"

```
rho_1LT=density(R744;T=T_LTev+0,1;P=P_LTev) "no overheating, dry evaporator"
```

"Circle main calculation"

"Compressor AC side"

```
s_1AC=entropy(R744;T=T_1AC+0,1;P=P_ACev) "suction entropy"
```

$h_{2ACis} = \text{enthalpy}(R744; s = s_{1AC}; P = P_{GC})$ "discharge ideal enthalpy"
 $h_{2AC} = h_{1AC} + (h_{2ACis} - h_{1AC}) / \eta_{isAC}$ "discharge real enthalpy"
 $T_{2AC} = \text{temperature}(R744; P = P_{GC}; h = h_{2AC})$ "discharge temperature"
 $W_{AC} = m_{AC} * (h_{2AC} - h_{1AC})$

"Compressor RSW side"

$s_{1RSW} = \text{entropy}(R744; T = T_{1RSW} + 0, 1; P = P_{RSWev})$ "suction enthalpy"
 $h_{2RSWis} = \text{enthalpy}(R744; s = s_{1RSW}; P = P_{GC})$ "discharge ideal enthalpy"
 $h_{2RSW} = h_{1RSW} + (h_{2RSWis} - h_{1RSW}) / \eta_{isRSW}$ "discharge real enthalpy"
 $T_{2RSW} = \text{temperature}(R744; P = P_{GC}; h = h_{2RSW})$ "discharge temperature"
 $W_{RSW} = m_{RSW} * (h_{2RSW} - h_{1RSW})$

"Compressor LT side"

$h_{1LT} = \text{enthalpy}(R744; T = T_{LTev} + 0, 1; P = P_{LTev})$ "suction enthalpy"
 $s_{1LT} = \text{entropy}(R744; T = T_{LTev} + 0, 1; P = P_{LTev})$ "suction enthalpy"
 $h_{2LTis} = \text{enthalpy}(R744; s = s_{1LT}; P = P_{GC})$ "discharge ideal enthalpy"
 $h_{2LT} = h_{1LT} + (h_{2LTis} - h_{1LT}) / \eta_{isLT}$ "discharge real enthalpy"
 $T_{2LT} = \text{temperature}(R744; P = P_{GC}; h = h_{2LT})$ "discharge temperature"
 $W_{LT} = m_{LT} * (h_{2LT} - h_{1LT})$

"Gas-cooler side"

$m_{GC} = (m_{LT} + m_{AC} + m_{RSW})$ "mass flow in gas-cooler"
 $h_{3GC} = (m_{LT} * h_{2LT} + m_{RSW} * h_{2RSW} + m_{AC} * h_{2AC}) / m_{GC}$ "enthalpy outlet from GC"
 $T_{3GC} = \text{temperature}(R744; P = P_{GC}; h = h_{3GC})$ "temperature inlet to GC"
 $h_{4GC} = \text{enthalpy}(R744; T = T_{4GC}; P = P_{GC})$ "enthalpy out of gas-cooler"
 $Q_{GC} = m_{GC} * (h_{3GC} - h_{4GC})$ "capacity of gas-cooler"
 $\rho_{3GC} = \text{density}(R744; T = T_{3GC}; P = P_{GC})$
 $\rho_{4GC} = \text{density}(R744; T = T_{4GC}; P = P_{GC})$

"Internal heat exchangers"

"IHE1 GC flow vs AC flow"

$T_{coldIHE1in} = T_{ACev}$ "cold side temperature"
 $T_{coldIHE1out} = e_{effIHE1} * (T_{4GC} - T_{ACev}) + T_{ACev}$ "look at e_eff description"
 $h_{coldIHE1in} = \text{enthalpy}(R744; T = T_{ACev} + 0, 1; P = P_{ACev})$
 $h_{coldIHE1out} = \text{enthalpy}(R744; T = T_{coldIHE1out}; P = P_{ACev})$
 $T_{hotIHE1in} = T_{4GC}$
 $T_{hotIHE1out} = \text{temperature}(R744; P = P_{GC}; h = h_{hotIHE1out})$
 $h_{hotIHE1out} = h_{hotIHE1in} - m_{AC} * (h_{coldIHE1out} - h_{coldIHE1in}) / m_{GC}$
 $h_{hotIHE1in} = h_{4GC}$
 $Q_{IHE1} = m_{AC} * (h_{coldIHE1out} - h_{coldIHE1in})$
 $h_{1AC} = h_{coldIHE1out}$

$T_{1AC} = \text{temperature}(R744; P = P_{ACev}; h = h_{1AC})$
 $\rho_{hotIHE1out} = \text{density}(R744; T = T_{hotIHE1out}; P = P_{GC})$
 $\rho_{coldIHE1out} = \text{density}(R744; T = T_{coldIHE1out}; P = P_{ACev})$

"IHE2 GC flow vs RSW flow"

$T_{coldIHE2in} = T_{RSWev}$ "cold side temperature"
 $T_{coldIHE2out} = e_{effIHE2} * (T_{hotIHE2in} - T_{RSWev}) + T_{RSWev}$ "look at e_eff description"
 $h_{coldIHE2in} = \text{enthalpy}(R744; T = T_{RSWev} + 0, 1; P = P_{RSWev})$
 $h_{coldIHE2out} = \text{enthalpy}(R744; T = T_{coldIHE2out}; P = P_{RSWev})$
 $T_{hotIHE2in} = T_{hotIHE1out}$
 $T_{hotIHE2out} = \text{temperature}(R744; P = P_{GC}; h = h_{hotIHE2out})$
 $h_{hotIHE2out} = h_{hotIHE2in} - m_{RSW} * (h_{coldIHE2out} - h_{coldIHE2in}) / m_{GC}$
 $h_{hotIHE2in} = h_{hotIHE1out}$
 $\{Q_{IHE2} = m_{RSW} * (h_{coldIHE2out} - h_{coldIHE2in})\}$
 $Q_{IHE2} = m_{GC} * (h_{hotIHE2in} - h_{hotIHE2out})$
 $h_{1RSW} = h_{coldIHE2out}$
 $\{h_{1RSW} = Q_{IHE2} / (m_{RSW} + 0,00000001) + h_{coldIHE2in}\}$
 $T_{1RSW} = \text{temperature}(R744; P = P_{RSWev}; h = h_{1RSW})$

$\rho_{hotIHE2out} = \text{density}(R744; T = T_{hotIHE2out}; P = P_{GC})$
 $\rho_{coldIHE2out} = \text{density}(R744; T = T_{coldIHE2out}; P = P_{RSWev})$

$B_IHE2 = (Q_RSW) * \text{density}(R744; T=T_1RSW; P=P_RSWev) / (\text{density}(R744; T=T_coldIHE2in+0,1; P=P_RSWev) * (Q_RSW - Q_IHE2))$

"Throttling to AC pressure"

$x_AC = \text{quality}(R744; T=T_ACev; h=h_hotIHE2out)$ "gass fraction at AC"

$m_ACgas = x_AC * m_GC$

$\Delta h_AC = \text{enthalpy_vaporization}(R744; T=T_ACev)$

$Q_AC = \text{flow_ac}(m_AC; m_ACgas) * (m_AC - m_ACgas) * \Delta h_AC$

$\rho_ACexp = \text{density}(R744; x=x_AC; P=P_ACev)$

"Throttling to RSW pressure"

$x_RSW = \text{quality}(R744; T=T_RSWev; h=h_ACliq)$

$h_ACliq = \text{enthalpy}(R744; T=T_ACev-0,01; P=P_ACev)$

{ $Q_RSW = m_RSW * (h_1RSW - h_ACliq)$ }

$Q_RSW = (m_RSW + \text{flow_rsw}(m_AC; m_ACgas)) * (h_coldIHE2in - h_ACliq)$

"Trottling to LT pressure"

{ $x_RSW = \text{quality}(R744; T=T_RSWev; h=h_ACliq)$ }

$h_ACliq = \text{enthalpy}(R744; T=T_ACev-0,01; P=P_ACev)$

{ $Q_RSW = m_RSW * (h_1RSW - h_ACliq)$ }

$\rho_ACliq = \text{density}(R744; T=T_ACev-0,01; P=P_ACev)$

$\rho_ACgas = \text{density}(R744; T=T_ACev+0,01; P=P_ACev)$

"Ejector calculation"

$s_1motive = \text{entropy}(R744; T=T_hotIHE2out; P=P_GC)$

$h_1motive = h_hotIHE2out$

$h_2motive = \text{enthalpy}(R744; s=s_1motive; P=P_ACev)$

$s_1suction = \text{entropy}(R744; T=T_RSWev+0,01; P=P_RSWev)$

$\rho_throttlingRSW = \text{density}(R744; h=h_ACliq; P=P_RSWev)$

$\rho_RSWliq = \text{density}(R744; T=T_RSWev-0,01; P=P_RSWev)$

$\rho_RSWout = \text{density}(R744; x=0,66; P=P_RSWev)$

$m_RSWliqflow = (m_RSW + \text{flow_rsw}(m_AC; m_ACgas)) * 1,5$

$\rho_RSWgas = \text{density}(R744; T=T_RSWev+0,01; P=P_RSWev)$

"COP"

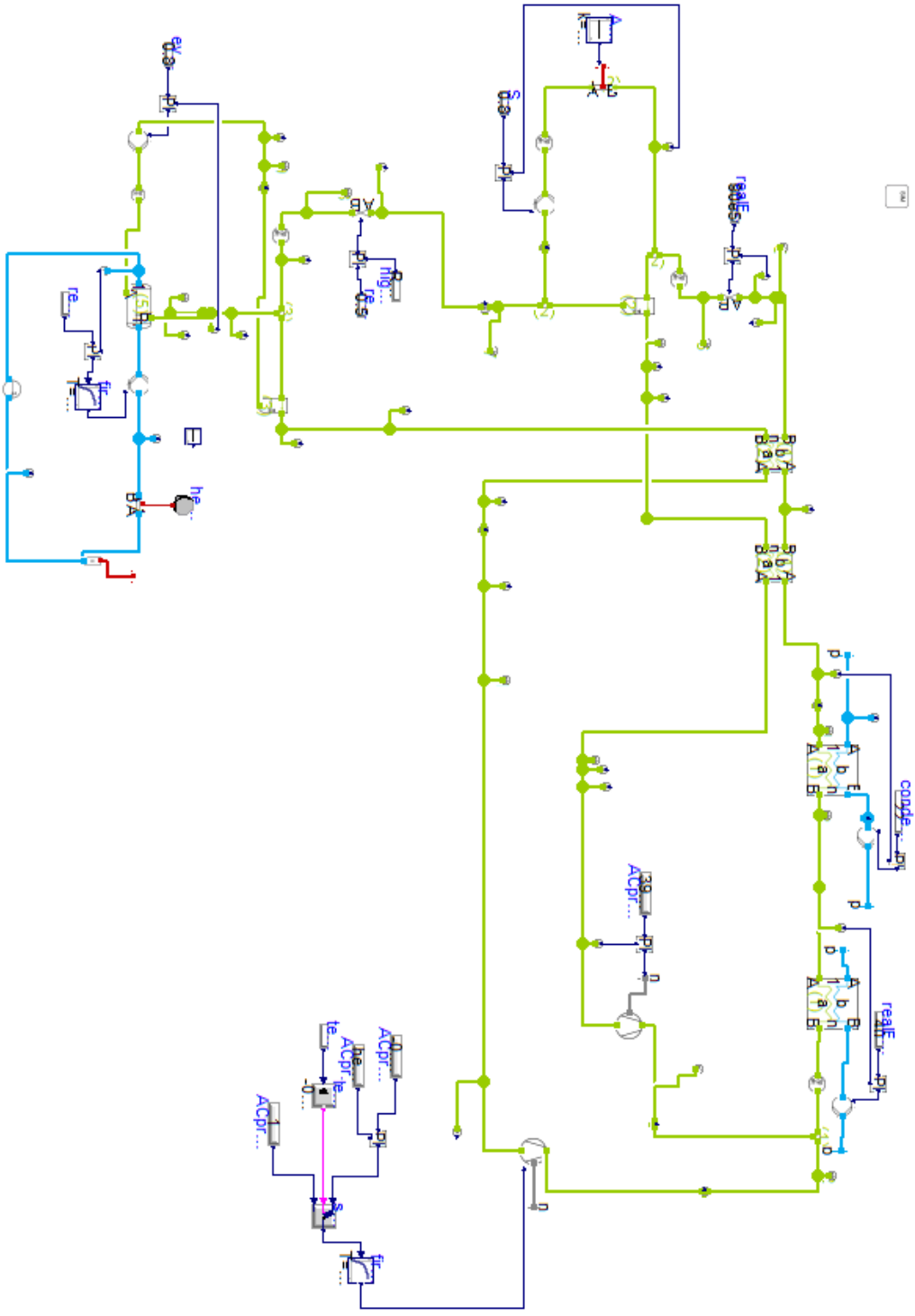
$COP_RSW = Q_RSW / (W_RSW + 0,0000001)$

$COP_AC = Q_AC / (W_AC + 0,00000001)$

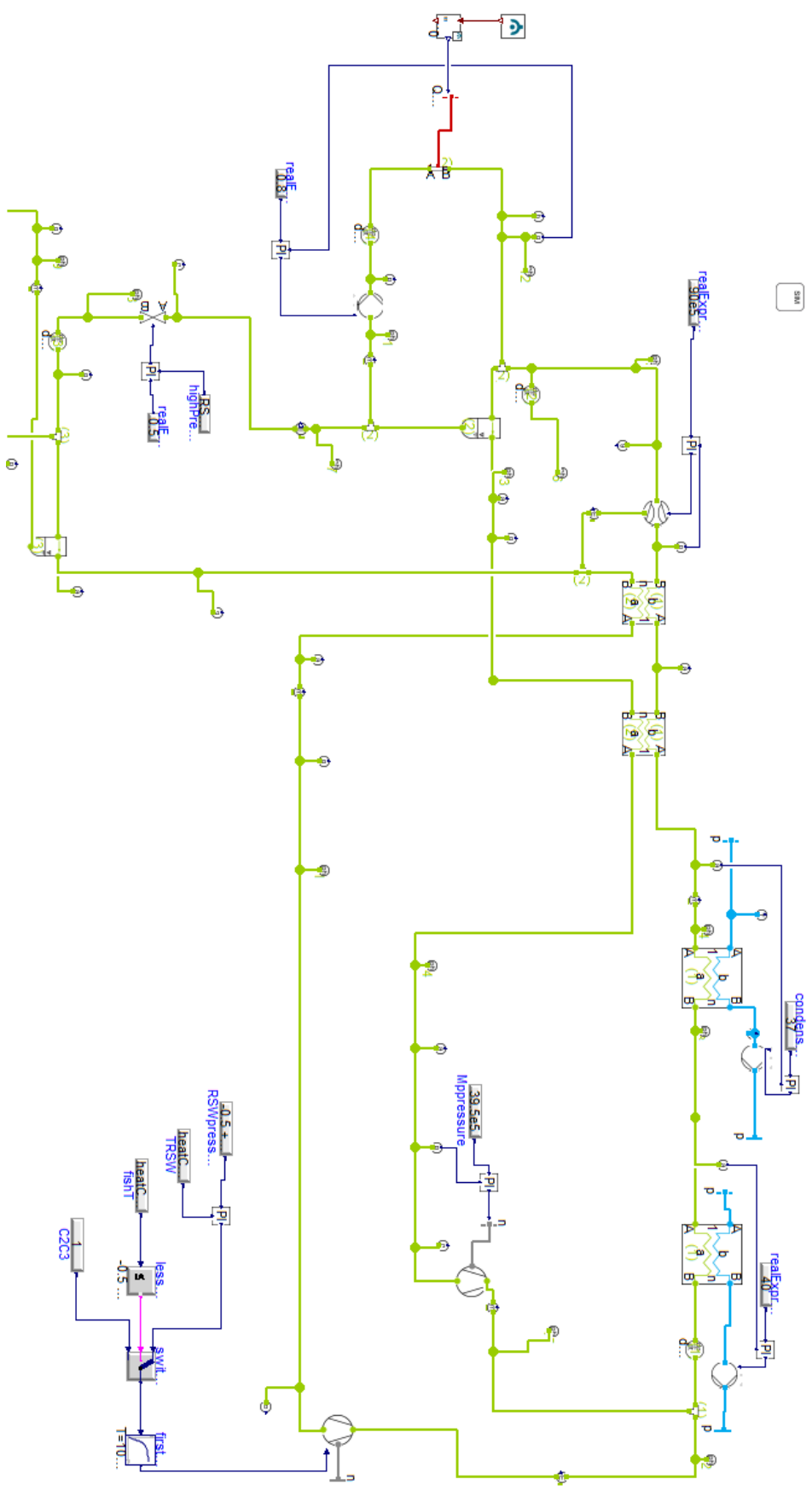
{ $COP_LP = Q_LP / (W_LP + 0,00000001)$ }

$COP_tot = (Q_RSW + Q_AC) / (W_AC + W_RSW)$

Appendix B: Dymola energy models



100



Appendix C: Ohrid conference paper

Simulation of a carbon dioxide (R-744) refrigeration system for fishing vessel

Pavel SEMAEV^a, Engin SÖYLEMEZ^a, Ignat TOLSTOREBROV^a, Armin HAFNER^a,
Kristina N. WIDELL^(b), Thomas LUND^(c), Jostein ØY^(d), Jan Petter URKE^(d)

- (a) Norwegian University of Science and Technology, NTNU, 7194 Trondheim, Norway
pavelse@stud.ntnu.no, Engin.soylemez@ntnu.no, ignat.tolstorebrov@ntnu.no,
armin.hafner@ntnu.no
- (b) SINTEF Ocean AS, Trondheim, Norway, Kristina.Widell@sintef.no
- (c) Danfoss Climate Solution 6000 Kolding, Denmark, thomaslund@danfoss.com
- (d) MMC First Process AS, 6260 Ålesund, Norway, Jostein.Oy@mmcfp.no

ABSTRACT

The paper describes architecture of a prototype industrial CO₂ trans-critical system for production of refrigerated sea water (RSW) for either fishing vessels or land-based process plants. The refrigeration system was designed to cover cooling demands of RSW (up to 450 kW), air-conditioning (up to 170 kW) and freezing equipment (up to 82 kW at -25 °C). Four system design cases were evaluated: one stage compression, two-stage expansion with auxiliary compressor, three stage expansion with parallel compressors and two stage expansion supported by ejector. The optimum high side pressure level and the effectiveness of internal heat exchanger were investigated to optimize the four system designs with respect to capacity, seawater temperature and COP. The system performance was evaluated for fish chilling on-board, including both chilling and temperature maintenance periods. Analysis shows a 28% difference in energy demand after 42 hours of operation, when applying the ejector supported solution. Considering that electricity onboard fishing vessels is provided by fossil fuel based generators, the decrease in energy demand results in lower total greenhouse gas emissions.

Keywords: Refrigerated sea water, trans-critical CO₂, Ejector

1. INTRODUCTION

Implementation of transcritical CO₂ refrigeration systems is gaining momentum and find various application areas from commercial to industrial systems (Accelerate, 2020). This is because of the detrimental effects of non-natural (synthetic) refrigerants (also called F-gases) on the environment (J.L. Dupont, 2019) (Sovacool, 2021); legislative pressure to phase out F-gases (K. Zolcer Skačanová, 2019); the development of various solutions for increasing performance of CO₂ refrigeration systems (Paride Gullo, 2018); and heat recovery integration which enables higher system coefficient of performance (COP). In addition to these aspects, the thermodynamic and transport properties of CO₂ make it an ideal candidate in most applications (Pearson, 2005).

One of the promising sectors of application of the transcritical CO₂ system is the fisheries. CO₂ is a non-toxic and non-flammable refrigerant, which are critical required properties particularly for the systems installed in fishing vessels. The legislative measures to lessen GHG emissions by phasing out F-gases are also creating pressure on the fishery sector due to the fact that R-22 (HCFC-22), which depletes the ozone layer and causes the greenhouse effect, is still used in 70% of the refrigeration systems installed in fishing vessels (UNEP, 2016).

In this study, a simulation model was developed for a prototype transcritical CO₂ refrigeration system, which was designed to meet air condition (AC) and refrigerated sea water (RSW) cooling demands on fishing vessels and at land-based process plants. The four different system design were investigated and discussed.

2. METHODS

2.1. System design and cases

The transcritical CO₂ system was equipped with three parallel compressors and it is schematically shown in Figure 1 . Compressor C1 was equipped with a frequency converter, while the other two were controlled by ON/OFF regulation. The compressors were activated based on the requested capacity, which increases systems flexibility regarding energy demand and operational conditions.

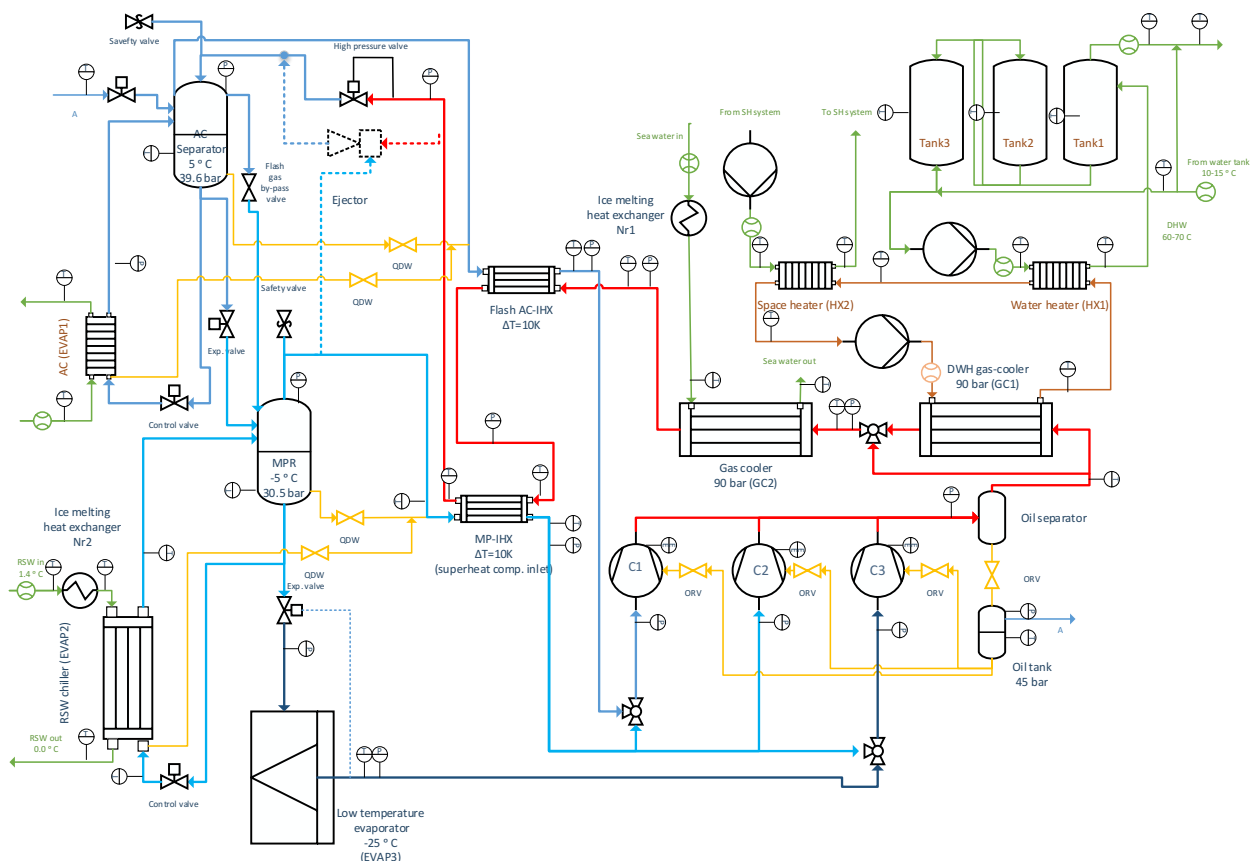


Figure 1: Principal sketch of the transcritical CO₂ refrigeration system

The system utilized the benefits of a transcritical CO₂ loop by energy recovery from the gas coolers (GC1 and GC2). It was designed to supply domestic hot water (DHW) and space heating (SH). The hydronic subsystem provided heat through two heat exchangers in series, HX1 and HX2 in Figure 1, at high and medium temperatures. During operation conditions with negligible DHW and SH demands, the heat was rejected through GC2 while avoiding GC1 by a three-way bypass valve. The CO₂ entered the gas cooler as vapour and was cooled down to by seawater. The system is equipped with two internal heat exchangers, AC-IHX and MP-IHX.

The main function of the CO₂ system was to provide RSW, where the cooling load was the controlling parameter. The set temperature in the RSW tanks was approximately -0.5 °C. To ensure sufficient cooling, CO₂ was set to enter the RSW evaporator (EVAP 2 in Figure 1) at approximately 30.5 bar and -5 °C. EVAP 2 functioned as a gravity-fed flooded evaporator and operated in conjunction with a medium-pressure receiver

(MPR in Figure 1). Integration to meet AC cooling needs was done by including a flooded evaporator (EVAP 1) and a separator (AC separator) between the high-pressure regulating valve and medium pressure receiver. The AC and the low temperature (LT) evaporating temperatures were 5°C and -25°C, respectively. The LT evaporator (EVAP 3) ran on direct expansion conditions, meaning a section of the evaporator was used to superheat the refrigerant before entering the LT compressor (C3). The system was equipped with multi-ejector rack parallel to the high-pressure valve, marked with dashed lines in Figure 1.

The described system design had multiple system configuration that could provide the requested cooling onboard. The configuration included the following options:

- CASE 1: All the three compressors (C1, C2, C3) were available to provide the requested RSW capacity.
- CASE 2: AC and RSW chilling, where compressor C1 was responsible for AC, while rest for RSW chilling.
- CASE 3: The system provided AC, RSW and LT cooling, where C1 was responsible for AC, C2 responsible for RSW and C3 responsible for LT storage. CASE 3 was a local solution of CASE 2.
- CASE 4: The parallel compression ran in conjunction with the ejector rack, providing AC and RSW cooling (CASE 2 + ejector). The ejector removed part of refrigerant vapour out of the RSW separator, hence unloading the RSW compressors.

2.2. Equipment

The CO₂ system had three semi-hermetical compressors, type: HGX46/ 400-4 ML CO2T. Each compressor had six reciprocating cylinders with a suction gas-cooled motor and a swept volume of 400 m³. One compressor was equipped with a frequency converter with a range of 20-70 Hz.

The outlined gas coolers (GC1 and GC2) are type Alfa Laval AXP112, manufactured by Alfa Laval. The heat exchanger was a brazed plate heat exchanger with external frames made of carbon steel. The capacity of the gas cooler was determined by the number of plates. The internal heat exchangers in the presented system layout were also manufactured by Alfa Laval, type AXP52. The benefits of the AXP heat exchangers are compactness, ease of installation, self-cleaning, low level of service and are gasket free.

Isotherm manufactures RSW and AC evaporator (EVAP1 and EVAP2). Configuration of these heat exchanger was a shell and tube heat designed for usage with CO₂ and seawater. The designed cooling capacity of the RSW evaporator was 450 kW. Danfoss provides the ejector, type “Multi ejector”. Each ejector block had a range of ejectors mounted vertically and in different sizes. Multi ejector was available with 4 to 6 ejectors and matches the capacity demand using different numbers and combinations.

2.3. Simulations

To evaluate the described refrigeration unit, models were built in the simulation software Engineering Equation Solver (EES) and Dymola. EES is a software package used to solve system of nonlinear equations. It is especially well suited to build a vapour compression refrigeration system as it does not require special coding. EES has a complete database for the properties of different refrigerant applied in the refrigeration system, such as R744 (carbon dioxide). Dymola is a modelling and simulation software based on the open Modelica modelling language. The ad-on libraries, *TIL-Media* and *TIL 3.5.0* were used as they provide many common pre-modelled components and refrigerant used in the refrigeration system.

The EES tool was applied to develop steady-state performance analysis, whereas Dymola was used for dynamic load simulations. Creating simulation models accounting for every detail of the RSW system and its

configurations is time-consuming and influence reliability and simulation time. Therefore, several simplifications were made. The most important were constant heat transfer coefficient and not accounting for pressure drop in components.

3. RESULTS AND DISCUSSION

3.1. Influence of internal heat exchangers on system performance

The internal heat exchangers (AC-IHX and MP-IHX) had two main functions. The IHX superheats the gas leaving the separator, and at the same time, subcools the liquid leaving the condenser. This reduces the expansion losses and increases the total refrigeration capacity of the system. The influence of IHX in a transcritical CO₂ system has been investigated in several studies, concluding with an increase in system COP by up to 12% (E. Torrella, 2011).

The refrigeration capacity of RSW production was calculated for different seawater temperatures and they are presented in Table 1. The influence of the efficiency of IHXs on refrigeration capacity depends on the system configuration. For CASE 1, the change was minor: at a seawater temperature of 15 °C with 90% effectiveness, the value of refrigeration capacity was 3% less when compared with the value at 10% effectiveness. For CASE 4, the change was 15%. However, one trend was noticed throughout all the four configurations. The RSW refrigeration capacity was larger, utilizing a lower efficient IHX at seawater temperatures below the critical temperature of CO₂ (<30 °C in Table 1). With an efficient IHX, the volumetric cooling effect ($\frac{m^3}{kW}$) of IHX will increase, and the start of the compression line will move to an area of greater superheat where the isentropic compression lines become flatter. This results in a higher enthalpy difference during compression, increasing power demand and lower refrigeration capacity at RSW. Based on the presented calculations, it is advised to cut off the internal heat exchangers using two bypass valves at seawater temperatures lower than 30 °C, regardless of the chosen system configuration.

Table 1: Influence of internal heat exchanger efficiency on system configurations at multiple seawater temperatures (the same efficiency for both IHX) on refrigeration capacity at RSW

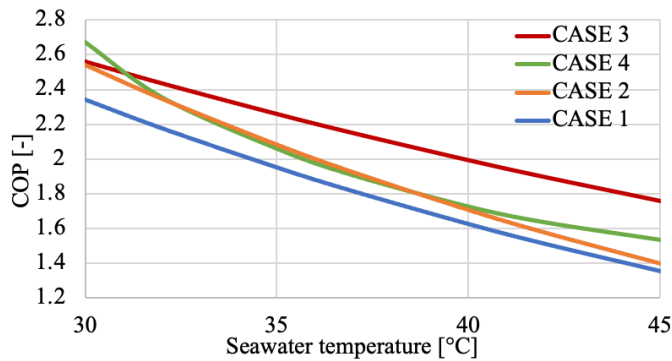
Operation mode	η_{IHX}	$\dot{Q}_{RSW} (T_{SW} = 15\text{ }^{\circ}\text{C})$	$\dot{Q}_{RSW} (T_{SW} = 20\text{ }^{\circ}\text{C})$	$\dot{Q}_{RSW} (T_{SW} = 25\text{ }^{\circ}\text{C})$	$\dot{Q}_{RSW} (T_{SW} = 30\text{ }^{\circ}\text{C})$	$\dot{Q}_{RSW} (T_{SW} = 35\text{ }^{\circ}\text{C})$
CASE 1	10 %	425.5 kW	398.7 kW	357.1 kW	299.4 kW	253.1 kW
	54 %	416.6 kW	393.0 kW	353.9 kW	300.7 kW	240.8 kW
	90 %	411.4 kW	387.0kW	352.5 kW	307.9 kW	229.4 kW
CASE 2	10 %	336.5 kW	344.9 kW	333 kW	300.73 kW	248.1 kW
	54 %	308.1 kW	304.3 kW	295.6 kW	281.96 kW	263.4 kW
	90 %	292.2 kW	284.4 kW	276.2 kW	267.5 kW	258.3 kW
CASE 3	10 %	160.9 kW	161.4 kW	159.3 kW	152.9 kW	143.8 kW
	54 %	147.6 kW	144.0 kW	141.8 kW	138.0 kW	135.5 kW
	90 %	140.5 kW	136.13 kW	132.8 kW	127.6 kW	123.8 kW
CASE 4	10 %	426.5 kW	438.8 kW	417.8 kW	363.7 kW	276.3 kW
	54 %	384.0 kW	395.1 kW	382.8 kW	347.0 kW	287.7 kW
	90 %	361.8 kW	360.5 kW	348.9 kW	326.9 kW	294.5 kW

CASE 2 provided AC refrigeration capacity in the range of [0 kW – 170 kW] for seawater temperatures [15°C – 35°C]. CASE 3 provided a stable LT refrigeration capacity of 82 kW.

3.2. Optimization of gas cooler pressure with respect to the seawater temperature

At temperatures above the critical temperature of CO₂, it was important to keep the cycles high pressure at the optimal value to ensure good systems COP. High seawater temperatures result often in low COP when applying CO₂ without special system modifications. An increase in seawater leads to a decrease in enthalpy out of gas cooler, and corresponding decrease in systems refrigeration capacity. At the same time, power input increases, thus resulting often in a substantial decrease of COP.

Based on performed simulations, it was evident that there exists an optimal discharge pressure for each gascooler exit temperature, which gives a maximum COP. The systems COP increased quickly with increasing gas cooler pressure to the optimum value, when the high side pressure was further increased COP slowly decreased. The slight decrease can be advantageous, as the lower gradient makes the system's performance less sensitive to high-pressure control. Furthermore, based on the optimum COP values, optimum pressure levels were calculated for each of the cases and plotted in Figure 2. The optimum COP values were curve fitted at multiple seawater temperatures in the range of 30°C to 45°C. Figure 2 indicates the difference between CASE 1 and 4, when the unit produces RSW. As a result of three stage expansion for CASE 3, a comparable high efficiency was achieved.



Operation mode	Refrigeration at
CASE 1	RSW
CASE 2	RSW and AC
CASE 3	RSW, AC and LT
CASE 4	RSW

Figure 2: Optimum gas cooler pressure lines for the reviewed system configurations at seawater temperatures 30 °C or higher, IHX efficiency 30%.

According to S.M.Liao, the optimal gas cooler pressure for a transcritical CO₂ system depends on three parameters: the temperature out of the gas cooler, the evaporating temperature and the compressors isentropic efficiencies (S.M Liao, 2000). In all presented cases, the evaporating temperature was constant. Accordingly, the optimal pressure was only affected by the temperature of refrigerant out of the gas cooler, which was assumed to be 5 K higher than the seawater temperature. Curve fitting the optimum gas cooler pressure developed in Figure 2 yielded the correlations presented in Table 2. The correlations can be used in further simulations to operate at the optimum discharge pressure. One should note, at seawater temperatures above 40°C, the gas cooler pressure should be at 110 bar, due to the compressor's application range. The correlations obtained by S.M.Liao et al. are different when compared to equations presented in Table 2, as they consider the evaporating temperature as well (S.M Liao, 2000).

Table 2: Optimum gas cooler pressure formulas assuming seawater temperature of 30 °C or higher.

Operation mode	Optimum gas cooler pressure formula [bar]
CASE 1	$2.4336 * (T_{SW} + 4) + 1.4614$
CASE 2	$2.209 * (T_{SW} + 4) + 9.1057$
CASE 3	$1.473 * (T_{SW} + 4) + 30.446$
CASE 4	$-0.0738 * T_{SW}^2 + 7.745 * T_{SW} - 81.72$

3.3. Predictions of system performance for fish chilling on board

RSW chilling onboard fishing vessels can be divided into three periods: 1) Prechilling, 2) Chilling and 3) Maintenance. Prechilling is cooling down the seawater in the RSW tank. The chilling period begins when the fish has been loaded in the RSW tank and lasts until a set temperature of seawater is reached in the chilling tank. Factors that influence the length of the chilling period are quantity of fish, amount of seawater and capacity of the refrigeration system. Maintenance chilling lasts until the unloading. During maintenance, the heat loads are primarily due to transmission losses, the length of this period can be up to 39 hours for vessels going far to the sea (E. S. Svendsen, 2021). So, high system COP, especially during the maintenance period, is crucial to ensure the overall efficiency of RSW systems.

Based on the reported chilling load data from a research cruise, which assessed the energy efficiency of onboard RSW system, two simulation scenarios were developed using Dymola to examine predictions of system performance for CASE 1, CASE 2 and CASE 4. The catch size was assumed to be 59 m³, consisting of mackerel. Results present the chilling and maintenance periods, Figure 3a and 3b.

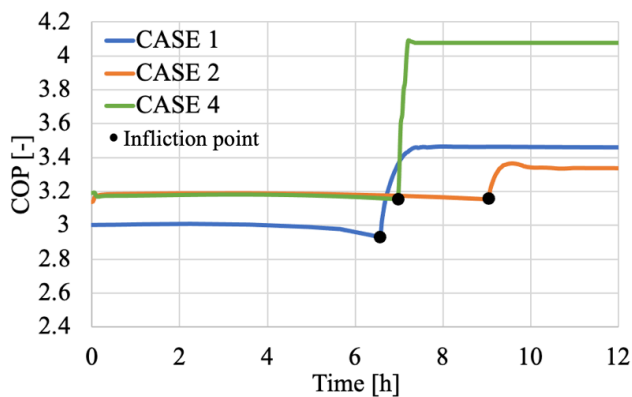


Figure 3a: Seawater temperature at 18 °C.

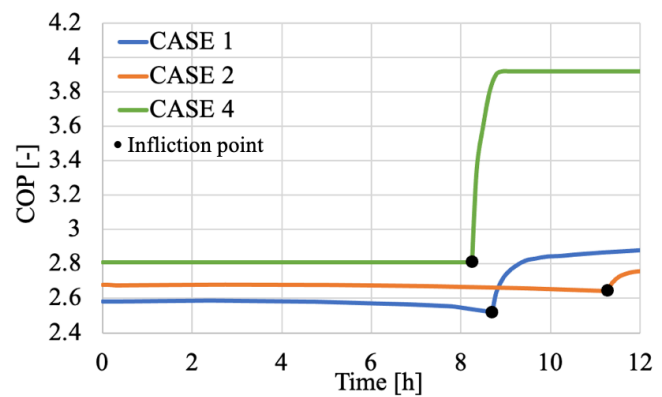


Figure 3b: Seawater temperature at 28 °C.

Figure 3: Systems COP during chilling and maintenance period

The maintenance period started when the set temperature was reached in the RSW tank of seawater and fish mixture (-0.5 °C), visualized as the inflection point in Figure 3. CASE 2 and CASE 4 yielded a higher system COP during the chilling period, both in Figure 3a and 3b. This occurred because CASE 4 and CASE 2 used an auxiliary compressor after the first expansion. However, the chilling time was longer at seawater at 18 °C when compared to CASE 1. This was due to a higher chilling capacity of one stage compression, which occurs at low seawater temperatures. A significant increase in systems COP was observed after the inflection point. The increase of COP resulted from suction pressure increase during the maintenance period, due to the chosen control strategy at part load operation. Figure 3 presents a more considerable increase for CASE 4 because the ejector provided the requested maintenance cooling without using the RSW compressors.

Figure 4 shows the share of power consumption during the chilling and maintenance period. Less energy demand throughout the trip resulted in less fuel consumption, since the electric power onboard fishing vessels was provided by petrol engine. As shown, the length of maintenance period largely effects overall energy demand. As a result of higher system COP during maintenance, shown in Figure 3, CASE 4 had lower hourly energy demand when compared to CASE 2, shown in Figure 4a. The difference is visualised by a smaller gradient for CASE 4 line, in comparison with CASE 2 and CASE 1 line in Figure 4a. Accordingly, after 42 hours of operation time, CASE 4 achieved the lowest share of energy demand. The difference was 9% and 13%, respectively.

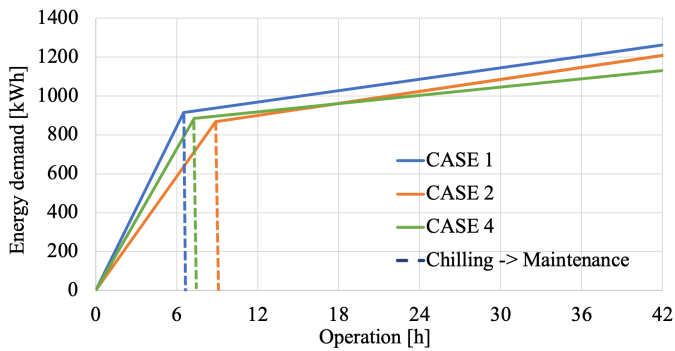


Figure 4a: Seawater temperature at 18 °C.

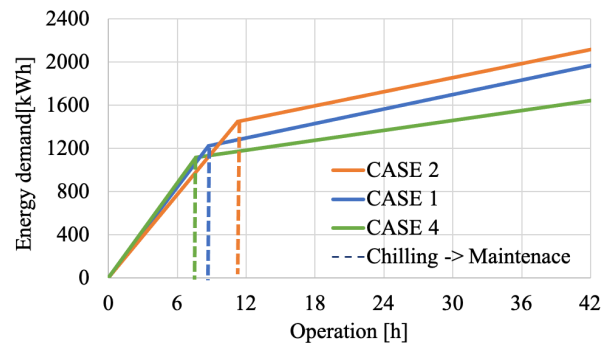


Figure 4b: Seawater temperature at 28 °C.

Figure 4: Energy demand during chilling and maintenance period

Figure 4b presents the overall energy demand, at seawater temperature of 28°C. High seawater temperature decreased the systems cooling effect and increased the transmission losses at RSW tank. CASE 4 resulted in shorter chilling time when compared to CASE 1 and CASE 2, shown in Figure 4b. The difference was 14% and 50%, respectively. A fast chilling can be dominant factor for the high seawater temperatures. Additionally, CASE 4 resulted in less hourly energy demand when compared with CASE 1 and CASE 2. The results were as expected, due to reduction in energy consumption utilizing an ejector for warmer climates. Additionally, CASE 4 delivered the requested cooling for RSW, applying the auxiliary compressor throughout the maintenance period. After 42 hours of operation, the difference in energy demand was 380 kWh comparing CASE 4 with CASE 1, and 525 kWh comparing CASE 4 with CASE 2. The low performance of CASE 2 when compared to CASE 1 is explained by refrigeration provided at two temperature levels (AC and RSW).

4. CONCLUSIONS

In this work, the performance of an industrial CO₂ transcritical system was analysed in a simulation model. Four cases were included, with different system configurations and considering the influence of heat exchangers and gas cooler pressure. The cases were RSW chilling (CASE 1), AC and RSW chilling (CASE 2), AC, RSW chilling and LT cooling (CASE 3), and parallel compression run in conjunction with an ejector rack (CASE 4).

The influence of the efficiency of IHX on refrigeration capacity depended on the selected system configuration. For CASE 1, the change was minor: at a seawater temperature of 15 °C with 90% effectiveness, the value of refrigeration capacity was 3% less when compared with the value at 10% effectiveness. For CASE 4, the change was 15%. However, one trend was noticed throughout all depicted operation modes. The RSW refrigeration capacity was larger when utilizing a lower efficient IHX at temperatures below the critical temperature of CO₂.

According to the simulation predictions, there was an optimal discharge pressure for a maximum COP. The systems COP increased steeply with increasing the gas cooler pressure to the extreme value and then slide decrease is observed with the further increasing of pressure. The slow decrease can be beneficial, as the lower gradient makes the system's performance less sensitive to the control of high pressure. The predictions also showed that the system COP at CASE 4 was the highest, because of ejectors. Less energy demand was predicted at CASE 4 throughout the chilling and temperature maintenance period. CASE 2 is arguably the least attractive solution due to the long chilling time and higher energy demand throughout the chosen time interval.

Based on this work, it can be said that the system benefits from the ejectors. However, further work is needed to enhance the developed simulation model. Additionally, a system will be built to conduct experiments considering the predictions.

ACKNOWLEDGEMENTS

The authors gratefully acknowledge the Research Council of Norway and industrial project partners for the financial support for carrying out the present research [NFR project No. 294662, CoolFish]. The CoolFish project includes research partners SINTEF Ocean (project manager), SINTEF Energy and NTNU. Industrial partners are MMC First Process, Selvåg Senior/Sørheim Holding, Danfoss, Øyangen, Perfect temperature group (PTG), Gasnor, Bluewild and Isotherm Inc. (USA).. Other partners that are involved are Institute of Refrigeration, South Bank University and Johnson Controls DK.

NOMENCLATURE

RSW	Refrigerated sea water	DMH	Domestic hot water
AC	Air condition	SH	Space heating
COP	Coefficient of performance	EES	Engineering Equation Solver
T_{SW}	Seawater temperature (°C)	LT	Low temperature
η_{IHx}	Effectiveness	IHX	Internal heat exchangers
\dot{Q}_{RSW}	Refrigeration capacity at RSW		

REFERENCES

- Accelerate, ACC. (2020). *Food Retail Best Practice*.
- E. Torrella, D. S. (2011). Energetic evaluation of an internal heat exchanger in a CO₂ transcritical refrigeration plant using experimental data. *International Journal of Refrigeration*, 40-49.
- Eirik Starheim Svendsen, M. S. (2021). *Energy measurements onboard pelagic*. Trondheim: SINTEF Ocean AS.
- J.L. Dupont, P. D. (2019). *38th Note on Refrigeration Technologies: The Role of Refrigeration in the Global Economy*.
- K. Zolcer Skačánová, M. B. (2019). Global market and policy trends for CO₂ in refrigeration. *International Journal of Refrigeration*, 98-104.
- Paride Gullo, A. H. (2018). Transcritical R744 refrigeration systems for supermarket applications: Current status and future perspectives. *International Journal of Refrigeration*, 269-310.
- Pearson, A. (2005). Carbon dioxide—new uses for an old refrigerant. *International Journal of Refrigeration*, 1140-1148.
- S.M Liao, T. Z. (2000). A correlation of optimal heat rejection pressures in transcritical carbon dioxide cycles. *Applied Thermal Engineering*, 831-841.
- Sovacool, S. G. (2021). Climate change and industrial F-gases: A critical and systematic review of development, sociotechnical and policy options for reducing synthetic greenhouse gas emissions. *Renew. Sustain. Energy REv*.
- UNEP. (2016). *Montreal Protocol on Substances that Deplete the Ozone Layer - Further information on alternatives to ozone-depleting substances*. Nairobi: Edward Elgar Publishing.